INVESTIGATION OF AMORPHOUS GeTeSeGa CHALCOGENIDES FOR PHYSICAL, STRUCTURAL, OPTICAL AND THERMAL PROPERTIES

Thesis Submitted in fulfilment of the requirement for the degree of

DOCTOR OF PHILOSOPHY

By

EKTA

(Enrollment no: 186905)

Under the supervision of

Prof. (Dr.) P.B. Barman & Prof. (Dr.) Pankaj Sharma

DEPARTMENT OF PHYSICS AND MATERIALS SCIENCE

JAYPEE UNIVERSITY OF INFORMATION TECHNOLOGY
WAKNAGHAT, DISTRICT SOLAN, H.P., INDIA
November 2022

ii

Cover Page	*i*
Copyright	*ii*
Table of content	*iii-v*
Declaration by scholar	*vii*
Supervisor's certificate	*ix*
Acknowledgement	*xiii-xiv*
Abstract	*xv*
List of Abbreviations	*xvii-xxi*
List of tables	*xxiii*
List of figures	*xxv-xxvii*
List of Publications	*xxix*
Conference / Workshop attended	*xxxi*

Table of contents

DECLARATION

I hereby declare that the work reported in Ph.D. thesis entitled **"Investigation of Amorphous GeTeSeGa Chalcogenides for Physical, Structural, Optical and Thermal Properties"** submitted at **Jaypee University of Information Technology, Waknaghat, India** is an authentic record of my work carried out under the supervisions of **Prof. (Dr.) P. B. Barman and Prof. (Dr.) Pankaj Sharma.**

I have not submitted this work elsewhere for any other degree or diploma. I am fully responsible for the contents of my Ph.D. Thesis.

Ekta

Enrollment No. 186905

Department of Physics and Materials Science,

Jaypee University of Information Technology,

Waknaghat, Solan, H.P. India-173234.

Date…………………
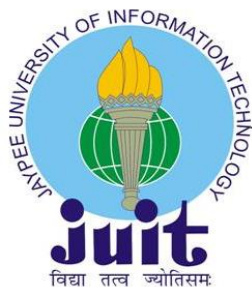
JAYPEE UNIVERSITY OF INFORMATION TECHNOLOGY
(Established by H.P. State Legislative vide Act No. 14 of 2002)
Waknaghat, P.O. Dumehar Bani, Kandaghat, Distt. Solan – 173234 (H.P.) INDIA
Website: www.juit.ac.in
Phone No. (91) 07192-257999 (30 Lines)
Fax: (91) 01792 245362

CERTIFICATE

This is to certify that the work reported in the Ph.D. thesis entitled **"Investigation of Amorphous GeTeSeGa Chalcogenides for Physical, Structural, Optical and Thermal Properties"**, submitted by **Ekta** at **Jaypee University of Information Technology, Waknaghat**, **India** is a bonafide record of her original work carried out under my supervision. This work has not been submitted elsewhere for any other degree or diploma.

Prof. (Dr.) P. B. Barman
Supervisor 1
Department of Physics and Materials Science
Jaypee University of Information Technology
Waknaghat, Solan, H.P. India-173234
Date…………………

Prof. (Dr.) Pankaj Sharma
Supervisor 2
Applied Science Department
NITTTR Chandigarh
Chandigarh. India- 160019
Date………………….

ix

x
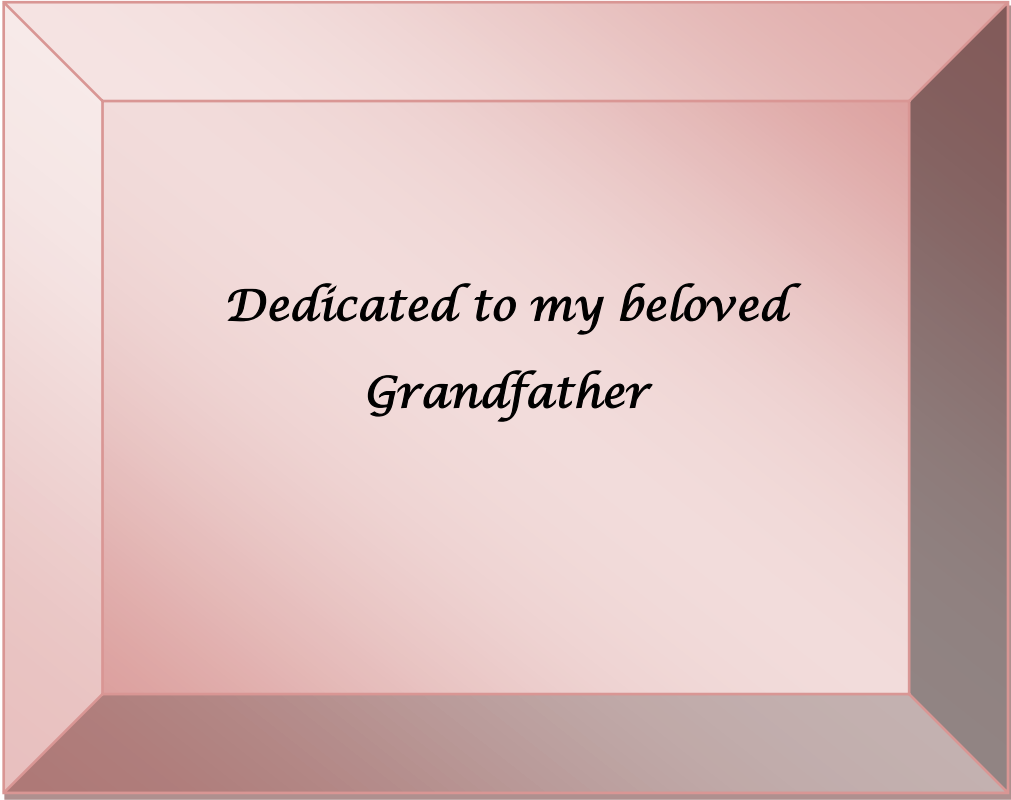
Dedicated to my beloved

Grandfather

<u>ACKNOWLEDGEMENTS</u>

*I am also grateful to all the members of technical and non-technical staff of the department **Er. Kamlesh Mishra, Mr. Ravendra Tiwari, Mr. Deepak Singh and Mr. Ghanshyam** for their help and precious assistance.*

*I have been very fortunate to meet people who have always been very kind and supportive. It is my pleasure to express my gratitude to my friends & juniors **Dipti, Sanjay, Monika, Pooja, Sweta, Rahul, Kalpana, Shiv Kumar (Senior)** and all the research scholars of the JUIT for keeping me blessed with best wishes. I want to say special thanks to my friend, room mate **Sargeet Kaur** for her continuous support and motivation during my hard times.*

*Finally, my deep and sincere gratitude to **my parents (Mr. R. P Duvedi & Mrs. Lata Duvedi**) for their continuous and unparalleled love, help and for supporting spiritually throughout my life. I am forever indebted to my parents for giving me the opportunities and experiences that have made me who I am. Also I would like to express my heartfelt gratitude to my father in law **Capt. Y. R. Sharma** & mother in law **Mrs. Anjana Sharma** without their unconditional support this task would not have been accomplished. There are moments in life when you feel direntionless. You get frustated and demoralized and need a boost. I want to express my special thanks to my husband cum friend **Ritesh Sharma** for always supporting and guiding me during this tenure. I would like say specially thanks to my sister (**Shanu**), brother (**Abhinav**) and brother in law (**Nirdesh**) for their continuous support and never let me felt abandoned. I also my sincere gratitude to my uncle Mr. **Navdeep Prashar** for motivating me most of the time. From the core of my heart I would like to thank my Grandfather **Mr. Ramesh Duvedi**, who really encourages, motivates and supports me in every phase of my research work.*

DATE: (EKTA)

ABSTRACT

The amorphous chalcogenides are useful in optoelectronic and IR applications because of their unique properties *i.e*. higher linear and non- linear refractive index, lower phonon energy and IR transparency up to far-IR region. Tellurium based gallium doped chalcogenides possess more thermal stability and high refractive index as compared to others. The bulk GeTeSeGa chalcogenides are prepared by traditional melt quenching approach. However, thin films are deposited on glass substrates by thermal evaporation method. With the rise of Ga content in the material, red shift in the wavelength is observed. The value of refractive index increases from 4.11 to 5.69 at 1μm while the value of optical band gap decreases from 0.952 eV to 0.790 eV with the Ga content. Further, with the inclusion of Ga the stability parameter ΔT increases which leads to the improvement of thermal stability of prepared glassy matrix. The GeTeSeGa system may be suitable in NIR imaging, IR detectors, optoelectronic and optical fiber applications.

List of Abbreviations

XRD	X-ray diffraction
EDS	energy-dispersive X-ray spectroscopy
VB	valence band
CB	conduction band
SRO	Short-range order
MRO	Medium range order
SRMRO	Short-range MRO
IRMRO	Intermediate-range MRO
LRMRO	Long-range MRO
HRSEM	High resolution scanning electron microscopy
HMFG	Heavy metal fluoride glass
O	Oxygen
S	Sulphur
Se	Selenium
Te	Tellurium
Po	Polonium
LP	Lone pair
σ	bonding
σ^*	Antibonding
O_3	Ozone
Sb	Antimony
Sn	Tin
Ga	Gallium
Ge	Germanium

FTIR	Fourier transform infrared spectroscopy
CRN	Continuous random network
CONM	Chemically Ordered Network Model
RCNM	Random Covalent Network Model
CFO	Cohen Fritzsche Ovshinsky
MDS	Mott Davis and Street
T	Transmittance
R	Reflection
CBA	Chemical Bond Approach
<r>	Average or mean coordination number
N_b	Bond bending constraints
N_s	Bond stretching constraints
N_c	Total number of constraints
$<r_{eff}>$	Effective coordination number
M_f	Count of floppy modes
D_{CL}	Cross-linking density
ρ	Density
P.D	Packing density
δ	Compactness
FVP	Free volume percentage
V_m	Molar volume
L	Lone pair electrons
M_i	Molecular weight
N_A	Avogadro number
CE	Cohesive energy
E_g^{th}	Theoretical band gap
$\bar{H}_S$	Heat of atomization
I_c	Degree of ionicity
C_c	Degree of covalency
V_T	Theoretical volume
F	Field strength
R_p	Polaron radius

E_{A-B}	Heteropolar bond energy
E_{A-A}	Homopolar bond energy
$\overline{H}_S / <r>$	Average single bond energy
χ	Electronegativity
R	Stoichiometry deviation
<E>	Mean bond energy
λ	Wavelength
VFF	Valence field Theory
ν	Wavenumber
K	Force constant
μ	Reduced mass
K_r	Force constant by Gordy
K_{AB}	Force constant by Somayayulu
Bond order	N_{bo}
E_g^{opt}	Optical bandgap
n	Refractive index
α	Absorption coefficient
D_{op}	Optical density
k	Extinction coefficient
ψ	Penetration depth
n_2	Non-linear refractive index
$\chi^{(3)}$	Non-linear susceptibility
T_M	Maxima of transmittance
T_m	Minima of transmittance
s	Refractive index of glass substrate
x	Absorbance
m_o	Integer for maxima and half-integer for minima
d	Thickness
d_1	Mean thickness
d_2	Corrected thickness

ε	Dielectric constant
ε_r	Real part of dielectric constant
ε_i	Imaginary part of the dielectric constant
E_o	Single oscillator energy
E_d	Energy of dispersion
$E_g{}^{WDD}$	Average energy gap
ε_∞	Dielectric constant at a higher frequency
n_o	Static refractive index
M_{-1} & M_{-3}	Moments of εi
β	Dispersion parameter
N_e	Total count of valence electron per anion
f	Field strength
σ_{oc}	Optical conductivity
σ'	Real part of the optical conductivity
σ''	Imaginary part of the optical conductivity
N^*	Number of the carrier concentration
ε_L	Lattice dielectric constant
m^*	Effective mass of the charge carriers
λ_o	Oscillator wavelength
S_o	Average oscillator strength
ε_{opt}	Residual dielectric constant
$\hbar\omega_D$	Screened plasma energy
ω_p	Plasma frequency
N_{opt}	Optical carrier concentration
$m_c{}^*$	Effective mass of the electron
α_p	Electronic polarizability
R_m	Average molar refraction
R_L	Reflection loss
M	Metallization characteristics
η_{opt}	Optical electronegativity
NLO	Nonlinear optical
P	Polarization

T_o	Onset of crystallization
T_g	Glass transition temperature
ΔT	Thermal stability
T_m	Melting temperature
T_c	Crystallization temperature
GFT	Glass-forming tendency
GS	Glass-stability
T_{rg}	Reduced glass transition temperature
$H^{'}$	Thermal stability criterion
H_r	Hruby's criterion
k_H	Glass-formation factor

List of tables

List of Figures

xxvi

List of Publications

1. **Ekta Sharma,** P. B. Barman & Pankaj Sharma (2022). On the structural and optical aspects of GeTeSeGa thermally evaporated semiconducting thin films for infrared applications. **The European Physical Journal Plus** (Volume 137, p. 358). SCI Indexed (I.F: 3.911) .

2. **Ekta Sharma,** P. B. Barman & Pankaj Sharma (2021). Structural correlation of GeTeSeGa system by XRD and far-infrared spectroscopy. **Applied Physics A: Materials Science & Processing** (Volume 127, p. 1-10). SCI Index (I.F: 2.584) .

3. **Ekta Sharma**, P. B. Barman & Pankaj Sharma (2020). Evaluation of optical linear and non-linear parameters of thermally deposited GeTeSeGa thin films in NIR (1 µm -2.6 µm) wavelength range from their transmission spectra. **Optik: International Journal of Light and Electron Optics** (Volume 219, p.165181).SCI Index (I.F: 2.443) .

4. **Ekta Sharma**, H. H Hegazy, Vineet Sharma & Pankaj Sharma, (2019). Topological behavior and glassy framework of GeTeSeGa chalcogenide glasses. **Physica B: Condensed Matter** (Volume 562, p.100-106). SCI Index (I.F: 2.436) .

5. **Ekta Sharma**, Pankaj Sharma (2020). Applicability of different models of energy bandgap and refractive index for chalcogenide thin films. **Materials Today: Proc**. (Volume 28, p.92-95). Scopus Index.

6. **Ekta Sharma,** R. Sharma, V. Sharma, P. Sharma, (2018). Cohesive Energy Calculation of Quaternary Ge-Te-Se-Ga Chalcogenide Glasses using Chemical Bond Approach, **AIP Conf. Proc**. 020008 (Vol. 2050, No. 1, p. 020008). Scopus Index.

xxx

Conferences / Workshops attended

- Attended 3rd HP science congress 2018 held at IIT Mandi.

- Attended Five-day workshop on "Material Characterization Techniques" at Dr. B. R. Ambedkar National Institute of Technology, Jalandhar on June 17-21,2019.

- Attended Five-day workshop on "Innovative techniques of characterization, optimization and Data Analysis (ITCOD)" at Chitkara University Rajpura, Punjab on July 8-12,2019.

- Attended Three-day International Conference on "Advanced Materials and Nanotechnology (AMN 2020)" at Jaypee Institute of Information Technology, Noida (INDIA) on February20-22, 202019.

- Attended Three-day International virtual Conference on "Advances in Functional Materials (AFM2020)" at KIIT Bhubaneswar, Odisha (INDIA) on August 26-28, 2020.

- Attended Two-day International virtual Conference on "Frontiers in Manufacturing Technology (FMT 2020)" at KIIT Bhubaneswar, Odisha (INDIA) on October 13-14, 2020.

- Attended two days online Course on "Winter School on Materials Characterization techniques" at Manipal University Jaipur, on December 26-27, 2020.

- Attended One-week Online FDP on "Novel Materials" at NIT Raipur on September 24-28, 2021.

- Attended one-day webinar on "Synthesis, characterization and applications of Nano- materials" at Harcourt Butler Technical University Kanpur on October 28th, 2021.

Introduction

1. Introduction

The materials exist in three states based on the distance between their neighbouring atoms; solid, liquid and gaseous. The interatomic distance between the adjacent atoms in solid and liquid is of the order of few Å, whereas in the gaseous state, this distance is comparatively large. The material may be of various types *viz.* metals, wood, glass, ceramics and plastic *etc.* The advancement of materials has resulted in the emergence of several periods like the Stone Age, Bronze Age and Steel Age. Material Science is the oldest kind of applied and engineering science. It is an applied science which links between the properties and structure of a material. This involves the evaluation of the material and how the structure of crystalline or non-crystalline material may be changed to affect the characteristics of a material. It helps in enhancing the characteristics to develop and improve the product suitable for society. The characteristics or properties may be divided into various categories such as physical, electrical, mechanical, optical, chemical and magnetic *etc*. Solid materials are classified as crystalline, non-crystalline or amorphous. The atoms in the crystalline materials are regularly arranged, whereas, in the non-crystalline/amorphous materials, atoms are arranged in irregular manner. Amorphous materials are gaining popularity because of wide range of applications in solid-state materials.

The understanding of materials occurred in 19th century when the thermodynamic properties related to the atomic structure in several phases were associated with the physical characteristics of the material. It is a multidisciplinary field comprised of the properties of matter and their uses in several areas of engineering and science. The structure is one of the most essential components in the field of materials science. This science measures the structure of a material from the atomic scale up to the macroscale. The structure of the material can be obtained by numerous techniques like x-ray diffraction (XRD), neutron or electron diffraction, Raman spectroscopy, chromatography, energy dispersive spectroscopy (EDS), thermal analysis and chemical analysis *etc*.

Solid-state is the study of solids or rigid matter by methods like metallurgy, electromagnetism, quantum mechanics and crystallography. These are characterized by the stronger interaction between their constituting particles such as molecules, atoms *etc*. The solids are materials with viscosities greater than $10^{14.6}$ poise. In contrast, fluids like gases and liquids have much low value.

1.1 Motivation behind the work

The study of amorphous materials characterized by a lack of long-range order has recently garnered much attention in condensed matter physics. Due to their high optical transparency, affordable manufacture and adaptability, glasses are the primary materials used in optical systems. In recent years, the innovation of materials with high refractive indexes and low band has been a growing area in science and technology. Semiconductors such as Ge, Si and InGaAs are the most commercialized for NIR sensing. However, InGaAs products are expensive to fabricate and require low temperatures. Hence, new materials that are flexible, cost-effective, have a tunable band gap, higher index of refraction and a high transparency window are needed. Chalcogenide materials are becoming more desirable because of their roles in near-infrared imaging (NIR). Chalcogenide glasses have outstanding properties for NIR imaging devices, such as a high NIR transmittance and high index of refraction ($n > 2$). The chalcogenide glasses possess 1000 times greater non-linearities than silica and hence are good candidates for mid-infrared supercontinuum (MIR SC) generation. Glasses that consist of polarizable atoms or ions, are likely to have large non-linear optical characteristics. In comparison to glasses, the crystals show non-linear effects. However, glasses lead due to more advantages, viz. low cost, large "refractive index" etc. Much work has been done on the binary, ternary and quaternary systems. However, low thermal stability and low transmission window are some drawbacks which are still there. The reports are available in the literature, but there is some drawback to the GeTeSe system. The glasses based on Se have good thermal stability; however, their IR cut-off window is limited due to Se. Also, Se shows ageing effect. On the other hand, Te-based glasses have a higher IR window. The Te-based glasses are the most potential materials out of the three chalcogens. The telluride-rich materials are seeking attention day by day because of their wider IR transparency up to far infrared region and their use in phase change memory (PCM) devices. These are used in waveguide-based applications like biosensors, optical fibers, spatial detection etc. Thermal and structural stability of amorphous materials are critical for these applications. The thermal stability of amorphous materials can be determined by the analysis of crystallization kinetics which can be derived from crystallization kinetics. The lower crystallization speed indicates better thermal stability. Because of the heavier masses of the constituent atoms in Te-based glasses, the vibration energies are shifted to the lower energy side, resulting in greater infrared transparency. As a result, understanding the crystallization kinetics of supercooled liquids

4

is essential for developing the optimal material composition. As compared to other chalcogens, Te atoms are heavier. Thus, a small quantity of Te addition stabilizes the glass formation. The metallic character of chalcogens increases from S, Se followed by Te. However, the robust metallic nature of Te leads to poor glass formation, which is the biggest drawback of Te-based glasses. To surmount this problem, it is required to include trivalent and tetravalent elements like Ga, As, Ge, Bi, Sb and I in Te rich system. From this perspective, Te-rich compositions have been considered. It is expected that the inclusion of Ga to the system may cause structural disorder, improving glass formation ability and possessing a broader IR window. The suitable composition has been investigated to maintain both the properties such as wider IR transmission and thermal stability of material. Also, in the recent era, the main interest is increasing in Ge, Te and Ga alloys for the far-Infrared transmission. The glasses based on GeTeGa have been recognized as a novel material for the ESA Darwin Mission.

1.2 Aim of the work

The chalcogenide glasses have unique properties as compared to oxide and fluoride glasses like wider infrared transmission window up to far-infrared region. The objective of the present work is to study variation of physical properties with Ga content in $Ge_{10}Te_{80}Se_{10-z}Ga_z$ (z = 0 to 10 at. %) glassy system. Also, the system has been investigated for optoelectronic applications having n > 2 and bandgap < 2 eV. System is investigated in far IR region. The thermal stability of these glasses suitable for optical fibers have also been carried out.

1.3 Outline of the thesis

The present thesis comprises the physical, structural, optical and thermal properties of Ge-Te-Se-Ga chalcogenide glasses synthesized by "conventional melt quenching" approach. The layout is divided into 6 chapters.

Chapter 1: Introduction

Chapter 2: Experimental details

Chapter 3: "Physical and structural properties of GeTeSeGa chalcogenide system".

Chapter 4: "Optical properties of GeTeSeGa chalcogenide thin films"

5

Chapter 5: Thermal properties of GeTeSeGa system.

Chapter 6: Summary and future scope.

1.4 Difference between crystal and amorphous semiconductors

The disordered atomic structure has a lower density and is more flexible. "An included ion can thus move smoothly, which is advantageous for solid-state battery applications" [1]. The glasses must have a quasi-equilibrium state that may be developed from a rapid melt quenching technique with a duration of milliseconds to minutes, depending on the material. Difference between crystalline and amorphous solids is depicted in table 1.1.

Table 1.1: Difference between crystalline and amorphous (non-crystalline) material [1].

Property	Crystal Material	Amorphous Material
Atomic position	Periodic	Periodicity lost
Order	long-range order	Short or medium-range order
Isotropy	No	Yes
Structure controllability	Atomic	Nano-scale
Homogeneity	Yes	Macroscopically yes
Stability	Yes	Meta-quasi
Dimension of the sample	Small	Large
Wave functions	Extended	Localized

1.5 Amorphous Semiconductors

Mott and Davis [2] have discussed the glasses among amorphous materials that may be solidified into the non-crystalline from the melt. Vitreous and Glassy words have been obtained from Latin and an Indo-European root [3]. The definition may be defined in mathematical notations as follow:

"Non-crystalline (disordered) ⊃ amorphous ⊃ glassy ≈ vitreous."

For example, an amorphous Si-H (Hydrogenated silicon) film possesses amorphous nature but is not glassy. It is formed from vapour and plasma phases. The film cannot be deposited by melt quenching of liquid Si [4].

Elliot and Phillips [5, 6] have preferred a different definition of glasses. They divided the non-crystalline solid into two parts; glassy and amorphous, depending on whether they exhibit the glass transition or not respectively. It is the gradual transition of glassy and supercooled liquids. Their results show that the glassy and amorphous are not compatible.

"Amorphous ∩ glassy (vitreous) = ϕ (empty set)"

In short, one can conclude that the definition given by Davis and Mott depends on the preparation techniques, whereas the definitions given by Phillips and Elliott depend on their properties.

There are generally two types of disorder that has been discussed; one is a compositional disorder that can be observed in binary crystalline alloys and another one is present in liquids and amorphous solids. Because of the absence of long-range order, the covalent chemical bonding exists in amorphous solids. The tailing states are created in the bandgap area due to spatial variation in bond angles, bond length and dihedral angles. Mobility edges are seen on the "valence band (VB) and conduction band (CB)". The boundaries between localized and delocalized states are defined by these edges. The disorder present in these materials is the main cause of these boundaries. This process is called Anderson Localization. Due to the absence of translational order in the amorphous solids, the Bloch theory of crystalline solids cannot be applied. However, the Hartree – Fock approximation, tight-binding model and density fluctuation model may be employed to understand the electronic characteristics of amorphous materials [7].

Several amorphous solids may be known as semiconductors in the sense that they do

not behave as good insulators or good conductors. However, instead they are poor conductors. Amorphous semiconductors are featured as :

1.   They possess transparency in the IR region
2.   The electrical properties of these solids are approximately comparable to intrinsic semiconductors or perfectly compensated semiconductors.
3.   Their conductivities at room temperature are less than 10^3-$10^4\Omega^{-1}cm^{-1}$.

1.5.1 Atomic structure of amorphous semiconductors

It is necessary to know about the structural arrangement of atoms in the amorphous solids to understand other vital chemical and physical characteristics. The structural order in the amorphous semiconductors may be classified as shown in figure 1.1 [8, 9].
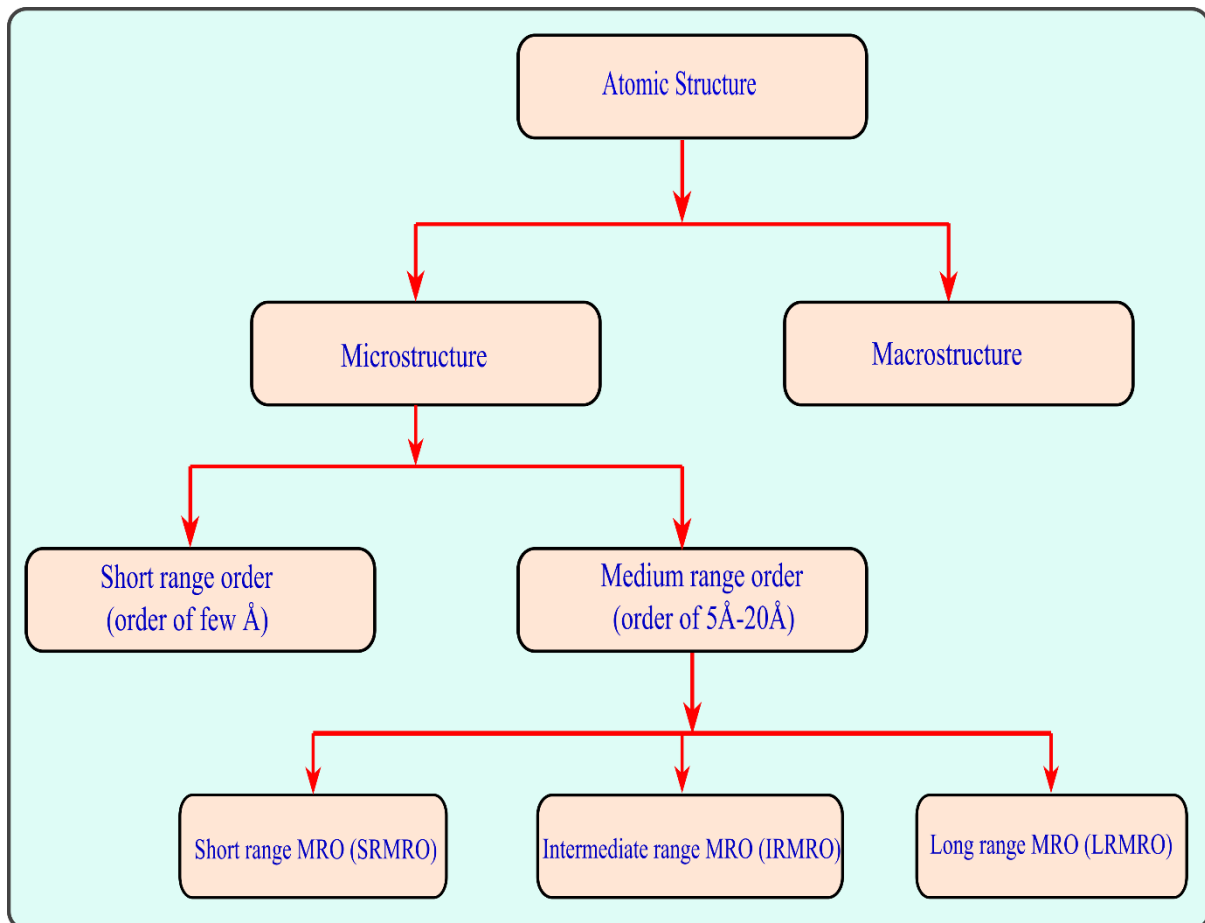
Figure 1.1: Atomic structure of amorphous solids

Short-range order (SRO) is the lowest structural order ~ 2-5Å [8]. In covalently bonded amorphous semiconductors *viz* chalcogenide glasses, the short-range order may be described in terms of coordination polyhedra. Hence, the parameters that are essential to define topological SRO are the type and number (N_j) of nearest neighbour "bond length r_{ij} and bond angle θ_{ijk}" subtended at the origin. The atom may be of type 'i' with neighbouring atoms j & k. However, atoms cannot be of a similar type.

"Medium range order or intermediate-range order (MRO or IRO)" in amorphous solids comes under the next higher level of the structural unit above SRO, possessing a length of 5-20 Å [8,10]. It may be characterized into three categories:

Short-range MRO (SRMRO) has a length scale of 3-5 Å. It may be associated with the kind of relation and relative orientation of pairs of coordinate polyhedral, which produce the basic structural units in short range order [10].

Intermediate-range MRO (IRMRO) has a length of 5-10 Å. It is concerned with the phase connection between the pairs of di - hedral angles for neighbouring bonds. As a result, "superstructural units" can be formed from aggregates of basic polyhedra linked together to form regular rings of atoms.

"Long-range MRO (LRMRO)" may be linked to the local dimensions of a covalent bonded amorphous network. This may be ascertained by finding the dimensions traced out locally over a distance of approximately 10 Å by bond percolation among the covalent bonds of the structure, ignoring the much weaker Van der Waals bonds [11].

Macroscopic structure: The SRO and MRO in amorphous semiconductors have been discussed in the preceding section, with the assumption that the structure is homogeneous at the microscopic level. However, several amorphous semiconductors possess inhomogeneity on the macroscopic level approximately 1µm like phase separation for a particular compositions of multicomponent melt quenched glasses and voids (pores) in the vapour deposited films. These inhomogeneities may be measured by using certain characteristics techniques such as optical microscopy, high-resolution transmission spectroscopy (HRSEM) and low angle (neutron or X-ray) scattering *etc*. [10]

1.5.2 Classification of amorphous Semiconductors

The distribution of amorphous semiconductors is shown in figure 1.2
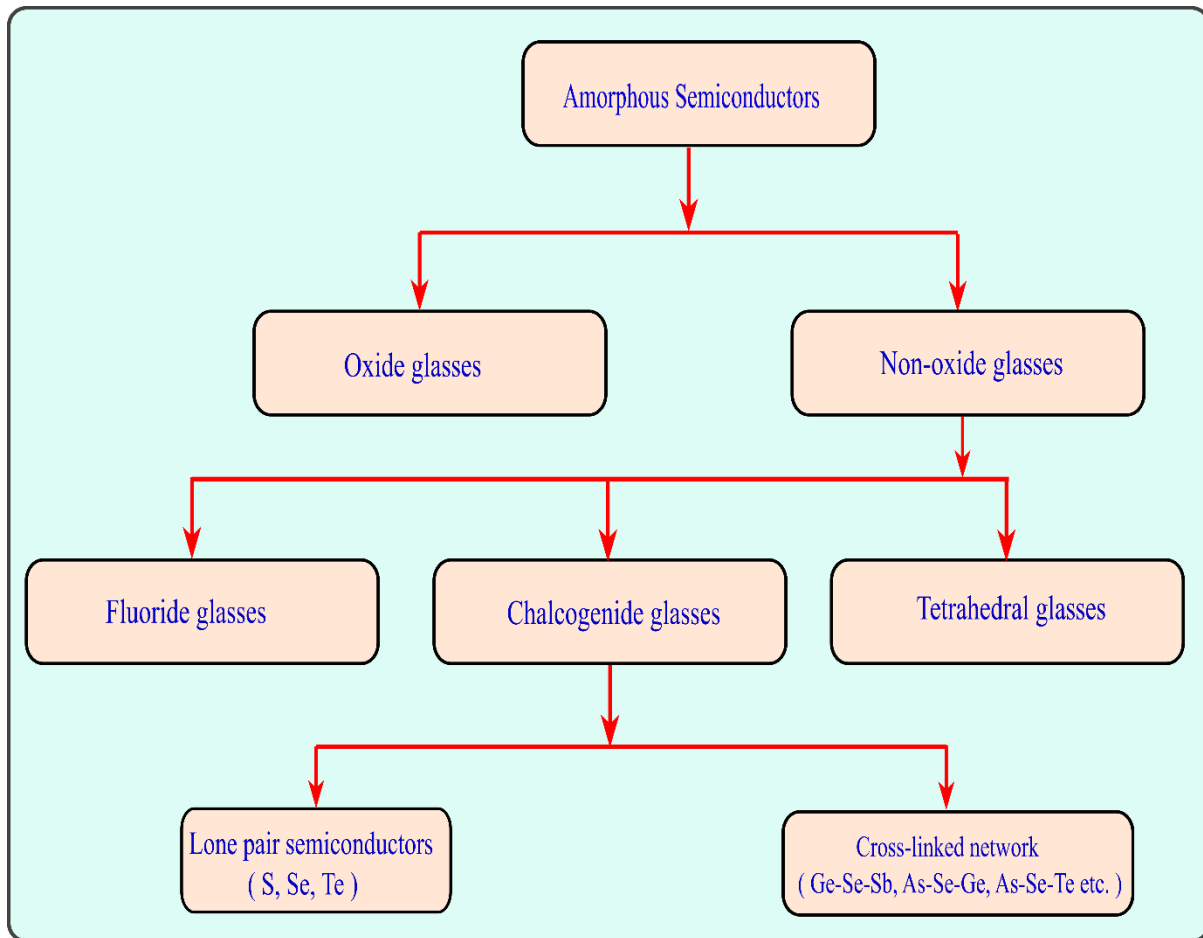
Figure 1.2: Distribution of amorphous Semiconductors

- ➢ **Ionic bonded or oxide amorphous semiconductors:** Ionic bonded or oxide glasses amorphous semiconductors are good insulators because electrons are bonded to their ions and do not participate in electrical conduction. Silica glasses (SiO_2) are favorable materials for long-distance optical fiber communication. The silica-based glass has a lower refractive index used for operating in nonlinear devices. Although these silica glasses require a high intensity of light for functioning. The transmission window of silica is in the range of 3 to 5 µm. Due to these limitations, it is necessary to obtain some new glass family suitable for optical applications in mid and far-IR region.

- ➢ **Non-Oxide or covalent bonded amorphous semiconductors:** The Non Oxide glasses are generally characterized in three classes; "fluoride, tetrahedral and chalcogenide glasses" (figure 1.2). The fluoride glasses are the classes of non-oxide

10

glasses composed of "Zirconium, barium, lanthanum, aluminum and sodium (ZBLAN)". Due to low viscosity of these glasses, crystallization is not totally ignored during glass transition processing. Heavy metal fluoride glass (HMFG) possesses less optical attenuation and is simple to prepare. However, HMFG have poor resistance to moisture and are fragile. For optical fibre applications, HMFG had a lower intrinsic loss than silica fibres in the mid-IR range.

1.6 Glass

Glasses may be described as amorphous semiconductors that can be cooled to a rigid condition without crystallization. Like all glasses, chalcogenide glasses possess "glass transition temperature (T_g)", that is critical for processing bulk glasses into thin films and optical fibres. The glassy industry is totally affected by the traditional silica-based materials, which provide a stable application in car industry, telecommunication, optics, building *etc*.

All oxide-based materials such as silicate, borate and phosphate glasses are developed from light elements of the periodic table and they form robust chemical bonding. Subsequently, the vibration modes possess higher energy, which leads to IR absorption limited to 3μm region. Thus these glasses are opaque above IR range.

1.7 Chalcogenide glasses

The group 16th of the periodic table is known as the chalcogens family (figure 1.3). The oxygen family is the name given to this group. It contains elements like oxygen (O), Sulphur (S), Selenium (Se), Tellurium (Te) and Polonium (Po).

Group→ Period↓	I(a,b) 1,11	IIa 2	IIIb 13	IVb 14	Vb 15	VIb 16	VIIb 17	VIIIb 18
1	H							He
2	Li	Be	B	C	N	O	F	Ne
3	Na	Mg	Al	Si	P	S	Cl	Ar
4	K/Cu	Ca	Ga	Ge	As	Se	Br	Kr
5	Rb/Ag	Sr	In	Sn	Sb	Te		

Figure 1.3: Location of chalcogens elements in the periodic table

The metallic nature rises with the rise of the atomic number of these group elements, *i.e.* S < Se < Te. Chalcogens elements S, Se and Te have covalent bonding structures. The word chalcogenide originated from the Greek word 'Chalcos' means Ore and gen means formation. So the meaning of chalcogenide is ore formation [12]. The elements are called chalcogenide as their atoms have a marked tendency to link together to form a long chain polymer [12]. The oxygen is also included in group 16th but has its own class *i.e.* oxide glasses. It possesses ionic bonding character and different properties compared to chalcogenide or non-oxide glass. Selenium is beneficial in glassmaking applications. Te materials are mostly suitable in electronic devices, solar cells and optical disks. All the chalcogens have six valence electrons having configuration $s^2 p^4$. s shell is filled with two electrons and the p shell has one filled electron pair, considered for non-bonding and two unfilled states (figure 1.4(a)).
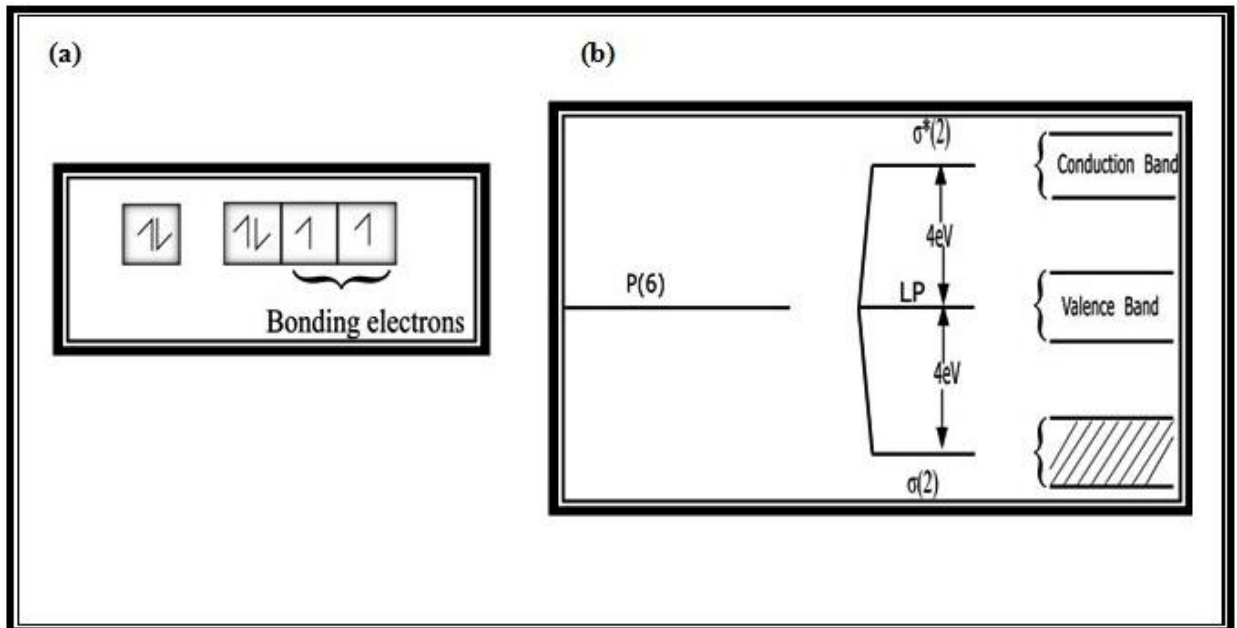
Figure 1.4: (a) Bonding electrons (b) Bonding in chalcogenide glasses given by Kastner [13]

The "lone pair electron" occupies the states at the top of the "valence band" due to the higher energy of unshared electrons than the bonding electrons. Now the valence band is no longer the bonding band as the lone pair (LP) and σ (bonding) is filled [14]. The lone pair lies between the "bonding (σ) and antibonding (σ*)" states. Moreover, the occupied states fall into the σ band while unoccupied states form the acceptor band above LP (figure 1.4(b)).

All the chalcogens play a vital role in biological functions such as a toxin or nutrient. Sulphur is rarely toxic and helpful in pure form. Se is also an essential nutrient, but more toxic than Sulphur. The unique characteristics of chalcogenide glasses are high "refractive index", wider infrared transmission (up to the far-infrared region), photosensitivity and low "phonon energy" which make them suitable for optoelectronic applications. It is not necessary to grow chalcogenide glasses on a single crystalline substrate due to their amorphous nature. The phonon energy and the electronic structure of chalcogenide glasses are two characteristics that have a significant influence on their interaction with light. The phonon energy of the material is used to estimate the infrared side of the transparent region, which leads to the wider transmission window extended up to the far-IR region (figure 1.5). The existence of heavy and large atoms causes the phonon energies at lower region and consequently

13

at longer wavelengths. Due to low phonon energy, chalcogenide glasses are used for infrared applications. The disorder and randomness produce localized electronic states that get extended into the prohibited bandgap. The presence of states has a profound impact on chalcogenide glasses's electrical and optical properties.
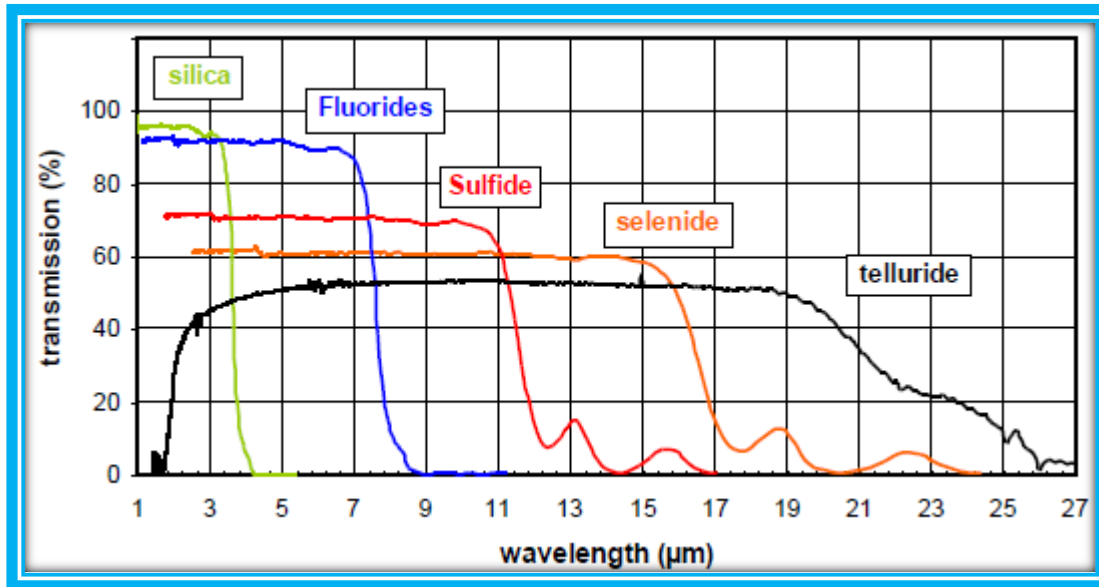
Figure 1.5: Comparison of transmission for chalcogenide glasses with fluoride & silica glasses [15]

The chalcogens have well-defined coordination numbers. Due to the existence of two-fold coordination, there is the presence of lone pair electrons in all chalcogens elements. The lone pairs do not contribute in chemical bonding so they show defects *viz* dangling bonds, vacancy and non-bridging atoms. The presence of defects creates energy levels in the bandgap and depict some peaks in density state distribution spectra.

One of the major distinctions among the chalcogenide and oxide glasses is the bandgap. The bandgap of the SiO_2 is about 10 eV, whereas the bandgap of chalcogenide glasses lies between 0.7 - 3 eV [16]. The chalcogenide glasses are known as soft semiconductors as their atomic structures are flexible. The bandgap of chalcogenide is similar to the bandgap of the semiconductors.

In the present era, key focus has been paid to the greenhouse effect that plays a crucial role in global warming. Many molecular species like CO_2, O_3, CH_4, H_2O *etc*.

14

exist in the atmospheric window. They show strong absorption bands in the mid-infrared (2.5 to 25µm) region. These molecules are considered as the main reason for global warming as they inhibit infrared light emitted by earth to escape into space. The transparency window in the near IR range is around 1.6 µm and 2.3 µm for the O-H absorption band [17]. The Ozone molecule (O_3) also possesses an absorption band in the 10 µm region. All specifications can be fulfilled only by the material which is made up of heavier atoms and has a low energy vibrational mode. The chalcogenide glassy materials such as Te, Se and S fulfils this requirement.

1.7.1 Types of chalcogenide glasses

Chalcogens have a small glass formation region [18]. Hence to enhance the glass-forming region, it is necessary to add network modifier with chalcogens like antimony (Sb), tin (Sn), gallium (Ga) and germanium (Ge) *etc*.

The chalcogenide glasses may be divided into two categories as:

i. "Lone-pair semiconductors: S, Se, Te, As_2S_3, As_2Se_3 *etc*.

ii. Cross-linking network: When one or more than one elements are combined with the binary system, the structure is cross-linked such as As-Se-Ge, Ge-Se-Sb, As-Se-Te *etc*".

The most promising chalcogenide material is Te-based chalcogenide glasses. These systems possess high IR transmission in mid to far IR region. The unique properties of these systems may be suitable in numerous hi-tech infrared applications *viz* space optics, biosensors helpful for environment and medicine [19-21]. The greatest limitation of Te based glasses is their higher metallic character, which tends to a strong tendency towards crystallization. This disadvantage also creates some complications in the processing of the glassy system. In recent days the main emphasis is kept on finding the system with appropriate optical, thermal and other properties. To surmount this problem, it is required to dope the system with the stabilizing components such as Ge, Se, Ga, I, In, Bi, As, *etc*.

1.8 Theoretical background

It was initially proposed that amorphous materials are structureless, as the word "structure" is employed only for crystalline materials. Thereafter, Ioffe and Regal [14] pointed out that the amorphous materials have an absence of long-range order and retain their semiconducting properties. The inadequacy of long-range order in amorphous systems indicates a shortage of translational periodicity [22, 23]. It is well known that several kinds of experimental techniques *viz* "x-ray diffraction (XRD), neutron diffraction, Fourier transform infrared spectroscopy (FTIR) and Raman spectroscopy" are being used to find the structure of amorphous semiconductors. Numerous models like the "continuous random network (CRN) model, chemically ordered network model (CONM), random covalent network model (RCNM)" [24-26] are discussed here to realize the compositional dependence of chalcogenide glasses. The network structure of amorphous materials can be characterized into three levels: i) The atomic coordination of each constituent element ii) distribution and counts of bonds and iii) the molecular structure of network forming groups of atoms [24].

In 1979 J. C. Phillips [26] proposed the basic idea on mechanical-constraint counting algorithms to describe the system's glass formation tendencies. The Philips –Thorpe model considered for non-oxide covalent materials such as chalcogenide glasses carries a microscopic approach by taking into account the connectivity of individual atoms. According to this theory, the glass-forming ability of a material is estimated by comparing the number of interaction force field constraints with the number of "degrees of freedom". For the 3-D space system, each atom consists of three translational "degrees of freedom". Due to the presence of constraints, these degrees of freedom can be removed. According to the topological constraint network theory, the average coordination number <r> is the main ruler of the physical properties of these covalent glasses.

The band models which have been used to discuss the behaviour of crystalline materials cannot be directly used for amorphous materials. In crystalline solids, the presence of a sharp edge in the density of states, produces well defined forbidden bandgap. It happens only due to the ideal long-range order and perfect short-range order in these materials. The non-crystalline materials have lack of periodicity. The periodic arrangement of atoms in the crystalline solids facilitates the calculation of electronic states mathematically by using Bloch theory, where as it becomes problematic in case of amorphous materials. The

electronic states in the amorphous solids can be discussed in terms of "tight-binding approximation and Hartree-Fock" calculations.

Different models have been formulated for the explanation of optical and electrical characteristics of amorphous solids in terms of states in the gap. These are mainly because of the existence of defects like weak and strained bonds. The electronic energy state of a semiconductor has delocalized states (also called an extended state) and the localized states *viz* dangling bonds and tails *etc*. The tail states in the amorphous solids are due to a compositional and translational disorder where the presence of short-range order gives rise to extended states. In amorphous semiconductors, these localized states are certain. These localized states are specific in the amorphous semiconductors. The energy separates the localized states from the extended states, referred as mobility edge [27]. Various models have been discovered to understand the solids band structures are as follow [17, 27-33]:

- ➢ Cohen Fritzsche Ovshinsky (CFO) model
- ➢ Mott -Davis Model
- ➢ Mott Davis and Street (MDS) model

There exist various approaches for the evaluation of optical constants *viz.* "refractive index (n) and extinction coefficient (k)", but here only those parameters are considered specific for thin films. Films are not self-supporting. These need some supporting substrate for their deposition, which results in a system consisting three dielectric media such as air, thin films and the substrate [34].

The optical properties of chalcogenide glasses have been studied from the last decades as these materials show high transparency up to far-infrared regions and are used in optical devices. When the light beam interacts with the material, it can be partially transmitted, partially absorbed or partially reflected.

The methods to calculate n and k are categorized into three modes *viz:*

- i)   Both reflection and transmittance (R and T)
- ii)   Only reflectance (R)
- iii)   Only transmittance (T)

Transmission is a characteristic of a material to permit the passage of radiation with some or none of the incident radiation being absorbed in the process. It has been observed that the presence of impurity absorption bands lowers the transmission window up to a specific region.

The transmission method is originally introduced by J.C. Manificier [35] and further expanded by Swanepoel [36, 37]. In this process, only the transmission spectrum has been used to determine the optical constants. Consider the thin film on the transparent glass substrate having "thickness d and complex refractive index $(n^* = n - ik)$". The refractive indices of air $n_a \sim 1$ and the refractive index of glass substrates s = 1.51 (figure 1.6).
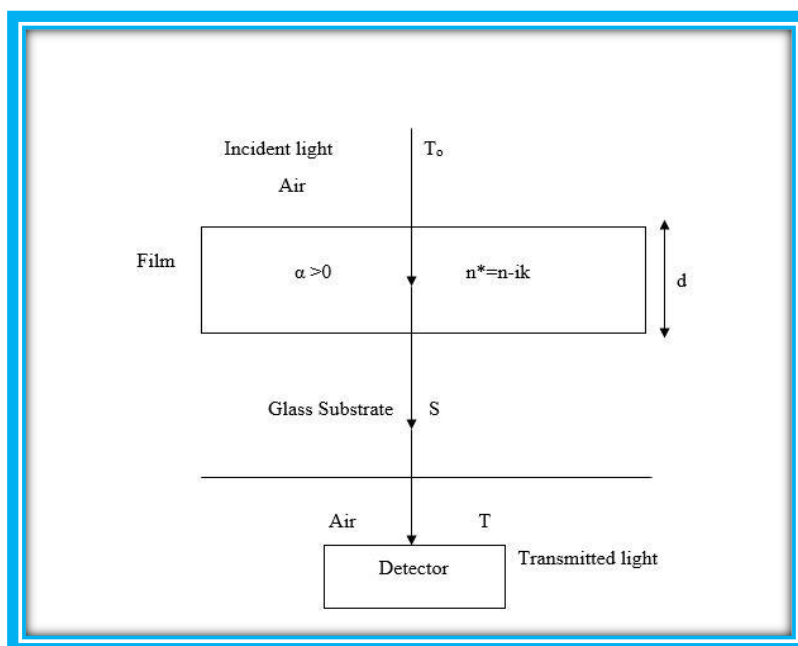
Figure 1.6: "System of an absorbing thin film on a thick transparent glass substrate"

If the thickness of the thin film is non-uniform, then interference fringes are absent and consequently, the transmission is a smooth curve rather than full spectrum. While for the uniform film thickness, the presence of interference effects produce the transmission spectra as depicted in figure 1.7.
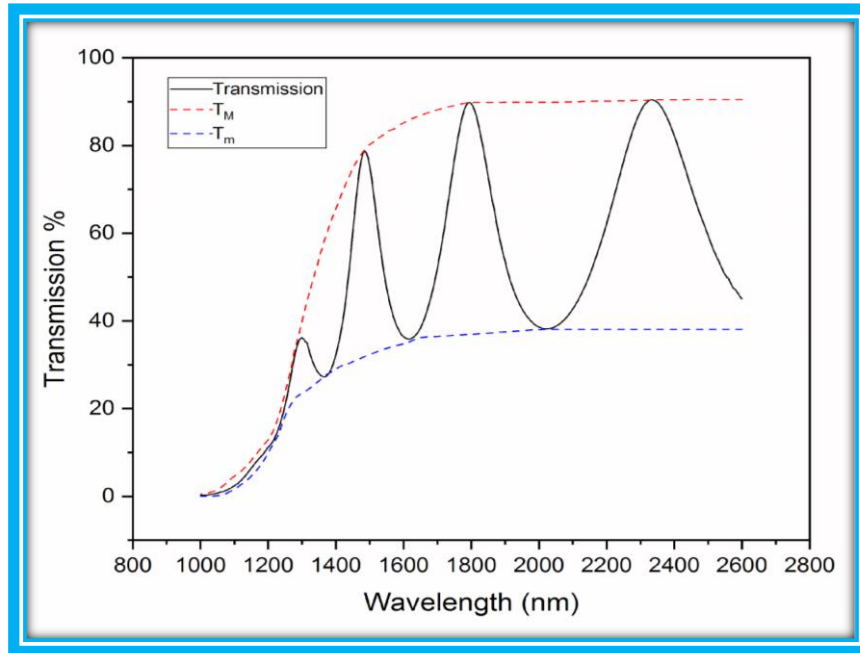
Figure 1.7: Graph of wavelength versus transmission showing upper and lower envelope for GeTeSeGa thin films

The thermal analysis method is a branch of analytical science in which the characteristics of analytes are examined as they vary with the temperature. Thermal analysis is defined as the variation of chemical and physical properties of the material with the change in temperature [38]. For example, the crystallization time should be lower for a rapid phase change materials used for storage devices. The thermal properties of glassy alloys cover a variety of aspects, such as the stability to devitrification and the glass transition temperature. The thermal variations in the material are because of endothermic (heat absorb) or exothermic (heat release) enthalpic reactions which are caused by vaporization and phase change *etc*. The oxidation, crystallization and some decomposition reactions are exothermic effects. On the other hand, dehydration, phase change, reduction and some decomposition reactions are endothermic [39]. The glasses are formed in the process of glass transition or vitrification. It is well known that amorphous materials have a tendency to relax towards equilibrium [39].

T_g is the temperature at which the material undergoes a state transformation (supercooled liquid to glassy solid). Also, several physical properties like hardness and volume, endure a dramatic transformation at this point.

The IR region is usually allocated into three regions as follow [40]:

19

Region	Wavenumber ($\bar{\upsilon}$)	Wavelength (λ)	Uses
Near- IR	$14000 cm^{-1}$ - $4000\ cm^{-1}$	$0.8\ \mu m$ -$2.5\mu m$	Harmonic vibration
Mid - IR	$4000\ cm^{-1}$ - $400 cm^{-1}$	$2.5\ \mu m$-$25\ \mu m$	Functional group identification
Far-IR	$400\ cm^{-1}$-$10\ cm^{-1}$	$25\ \mu m$-$1000\ \mu m$	Rotational Spectroscopy

IR spectra have mainly two regions *viz.* 0 to $1000\ cm^{-1}$ (fingerprint region) and 1000 –

$4000\ cm^{-1}$ (functional group region). The information about the structural positioning of the glass alloys may be determined from far-Infrared spectroscopy.

1.9 Applications

Amorphous chalcogenide glasses have gained a lot of enthusiasm as these prove to be the high-tech materials applicable in optics, chemistry, physics, biology, medicine, electronics, material science, engineering, optoelectronics *etc* (figure 1.8). After being exposed to electromagnetic radiation, these may experience major change in their physical and structural properties. These changes may be reversible or irreversible and used for device fabrication suitable for specific applications [41-45].
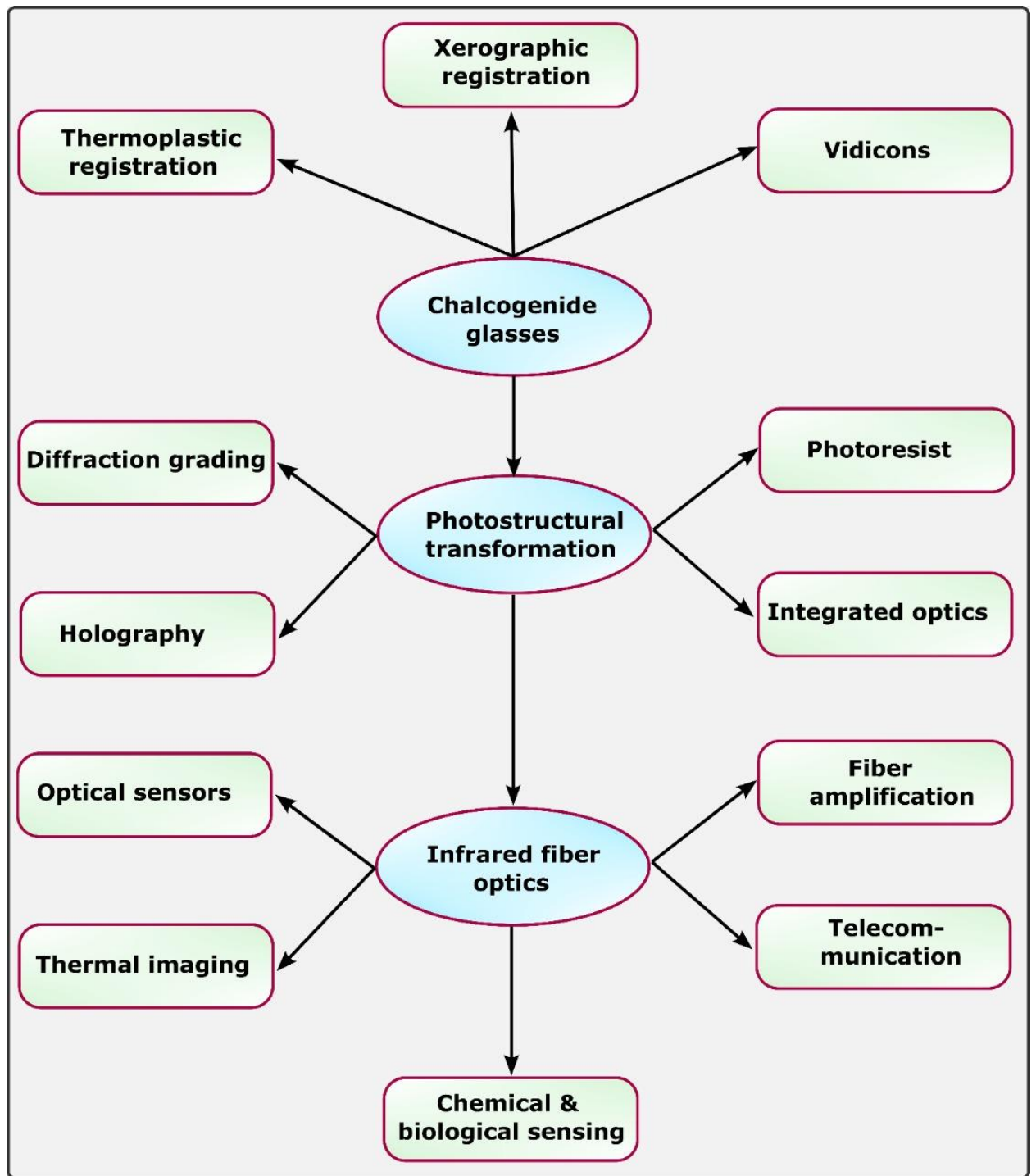
Figure 1.8: Flow chart of applications of chalcogenide glasses in different fields

1.10 Properties of chalcogenide glasses-A Literature Survey

From the literature survey, it has been found that work has been carried out for binary, ternary and quaternary chalcogenide glasses. The varied compound composition shows

very interesting properties, suitable for different optoelectronic applications. In this study, several glasses have been reviewed for their structural, optical, electrical and thermal properties.

1.10.1 Structural properties

The structural properties have been discussed with the help of "FTIR (Fourier Transform Infrared Spectroscopy), XRD (x-ray diffraction) and Raman spectroscopy". The spectra obtained from Raman and Infrared spectroscopy provide information about the bonding arrangement of constituent elements. The geometrical model for the ideal glass was firstly proposed by Zachariasen in 1932 [23]. The lone pairs do not contribute in chemical bonding so they show defects *viz.* dangling bonds, vacancy and non-bridging atoms. The presences of defects give rise to energy levels in the bandgap and also some peaks in density state distribution.

Rajneesh Kumar *et al.* [46] reported the impact of the addition of Tin (Sn) on the bonding arrangement of Se-Te alloys by "far-infrared transmission spectroscopy". Far-IR spectra shifted towards the higher frequency side with the appearance of new bands. It could be because of the absorption coefficient or light scattering caused by increasing defect centres with the Sn

concentration.

Neha Sharma *et al.* [47] investigated the bulk samples of Ge-Se-Sb-Te chalcogenide glasses by using far-IR spectroscopy in the range of $30cm^{-1}$-$350cm^{-1}$. The far-infrared analysis outcomes were also used to discuss the reduction in the optical bandgap of the prepared compositions. In comparison to other bonds, the bond energy of Te-Te and Ge-Te bonds is low. Because of the low bond energy, the overall energy of the system reduces, resulting in a decline in the "optical band gap".

The structural changes of metals and metal halides modified GeTe$_4$ glasses were studied using Raman spectroscopy [48]. The spectra of glasses were obtained in the range of 100 cm^{-1} – 300 cm^{-1} displayed four bands at $124cm^{-1}$ contributed by Ge-Te, 140 cm^{-1} & 159 cm^{-1} for Te-Te and 275 cm^{-1} for Ge-Ge vibrations. However, relative intensities of 140 cm^{-1} and 124 cm^{-1} bands are insensitive to composition changes. It should be noted that Ga and Ge are periodic table neighbours with similar size and electronegativity.

Yuju He *et al*. [49] revealed the consequence of doping of Al and AlCl$_3$ on the optical properties of Ge-Te-Ga "far-IR" transmitting glasses. The IR transmitting and thermal

stability properties were analyzed by "differential scanning calorimetry (DSC) and Fourier transform infrared spectroscopy (FTIR)". The inclusion of Al may successfully remove the impurities in Ge–Te–Ga because Al can grab the oxygen from the raw elements Ge, Te, and Ga. Thus it reduces possibility of combing oxygen combining with the metals Te, Ga and Ge.

M. Fabian *et al.* [50] studied the atomic structure of $Ge_xSb_{40-x}Se_{60}$ chalcogenide glasses by different characterizations like x-ray diffraction (XRD), neutron diffraction (ND) and far FTIR ($450cm^{-1}$ – $50cm^{-1}$) reflectance spectroscopy. With the increment in Sb content in the $Ge_xSb_{40-x}Se_{60}$ well-defined Sb-pyramidal units were formed. It may be attributed that the glassy network exhibits distinctive bands associated with Ge-Se and Sb-Se chemical bond vibration in $SbSe_3$ pyramidal and $GeSe_4$ tetrahedral units.

Baudet *et al.* [51] reported the structural analysis by Raman and XPS spectroscopy of RF sputtered $(GeSe_2)_{100-x}$ $(Sb_2Se_3)_x$ thin films. The wide band corresponds to vibration mode of corner linked $[GeSe_{4/2}]$ tetrahedra ($\sim200cm^{-1}$) and $[GeSe_{4/2}]$ tetrahedra connected by edges ($\sim215cm^{-1}$).

S. Ahmadpour *et al.* [52] reported the FTIR spectra of $Sn_x(Se_{0.6}As_{0.1}Ge_{0.3})_{100-x}$ (x=0 to 6 at. %) chalcogenide glasses in the range of 2.5µm -13.5µm. The increment of Sn concentration enhances the system connectivity. The FTIR spectra also verified the existence of distinct impurities. The inclusion of Sn (up to 3%) the IR transmittance declines because it works as modifier. However, addition of Sn (at 6%) shows inverse results. Thus for sn (at 6%), it acts as networker in the composition.

M. Ghayeblooa *et al.* [53] studied the impact of CsI on the $(Se_{40}S_{20}Ge_{20}Sb_5As_{15})_{1-x}$ chalcogenide glassy system synthesized by conventional "melt quenching" method. The absorption peak of Se-O-H, S-H, H_2O, Ge-O, and Ge-O, located at 2.85 µm, 4 µm, 6.26 µm, 7.9 µm, and 12.5 µm corresponds to oxides and hydrides impurities. With the increment of CsI percentage to the glass composition, the infrared transmission decrease. It follows the same trend as the "glass transition temperature". It could be due to the reduction in connectivity of the glassy network with CsI addition.

1.10.2 Physical properties

Ishu Sharma *et al.* [54] studied the compositional dependent and topology of physical parameters of $Ge_{18}Se_{72-x}Te_{10}Bi_x$ (x= 0 to 10 at. %) glassy alloys. The physical parameters like "mean coordination number (<r>), the number of constraints, density (ρ), lone pair

electrons (L), mean bond energy (<E>), cohesive energy (CE)" and other parameters are estimated. The value of <r> increased by the enhancement of Bi in the system. Using <r> values, lone pair electrons" had been estimated. By adding Bi content, the value of L decreases which may be attributed to the interaction of lone pair bridging Se atoms and Bi ions

J. Sharma *et al.* [55] revealed the influence of Ge addition on the physical and dielectric properties of $Se_{75}Te_{25}$ and $Se_{85}Te_{15}$ chalcogenide system. The physical parameters like "mean coordination number, counts of constraints, and average heat of atomization" enhances. However, "electronegativity, lone pair electrons, a fraction of floppy modes and stoichiometry (R)" parameters decrease with the increase of Ge concentration. This is due to addition of four fold Ge as compared to other two (have two-fold coordination)

Ishu Sharma *et al.* [56] investigated the optical and physical characteristics of $Ge_{20}Te_{80-x}Sb_x$ (x=0 to 10 at. %) amorphous bulk and thin films. The values of the physical parameter <r> were utilized to estimate the value of L. With the increment of Sb, L values decreases. The density was calculated theoretically and experimentally. With the increase of Sb content; the ρ values increased attributed to the increase of refraction index values. Firstly, Te (two fold) chains cross linked with Ge (four fold) then by three-fold Sb. The rise in Sb in the system leads to increase in <r> values.

K.A Aly *et al.* [57] reported the investigation of topological and compositional dependence of $Cu_{2x}Ge_{30-x}S_{70-x}$ (0 to 5 at. %) glassy alloys. With the rise in Cu content, the value of <r> increased from 2.6 to 2.7. It may be due to the four-fold coordination of Cu. The compactness and density values are also enhanced, whereas molar volume values reduced. With the incorporation of Cu content, the "average heat of atomization and mean bond strength" depict a similar trend. It was noted that the optical gap reduced from 2.75eV to 2.28eV with the rise in Cu concentration due to reduction in S-S bonds.

L. Heireche *et al.* [58] investigated the physical properties of the $Se_{90-x}Zn_{10}Sb_x$ (x=0 to 6 at. %) glassy system. The values of the "average coordination number" rises from 2 to 2.06 with the antimony concentration. The number of constraints and fraction of zero frequency modes were also determined. The values of <r> were utilized to determine the lone pair electrons. The increase response is because of inclusion of adition of three fold coordinated Sb in place of two fold coordinated Se. T_g values decreases with Sb content which may be due to the reduction in mean bond strength. The R parameter was utilized to evaluate mean bond <E> and T_g.

Ahmed Saeed Hassanien *et al.* [59] reported the physical and optical properties of amorphous $Cu_xGe_{20-x}Se_{40}Te_{40}$ (x= 0.5 to 20 at. %) glassy system. The values of density and packing density increase with the rise of Cu concentration. It may be due to replacement of Ge (ρ_{Ge}=5.32g/cm^{-3}) with Cu (ρ_{Cu} = 8.92g/cm^{-3}). The values of CE increased from 1.099eV to 3.184eV, whereas counts of constraints (N_c) reduced from 3.2 to 4.4.

H. I. EI Saeedy *et al.* [60] investigated the physical properties of the $Cu_x(Ge_{30}Se_{70})_{100-x}$ glassy system. The physical parameters such as <r>, molar volume (V_m), ρ, compactness and CE were determined for the system. The "average coordination number" increases from 2.6 to 2.77. is ascribed to the addition of four-fold Cu atoms. The value of V_m reduces while the compactness and density values increase with the increase of Cu concentration. "The heat of atomization (H_s) and mean bond strength" showed a similar trend with the enhancement of Cu concentration. The increase of H_s with Cu addition is due to its higher value of H_{Cu} (81.1kcal/mol) as compared to others.

Imen Kebaili *et al.* [61] studied the physical properties and bandgap tuning of ternary $Sn_x(GeSe_2)_{100-x}$(x= 0 to 24 at. %). The influence of Sn on the physical parameters such as <r>, ρ, V_m, the heat of atomization and degree of ionicity has been studied. Using CBA, the values of cohesive energy were determined. With the enhancement of Sn content, the molar volume and density increased which is related to enhance cross linkage due to four-fold coordination of Sn in the material.

J. Kang *et al.* [62] studied the effect of Sn on physical, electrical and structural characteristics of $(Ge_{20}Se_{80})_{90-x}Sb_{10}Sn_x$ (x= 2 to 10 at. %) glassy system. The various physical parameters *viz* "<r>, number of constraints, L, stoichiometry parameter, electronegativity, T_g and mean bond energy" *etc*. were estimated. The increase in <E> may be due to higher bond energy of Se-Sn bond as compared to homopolar Se-Se bonds. With the enhancement of Sn, the <r> increased from 2.492 to 2.620, and the number of constraints increased from 3.23 to 3.55 respectively. Lone pair electrons were estimated from the mean coordination number and which reduces with Sn content. This is ascribed to the interaction of Sn ions with bridging Se atoms.

1.10.3 Optical Properties

When a beam of light interacts with the material, it can be partially transmitted, absorbed or reflected. Several researchers have reported the optical properties; *viz* "refractive index (*n*), extinction coefficient (*k*), optical bandgap (E_g^{opt}) and absorption coefficient (α)" for

various chalcogenide glasses.

Rittwick Mondal *et al.* [63] investigated the influence of sulphur concentration on the optical, and dielectric behaviour of xS-(1-x)(0.65Se-0.35Te) chalcogenide glassy alloys prepared from the "melt quenched" technique. By adding S amount in the system the "optical band gap (E_g^{opt})" had been found to increase and may be due to decrease in unsaturated defects which lead to increase of E_g^{opt} values. The reduction in electric polarizability corresponds to the decrease in n values of the material. With the addition of S amount in the system, the non-linear parameters like third-order non-linear susceptibility and non-linear refractive index were found to decline.

M. Rashad *et al.* [64] revealed the influence of different dopant on the optical constants for melt quenched $(Se_{90}Te_{10})_{95}M$ (M=Bi and Zn) system. The films were prepared by an evaporation process of thickness 100 nm on cleaned glass substrates. The optical band gap increases for Zn system due to decrement in defect states. However, it declines (1.28eV) for the Bi-doped system due to enhancement of localized states with Bi addition in system as compared to the pure $S_{90}Te_{10}$ system (1.85eV).

M.M. Soraya [65] investigated the optical and structural characteristics of the rapid melt quenched $Se_{85-x}Te_{15}In_x$ (x=0 to 10 at. %) amorphous system. The "refractive index" and thickness of the film were estimated by the Swanepoel method. By the incorporation of In content, the values of n and dielectric constant (ε) increases. The rise in value of n can be related to higher polarizability of In atoms (r = 2Å) compared to Se atoms (r = 1.22Å). For the non-direct transition, the "optical band gap" had been obtained from the Tauc method and the values of bandgap reduced (1.69 to 1.51) with the enhancement of In content. The decrease in E_g^{opt} was discussed according to CBA and electronegativity difference of constituent elements.

Ishu Sharma *et al.* [66] reported the optical and physical properties of $Pb_{10}Se_{90-x}Ge_x$ (x=0 to 10 at. %) chalcogenide glassy system. The bulk samples and thin films were prepared by traditional melt quenched and "thermal evaporation" techniques. E_g^{opt} was obtained by the "Tauc method". With the addition of Ge concentration, the values of optical band gap reduced from 1.6eV to 1.53 eV. Inclusion of Ge, rises the absorbance and creates the defects in the system. Further, it leads to widening of localized states and decrease in E_g^{opt} substantially.

Palwinder *et al.* [67] investigated the optical bandgap tuning of Ag added $Ge_2Sb_2Te_5$ thermally evaporated thin films. The transmission spectra of the prepared thin films were analyzed in the near-IR range (500nm-3300nm) at 300K. E_g^{opt} increases up to the addition of 3% Ag content. However, further addition of higher content of Ag, E_g^{opt} decreases. This behaviour is linked to decrement of density of states with Ag addition.

The optical properties of $Se_{86-x}Te_{10}Sb_4Bi_x$ quaternary thin films were studied by H. Nyakotyo et al. [68]. The transmission spectra of thin films had been obtained in the UV-Vis-NIR region (500-2500nm). By the enhancement of Bi in the material, the transmission increases while E_g^{opt} decreases. This decrease was interpreted based on the chemical bond approach. Additionally, reduction in E_g^{opt} values may be due to rise in defects states with Bi addition.

R. Raj *et al.* [69] investigated the optical and structural properties of thermal evaporated $(GeS_2)_{100-x}(Sb_2S_3)_x$ thin films. The values of the E_g^{opt} were reduced from 2.40eV to 2.34eV. With the enhancement of doping concentration, the values of "absorption coefficient, extinction coefficient, refractive index and Urbach energy" increases. The decrease in E_g^{opt} with Sb content was discussed according to Mott Davis model. Also increase of Sb concentration leads the formation of more defect states causes reduction in E_g^{opt}.

S. S. Fouad *et al.* [70] revealed the optical and physical properties of $Ge_{10}Se_{90-x}Te_x$ thin films. With the rise in Te concentration the joint density of states enhances while the bandgap of the film decreases. The increase in linear, non-linear refractive index, electronic polarizability and the third-order susceptibility has been observed with the increment of Te concentration in the Ge-Se system. This response has been explained by alloy effect. Moreover, these changes may be caused by variation in bond length and angles in the system. Further, the red shift in E_g^{opt} has also been explained by increasing the degree of disorder and density of states with Te addition.

E. R. Shaaban *et al.* [71] revealed the heating effect on the optical properties of the amorphous $As_{40}Se_{45}Se_{15}$ chalcogenide thin films. The bandgap was calculated by the Tauc method, which exhibits indirect allowed transition for the as-prepared and annealed samples. Moreover, with the increase of annealing temperature an increase crystallite size

for system was also observed. The reduction in E_g^{opt} may be ascribed to the quantum confinement phenomenon.

K. A. Aly *et al.* [72] investigated the optical properties of amorphous $As_{20}Se_{80-x}S_x$ films by using the transmission spectra. With the rise of the Sulphur concentration, the optical band gap increases however, the refractive index reduces. This reduction in E_g^{opt} may be due to widening of localized states and increase of defect states with S addition.

 D. C. Sati *et al.* [73] studied the role of substrate temperature (303K, 363K, 423K) on the non-linear optical properties of $Ge_{10}Se_{90-x}Te_x$ (x = 0 at. % to 50 at. %) thin films. The nonlinear "refractive index" enhances with Te and with the increase of substrate temperature. The best composition, $Ge_{10}Se_{40}Te_{50,}$ exhibits large non-linearity suitable material for high-speed communication, optical switching and IR optics.

Some recent literature data for the estimation of an optical constant by any means like transmission or reflection is described in the table 1.2.

Table 1.2: Literature review for optical properties of chalcogenide glasses

S. No	Composition	Type of study	Optical band gap	References
1.	$Ge_{0.17}Se_{0.83-x}Sb_x$	Transmittance & Reflectance	1.92 eV to 1.63 eV	[74]
2.	$Ge_xSb_{40-x}Se_{60}$	Transmittance & Reflectance	1.5 eV to 2.01 eV	[75]
3.	$(Se_{80}Te_{20})_{100-x}Zn_x$	Transmittance	1.28 eV to 1.33 eV	[76]
4.	$Ge_{15-x}Sb_xSe_{50}Te_{35}$	Transmittance & Reflectance	1.047 eV to 0.864 eV	[77]
5.	$Ge_xSe_{35-x}Te_{65}$	Transmittance	1.56 eV to 1.82 eV	[78]
6.	$Se_{40-x}Te_{60}Ag_x$	Transmittance	1.36 eV to 1.41 eV	[79]
7.	$(Ge_{11.5}Se_{67.5}Te_{12.5})_{100-x})Sb_x$	Transmittance	1.34 eV to 1.41 eV	[80]
8.	$Ge_{10}Se_{90-x}Te_x$	Transmittance	1.90 eV to 1.61 eV	[81]
9.	$Ge_{20}Sn_{10}Se_{70-x}Te_x$	Transmittance	1.57 eV to 1.35 eV	[82]
10.	$Se_{80-x}Te_{20}Sb_x$	Transmittance	1.35 eV to 0.80 eV	[83]

1.10.4 Thermal Properties

The thermal property provides the information of various reactions that take place with the variation in temperature. In recent era, "Differential scanning calorimeter (DSC) and differential thermal analysis (DTA)" are used to analyze the "glass transition temperature, crystallization temperature, activation energies" and other related parameters.

Glass is made from the corresponding melt so it naturally exhibits T_g. It is well understood that glass becomes viscous when it is heated, the glass rod is heated. Due to the slow softening, glasses may be deformed to random shapes by moulding, stretching and blowing *etc*. The "glass transition temperature T_g" may be described as the transforming temperature between the glassy and viscous supercooled liquid states.

If the cooling of the liquid is performed slowly, then it endures crystallization at melting temperature (T_m). This crystal to liquid transformation happened under the thermal equilibrium. On the other hand, if the liquid is cooled fastly, then it can diverge from the thermal equilibrium and become supercooled, not depicting any signature at T_m. Here "rapidly" means the time interval between 10^{-5} sec and 1day, depending upon the material. The time at which disordered material cannot get sufficient time to relax and become an ordered structure due to viscosity. In many disordered materials, thermal crystallization occurs when heated. The crystallization process takes place when amorphous material is subjected to pressure. The remarkable difference between the glass transition and glass crystallization is; glass crystallization appears exothermic while the transition is endothermic [84]. Crystallization is a form of structural relaxation that occurs when there is a transition from disorder to order. The crystals cannot directly transform to glasses, while the transformation between the glass and supercooled liquid can be reversible [85].

A. Kumar *et al.* [86] reported the calorimetric measurement of quaternary $Se_{78-x}Te_{20}Sn_2Cd_x$(x=0 to 6) to investigate the glass transition and crystallization kinetics of the samples. Increase in T_g may be linked to reduction in Se rings with decrease of Se concentration.

S. K. Pal *et al.* [87] reported the structural and thermal analysis of multicomponent Se-Te-Sn-Ge phase change materials (PCMs). The various kinetics parameters of the chalcogens rich non-oxide $Se_{78-y}Ge_yTe_{20}Sn_2$ (y = 0 to 6) were studied by DSC method in the non-

isothermal method. With the addition of Ge, the long polymeric chains are linked by four fold Ge in the system. It is composed of Se_8 rings and long polymeric chain.

Roman Svoboda *et al*. [88] investigated the crystallization kinetics of $(GeTe_4)_x(GaTe_3)_{100-x}$ glass for far-infrared optics by "differential scanning calorimetry (DSC), XRD, IR spectroscopy and Raman spectroscopy". The complex crystallization data comprises two primary overlapping peaks: one relates to the production of rhombohedral GeTe and Ga_2Te_5 phases, while the other corresponds to the precipitation of "hexagonal tellurium and formation of hexagonal Ga_2Te_5 phase".

P. Petkov *et al*. [89] investigated the thermal behaviour of $(GeTe_4)_{1-x}Ga_x$ and $(GeTe_5)_{1-x}Ga_x$ (x = 0 to 15 at. %) bulk chalcogenide glassy alloys by using DSC. The addition of Ga content affects the "T_g, crystallization temperature (T_c), melting temperature (T_m) and crystallization peak temperature". With the addition of Ga, a new stable phase $GaTe_3$ appeared. Moreover, another phase Ga_2Te_5 appeared along with $GaTe_3$ when the Ga content was about 20 mol%. The ternary phases were absent in all thermally treated samples. The thermal experiment also predicts the presence of $GaTe_4$ and $GaTe_5$ are composed of crystalline phases along with amorphous phases.

M. I. Abd- Elrahman *et al*. [90] investigated the thermal properties of $(Se_{90}Te_{10})_{100-x}In_x$ melt quenched chalcogenide alloys. The DSC had been adopted with different heating rates to investigate the T_g and fragility dynamics (< m >). With the increasing In concentration in the system, the increase in T_g was observed. By increasing temperature, the decrement in E_g is observed which is linked with the amount of free volume existing in the system. The generation of strong Se–In bonds (227.43 kJ/mol) at the expense of Se–Te bonds (185.04 kJ/mol) often results in an increase in T_g as In increases.

"Differential Scanning Calorimetry (DSC) and Thermomechanical analysis (TMA)" were employed to investigate the Thermo kinetic behaviour of $(GeTe_4)_y(GaTe_3)_{100-y}$ bulk infrared glasses as reported by Roman Svoboda *et al*. [91]. Addition of Ga content into the $GeTe_4$ system results in the production of eutectic near $(GeTe_4)_{67}(GaTe_3)_{33,}$ which is linked to diminishing melting temperature. To begin, adding Ga lowers the T_g by 4 °C while adding 20 mol % of Ga raises the T_g to 161°C.

Brian Jeevan Fernandes [92] reported the effect on crystallization kinetics of $Ge_{20}Te_{80-x}Sn_x$ chalcogenide glassy system with Sn addition. From DSC, the thermal parameters like glass T_g, T_m, onset crystallization (T_o), the activation energy of glass crystallization (E_c) had been evaluated using the Kissinger and Moynihan Models. With the incorporation of Sn, the glass-forming ability of the Ge-Te reduces, resulting in the narrow range of the glass forming region. The increase in T_g value with the addition of Sn to $Ge_{20}Te_{80}$ material can be explained due to semi metallic nature of S_n. Moreover, the introduction of S_n leads to the dominance of metallicity component resulting in decreased amorphous network connectivity and rigidity. Also it results in decrease in T_g value of for $Ge_{20}Te_{80-x}Sn_x$ system.

Vandita Rao *et al.* [93] stated the study of crystallization kinetics of $Se_{82-x}Te_{18}Sb_x$ glassy system prepared by the melt quenching method. With the enhancement of Sb content in Se-Te system and the increase in heating rate, the crystallization temperature increases. The activation energy (E_a) values of glassy system rises with Sb addition. It may be due to structural variation caused by addition of Sb atoms in the system.

Vandita Rao *et al*. [94] revealed the thermo mechanical properties of amorphous $Se_{78-x}Te_{20}Sn_2Sb_x$ (x = 0 to 6) prepared by "melt quenched technique". The bulk samples were characterized by "DSC and XRD techniques" for the phase transformation and structural analysis. The DSC analysis was performed at 10K/min for all the compositions. With the increase of Sb percentage, T_g and hardness behaviour increases. The activation energy of glasses rises with Sb addition. It may be due to structural variation caused by addition of Sb atoms in the system.

Alaa M. Abd- Elnaiem *et al*. [95] reported the thermal kinetics of the Zn_5Se_{95} glassy system by DTA under non-isothermal situations. For the estimation of activation energy of crystalline, Moynihan *et al*. Kissinger's and other approaches have been used. The fragility index of Zn_5Se_{95} glassy system calculated by the activation energy and glass transition values. Tg enhances with heating rate (β) because of increment in structural relaxations. Also it reduces relaxation time with increasing β.

Ningning Yin *et al.* [96] revealed the influence of Te content on thermal characteristics of

$Ge_{25}Sb_{10}Se_{65-x}Te_x$ glass system. The samples were developed by the melt quenching technique. DSC, TMA, FTIR and XPS had been used for the investigations. The values of T_g lie between 551.45 K - 514.56 K and ΔT (T_o-T_g) is greater than 110K. With the increment of Te concentration, the thermal coefficient values change from 1.87×10^{-5} to 1.82×10^{-5}. The chemical bond energy is the most important factor to estimate characteristic temperature. By adding Te, bond energy of Ge-Se (114.9kcal/mol) reduces. However, Ge-Te bond (94.8kcal/mol) increases. Thus, the reduction in average bond energy is obtained and subsequently the values of characteristic temperatures decreased.

The crystallization properties of $(As_{50}Se_{50})_{100-x}Ag_x$ (x=0 to 15) was reported by Mansour Mohamed et al. [97] With the enhancement of Ag concentration, the value of glass transition activation energy (E_a) reduces from 185.19 eV to 179.94 eV. This reduction in E_a may be ascribed to rise in internal energy of the system with Ag content.

1.10.5 Electrical properties

The electric transport properties of the Zn doped SeTe chalcogenide system had been studied in the frequency range 50 Hz-500 kHz under the temperature range 400K-520K by Arun Kumar et al. [98]. The presence of a sharp peak in the XRD pattern revealed the polycrystalline character of the samples. The doping of Zn influenced the dielectric and ac conductivity of the Se-Te-Zn system. The zinc atoms may enter or cross-link into the Se-Te system's chain or ring structure. As zinc concentration increases, zinc atoms behave as network formers instead of network converters.

Mansour Mohamed et al. [99] revealed the electrical properties of $As_{47.5}Se_{47.5}Ag_5$ thin films at distinct thicknesses of 174nm-1383nm. The DC conductivity of the films was studied in the temperature range 300K-588K. The variation in the film thickness strongly affect the optoelectronic properties of the prepared $As_{47.5}Se_{47.5}Ag_5$ thin films. The reduction in electrical conductivity with increasing film thickness might be related to rise in degree of disorder and structural defects in the investigated films. The reduction in activation energy values as film thickness increases is linked to an increase in the disorder of the atomic bonds between neighbours.

Alaa. M. Abd - Elanaiem *et al.* [100] investigated the effect of Ga and annealing temperature on electrical properties of $As_{30}As_{70-x}Ga_x$ melt quenched bulk and thermally evaporated thin films. At the room temperature by addition of 3 at. % of Ga, the electrical conductivity increased from $7.7 \times 10^{-4} \, \Omega^{-1}cm^{-1}$ to $8.04 \times 10^{-3} \, \Omega^{-1}cm^{-1}$. However, it decreased as the Ga content increased (> 3 at.%). Moreover, the changes in activation energy caused by Ga addition act to form newly charged centres in the mobility gap, which modifies the As-Te energy band.

Kristina O. Cajko *et al.* [101] investigated the electrical behaviour of $Ag_x(As_{40}S_{30}Se_{30})_{100-x}$ melt quenched chalcogenide alloys. The DC conductivity measurement was performed over a temperature range of 25 °C to 160°C. The "activation energy" of conduction was determined on the basis of "Arrhenius law" which indicated a semiconductor-like behaviour. The decrease in the activation energy values and increment in the DC conductivity values by inclusion of Ag result from increasing the density of "localized states" in the mobility gap. With the addition of Ag to the As–S–Se system, an increase in DC conductivity observed. This corresponds to a decrease in activation energy. The rise in conductivity with Ag concentration could be due to an increase in the density of "localized states" in the system.

Yaseer B. Saddeek [102] reported the effect of Sn to $(GeSe_2)_{1-x}Sn_x(0 \leq x \leq 0.12at.\%)$ glasses on the electrical and mechanical properties. The temperature dependence of electrical parameters had been analysed in the temperature range from 300K-450K. With the increase of Sn content both the electrical conductivities (ΔE_{dc}) and thermoelectric activation energies (ΔE_{th}) decreased according to "Mott and Davis model". These results corresponded to the enhancement in the "width of localized states" due to the presence of Ge-Ge bonds. Sn is more electropositive "($\chi S_n = 1.88$) than Ge ($\chi_{Ge} = 2.05$) and Se ($\chi_{Se} = 2.55$)". Thus increasing the concentration of electropositive element in the host matrix increases its electrical conductivity.

Pankaj Sharma *et al.* [103] investigated the electrical properties of $Ge_{17}Se_{74}Sb_9$ melt quenched thermally evaporated thin films. The I-V characteristics were analyzed at temperatures from 289K to 348K. The linear nature of the I-V curve indicates that the conduction mechanism was ohmic in nature. With the enhancement in temperature, the

resistivity of thin films decreased implying the semiconducting behaviour of thin films. Moreover, "the activation energy" decreased with the increase of voltage applied across the films. This is owing to the fact that the density of thermally produced charge carriers increases with temperature, which in turn raises the density of charge carriers.

K. A. Aly *et al.* [104] reported the effect of temperature dependence over the range of 300K-450K of $Ge_{20}Se_{80-x}In_x$ chalcogenide thin films. By adding In into the Ge-Se matrix, the conductivity (σ) and Seeback coefficient (S) increased while the "activation energy for electrical conductivity (ΔE) and activation energy for thermoelectric (ΔE$_s$)" decreased. The mobility of $Ge_{20}Se_{80-x}In_x$ thin films with In content increases. It is well known that mobility (μ) is directly proportional conductivity (σ). The inclusion of In results in a decrease in activation energy (ΔE) and as a result, both increase with rising In content.

H.H. Hegazy *et al.* [105] reported the thermoelectric and electrical characteristics of $Ge_{25}Se_{65}Sb_{10-x}Cu_x$ thin films in the temperature range of 300K - 400K. With the enhancement of Ge content, the electric conductivity increased from 2.89×10^{-9} m^{-1} to 6.39×10^{-7} m^{-1}. The positive values of thermoelectric power and negative temperature dependence for all compositions had been found. As the temperature and Cu concentration rises, the values of activation energy decrease. Consequently, the values of free carrier concentration increases. When the temperature rises, the energy of the VB rises, permitting electrons to jump to the CB leaving holes behind. The free electrons and holes improved charge carrier concentration, which increased the conductivity.

The electric conductivity and dielectric investigation of $Ag_{0.5}(As_{40}S_{30}Se_{30})_{99.5}$ glassy system at a different temperature in the frequency range 100Hz to 1MHz had been investigated by Kristina O. Cajko [106]. AC conductivity has a frequency dependency that follows "Jonscher's power Law". However, DC conductivity has an Arrhenius behaviour. The dielectric properties such as "real and imaginary parts of dielectric constants" were reduced with the frequency and enhanced with the temperature. The values of maximum barrier height W_m were determined by the dielectric loss data.

H. Bennaji *et al*. [107] revealed the electric, thermal and dielectric properties of $Sn_3Sb_2S_6$ thin films for solar cell applications. The impedance spectroscopy had been adopted to determine the dielectric and electrical properties of the sample. AC conductivity obeyed

the Jonscher's power Law and DC conductivity followed Arrhenius behaviour. The results indicated that the conduction process was thermally activated and the value of activation energy was found to be 0.813eV.

E. R. Shaaban *et al.* [108] reported the short resistance temperature-dependent, electrical and thermal analysis of $As_{40}Se_{60-x}S_x$ thin films. The films had a thickness of 1000 nm and a heating rate of 5K/min for estimating sheet resistance. The values of the sheet resistance (R_s) decreased abruptly when the temperature increased from 300K to 390K. This is due to the grain growth in the film due to increase in temperature.

R. Neffati *et al.* [109] reported the electric and thermoelectric power for $((SbSn)_xSe_{100-x})$ system. The DC conductivity obeyed Arrhenius response in the temperature range (300-450K). By adding SbSn content, the values of activation energies decreased from 0.87 to 0.74 eV. Some parameters such as concentration, charge carrier, relaxation time and mobility were determined for different investigated samples. It had been observed that with the raising SbSn content causes a drop in activation energy (band gap). The introduction of SbSn generates more cross linking and decreases polymerization of the Se chain. This outcome results in reduction in band gap due to formation of heteropolar bonds. Further, the rise in SbSn and the substitution of Se–Se bonds by Sn–Se and Sb–Se bonds, can be linked to reduction in activation energy values due to overall reduction in the band gap.

References

[1] K.Tanaka & K. Shimakawa., "Amorphous chalcogenide semiconductors and related materials", Springer Science & Business Media, 2011.

[2] N.F. Mott & E.A Davis., "Electronic Processes in Non-Crystalline Materials", 2nd ed. Clarendon, Oxford, 1979.

[3] R. H. Doremus., "Glass Science", 3rd ed. Wiley, New York, NY, 1994.

[4] M. H. Bhat, V. Molinero, E. Soignard, V. C Solomon, V.C. Sastry, S. Yarger, J. L. Angell., "Vitrification of a monatomic metallic liquid", Nature, vol. 448, pp. 787–790, 2007.

[5] J. C. Phillips., "Structural principles of amorphous and glassy semiconductors", J. Non-Cryst. Solids, vol. 35–36, pp. 1157–1165, 1980.

[6] S. R. Elliott., "Physics of Amorphous Materials", 2nd ed. Longman Scientific & Technical, Essex, 1990.

[7] K. Morigaki & C. Ogihara., "Amorphous semiconductors: Structure, optical, and electrical properties", Springer Handbook of Electronic and Photonic Materials, 1-1 Springer, Cham, 2017.

[8] C. Wright, R. A. Hulme, D. 1. Grimley, R. N. Sinclair, S.W. Martin, D. L. Price and F. L. Galeener., "The structure of some simple amorphous network solids revisited", J. Non-Cryst. Solids, vol.129, pp.213, 1991.

[9] S. R. Elliott., "Physics of amorphous materials", Longman Inc., New York, 1983.

[10] R. Zallen., "Physics of Amorphous Solids", John Wiley & Sons, New York, 1983.

[11] M. Popescu., "Non-Crystalline Chalcogenides", Dordrecht: Kluwer Academic 2000.

[12] S. R. Elliott., "Chalcogenide glasses", New York: Materials Science and Technology, 1991.

[13] M. Kastner., "Bonding bands, lone-pair bands, and impurity states in chalcogenide semiconductors", Phys. Rev. Lett, vol. 28, pp. 355, 1972.

[14] F. Ioffe & A. R. Regel., "Progress in Semiconductors", AF Gibson. FA Kroger and RE Burgess (London: Heywood) vol 4, 237 (1960).

[15] S. Cui, R. Chahal, C. Boussard-Pledel, V. Nazabal, J. L. Doualan, J. Troles & B. Bureau., "From selenium-to tellurium-based glass optical fibers for infrared spectroscopies", Molecules, vol. *18, no.* 5, pp. 5373-5388, 2013.

[16] S. Maurugeon, B. Bureau, C. B.Pledel, A. J. Faber, X. H. Zhang, W. Geliesen and J. Lucas., "Te-rich Ge–Te–Se glass for the CO_2 infrared detection at 15 μm", J. Non-Cryst. Solids, vol. 355, pp. 2074–2078, 2009.

[17] N. A. Goryunova and B. T. Kolomiets., "New vitreous semiconductors", Zhurn. Techn. Fiz, vol. 25, pp. 984, 1955.

[18] P. Houizot, C. Boussard-Pledel, A. J. Faber, L. K. Cheng, B. Bureau, P. A. Van Nijnatten., "Infrared single mode chalcogenide glass fiber for space", Opt Exp, vol. 15, pp. 12529-12538, 2007.

[19] A. Leger., "Strategies for remote detection of life DARWIN-IRSI and TPF missions", Adv. Space Res, vol. 25, pp. 2209, 2000.

[20] D. Le Coq, K. Michel, J. Keirsse, C. Boussard-Pledel, G. Fonteneau, B. Bureau, J.-M. Le Quere, O. Sire and J. Lucas., "Infrared glass fibers for in-situ sensing, chemical and biochemical reactions", C R Chim, vol. 5, pp. 907-913, 2002.

[21] G. Lucovsky and T.M. Hayes., "Amorphous Semiconductors", Berlin: Springer Verlag, 1985.

[22] R. Zallen., "The Physics of Amorphous Solids", USA: John Wiley, 1998.

[23] W. H. Zachariasen., "The atomic arrangement in glass", J. Am. Chem. Soc, vol. 54 pp. 3841, 1932.

[24] G. Lucovsky , F. L. Galeener , R. C. Keezer , R. H. Geils and H . A. Six., "Structural interpretation of the infrared and Raman spectra of glasses in the alloy system $Ge_{1-x}S_x$", Phys. Rev. B, vol. 10, pp. 5134, 1974.

[25] P. Tronc, M. Bensoussan, A. Brenac, C. Sebenne., "Optical-Absorption Edge and Raman Scattering in Ge_xSe_{1-x} Glasses", Phys. Rev. B, vol. 8, no. 5947, 1973.

[26]   J. C. Phillips., "Topology of covalent non-crystalline solids: Short-range order In Chalcogenide Alloys", J. Non. Cryst. Solids, vol. 34, pp.153–181, 1979.

[27]   N. F. Mott., "Electrons in disordered structures", Adv. Phys, vol. 16, no. 144, 1967.

[28]   W. E. Spear, P.G. Lecomber and A. J. Snell., "An investigation of the amorphous-silicon barrier and pn junction", Philos. Mag. B, vol. 38, no. 3, pp. 303-317, 1978.

[29]   E. A. Davis and N. F. Mott., "Conduction in non-crystalline systems V. Conductivity, optical absorption and photoconductivity in amorphous semiconductors", Phil. Mag, vol. 22, no. 179, pp. 903-922, 1970.

[30]   R. A. Street and N.F. Mott., "States in the gap in glassy semiconductors", Phys Rev Lett, vol. 35, no. 19, 1293, 1975.

[31]   N. F. Mott , E.A. Davis and R. A Street., "States in the gap and recombination in amorphous semiconductors", Phil Mag, vol. 32, no. 5, pp. 961-996, 1975.

[32]   N. F. Mott, "Conduction in non-crystalline systems: VII. Non-ohmic behaviour and switching", Phil. Mag, vol. 24, no. 190, pp. 911-934, 1971.

[33]   P. W. Anderson., "Model for the electronic structure of amorphous semiconductors", Phys. Rev. Lett, vol. 34, no. 15, pp. 953, 1975.

[34]   K. Kumari, R. Kumar and P. B. Barman., "Tuning of structural, magnetic and optical properties of $NiFe_2O_4$ films by implementing high magnetic fields", Thin Solid Films, vol. 712, pp.138321, 2020.

[35]   J. C. Manificier, J. Gasiot and J. P. Fillard., "A simple method for the determination of the optical constants n, k and the thickness of a weakly absorbing thin film", J. Phys. E: Sci. Instrum, vol. 9, no. 11, pp. 1002, 1976.

[36]   R. Swanepoel., "Determination of the thickness and optical constants of amorphous silicon", J. Phys. E: Sci. Instrum, vol.16, no.12, pp. 1214, 1983.

[37]   R. Swanepoel., "Determination of surface roughness and optical constants of inhomogeneous amorphous silicon films", J. Phys. E: Sci. Instrum, vol. 17, no. 10, pp. 896, 1984.

[38]   P. J. Haines, M. Reading and F. W. Wilburn., "Differential thermal analysis and differential scanning calorimetry", Elsevier Science BV. Handbook of Thermal Analysis and Calorimetry, vol. 1, pp. 279-361, 1998.

[39]   I. M. Hodge I M and A. R. Berens., "Effects of annealing and prior history on enthalpy relaxation in glassy polymers. 2. Mathematical modeling", Macromolecules, vol. 15, no. 3, pp. 762-770, 1982.

[40]   https://chem.libretexts.org/ Bookshelves / Physical and Theoretical Chemistry Textbook Maps / Supplemental Modules (Physical and Theoretical Chemistry) / Spectroscopy / Vibrational Spectroscopy / Infrared Spectroscopy / Infrared Spectroscopy.

[41]   M. Popescu., "Disordered chalcogenide optoelectronic materials: phenomenon and applications," J. Optoelectron. Adv. Mater. vol. 7, pp. 2189-2210, 2005.

[42]   J. S. Sanghera, I. D. Aggarwal., "Active and passive chalcogenide glass optical fibers for IR applications: a review", J. Non. Cryst. Solids, vol. 257, pp. 6–16, 1999.

[43]   M. Frumar, J. Jedelsky, B. Frumarova, T. Wagner, M. Hrdlicka., "Optically and thermally induced changes of structure, linear and non-linear optical properties of chalcogenides thin films", J. Non. Cryst. Solids, vol. 327, pp. 399–404, 2003.

[44]   S. Cui, C. Boussard-Pledel, J. Lucas, B. Bureau., "Te-based glass fiber for far-infrared biochemical sensing up to 16 μm", Opt. Express, pp. 22, 2014.

[45]   M. Alshaaer, K. Issa, A. Qazaq and G. Saffarini., " Effects of magnetite incorporation in a chemically bonded phosphate ceramic", J . Phys. Chem. Solids, vol. 162, pp. 110531, 2022.

[46]   R. Kumar, P. Sharma, S.C Katyal, P. Sharma and V.S Rangra., "A study of Sn addition on bonding arrangement of Se-Te alloys using far infrared transmission spectroscopy", J. Appl. Phys, vol. 110, no. 1, pp. 013505, 2011.

[47]   N. Sharma, S. Sharda, V. Sharma, P. Sharma., "Far-infrared investigation of ternary Ge-Se-Sb and quaternary Ge-Se-Sb-Te chalcogenide glasses", J. Non. Cryst. Solids, vol. 375, pp. 114–118, 2013.

[48]   J. Sun, Q. Nie, X. Wang, S. Dai, X. Zhang, B. Bureau, C. Boussard, C. Conseil and H. Ma., "Structural investigation of Te-based chalcogenide glasses

using Raman spectroscopy", Infrared Phys. Technol, vol. 55, no. 4, pp. 316-319, 2012.

[49]   Y. He, X. Wang, Q. Nie, Y. Xu, G. Wang, T. Xu and S. Dai., " Optical properties of Ge–Te–Ga doping Al and $AlCl_3$ far infrared transmitting chalcogenide glasses", Infrared Phys. Technol, vol. 58, pp.1-4, 2013.

[50]   M. Fabian, N. Dulgheru, K. Antonova, A. Szekeres and M. Gartner., "Investigation of the atomic structure of Ge-Sb-Se chalcogenide glasses", Adv. Condens. Matter Phys, 2018.

[51]   E. Baudet, C. Cardinaud, A. Girard, E. Rinnert, K. Michel, B. Bureau and V. Nazabal., "Structural analysis of RF sputtered Ge-Sb-Se thin films by Raman and X-ray photoelectron spectroscopies", J. Non. Cryst. Solids, vol. 444, pp. 64-72, 2016.

[52]   S. Ahmadpour, M. Rezvani and P. Bavafa., "The effect of Sn on the physical and optical properties of $(Se_{0.6}As_{0.1}Ge_{0.3})_{100-x}Sn_x$ glasses", Spectrochim. Acta A Mol. Biomol. Spectrosc, vol. 205, pp. 258-263, 2018.

[53]   M. Ghayebloo, M. Rezvani and M. Tavoosi., "The effect of CsI on the thermal and optical properties of IR transparent Se-S-Ge-Sb-As chalcogenide glasses", Infrared Phys. Technol, vol. 108, pp. 103352, 2020.

[54]   I. Sharma and A. Z. Khan., "An assessment of topology and compositional dependent physical parameters of Ge-Se-Te-Bi lone pair semiconductors", J. Optoelectron. Adv. Mater, vol. 19, pp. 778-787, 2017.

[55]   J. Sharma and S. Kumar., "Role of Ge incorporation in the physical and dielectric properties of $Se_{75}Te_{25}$ and $Se85Te15$ glassy alloys", Pramana, vol. 86, no. 5, pp. 1107-1118, 2016.

[56]   I. Sharma, P. Kumar and S. K. Tripathi., "Physical and optical properties of bulk and thin films of a–Ge–Sb–Te lone-pair semiconductors", Phase Transitions, vol. 90, no. 7, pp. 653-671, 2017.

[57]   K. A. Aly, A. Dahshan and Y. Saddeek., "Compositional and topological analysis of $Cu_{2x}Ge_{30-x}S_{70-x}$ lone pair semiconductors", Appl. Phys. A, vol. 127, no. 8, pp. 1-7, 2021.

[58]   L. Heireche, M. M. Heireche, M. Belhadji., "The Study of Physical Parameters of SeZnSb Chalcogenide Glasses", Journal of Non-Oxide Glasses, vol. 10, no. 3, pp. 83-90, 2018.

[59]   M. Ahmad, K. A. Aly, A. Dahshan, M. M. Soraya and Y. B. Saddeek., " Study of the physical properties of quaternary Ge–As–Te–Pb thin films for technology applications", Appl. Phys. A, vol. 126, no. 7, pp. 1-6 , 2020.

[60]   H. El Saeedy, H. A. Yakout, K. A. Aly, Y. B. Saddeek, A. Dahshan, H. A. A. Sidek, K. A. Matori, M. H. M. Zaid, and H. M. H. Zakaly., "Synthesis and theoretical characterization of ternary $Cu_x(Ge_{30}Se_{70})_{100-x}$ glasses", Results Phys, vol. 23, pp. 104026, 2021.

[61]   I. Kebaili, I. Boukhris, R. Neffati, S. Znaidia, Y. B. Saddeek, K. A. Aly and A. Dahshan., "Theoretical characterization and band gap tuning of Sn_x $(GeSe_2)100-x$ thin films", Mater. Chem. Phys, vol. 25, pp. 123133, 2020.

[62]   J. Kang, R. K. Kotnala and S. K. Tripathi., "Effect of Sn incorporation on structural, physical and electrical properties of Ge-Se-Sb-Sn thin films", Chalcogenide Lett, vol. 17, no. 12, 2020.

[63]   R. Mondal, D. Biswas, S. Paul, A. S. Das, C. Chakrabarti, D. Roy, S. Bhattacharya, and S. Kabi., "Investigation of microstructural, optical, physical properties and dielectric relaxation process of sulphur incorporated selenium–tellurium ternary glassy systems", Mater. Chem. Phys, vol. 257, pp. 123793, 2021.

[64]   M. Rashad, N. M. Shaalan, AAl Abd-Elmageed, R. Amin, M. M. Hafiz, and A. A. Abu-Sehly., "The effects of different dopant on the optical parameters for selenium tellurium thin films", Optik, vol. 241, pp.166102, 2021.

[65]   M. M. Soraya., "Structural and optical properties of $Se_{85-x}Te_{15}In_x$ chalcogenide thin films for optoelectronics", Appl. Phys. A, vol. 126, no. 8, pp. 1-9, 2020.

[66]   I. Sharma and A. S. Hassanien., "Effect of Ge-addition on physical and optical properties of chalcogenide $Pb_{10}Se_{90-x}Ge_x$ bulk glasses and thin films", J Non Cryst Solids, vol. 548, pp. 120326, 2020.

[67]   P. Singh, R. Kaur, P. Sharma, V. Sharma, M. Mishra, G. Gupta and A. Thakur., "Optical band gap tuning of Ag doped $Ge_2Sb_2Te_5$ thin films., J. Mater. Sci.: Mater. Electron, vol. 28, no. 15, pp.11300-11305, 2017.

[68]   H. Nyakotyo, T. S. Sathiaraj and E. Muchuweni., "Optical properties of electron-beam deposited quaternary $Se_{86-x}Te_{10}Sb_4Bi_x$ ($0 \leq x \leq 8$) chalcogenide alloys", Infrared Phys. Technol, vol. 85, pp. 99-108, 2017.

[69] R. Rajnish, P. Lohia and D. K. Dwivedi., "Investigation of structural and optical properties of $(GeS_2)_{100-x}(Sb_2S_3)_x$ (x = 15, 30, 45, 60) chalcogenide glasses for mid infrared applications" Optik, vol. 218, pp.165041, 2020.

[70] S. S. Fouad, G. A. M. Amin and M. S. El-Bana., "Physical and optical characterizations of $Ge_{10}Se_{90-x}Te_x$ thin films in view of their spectroscopic ellipsometry data", J Non Cryst Solids, vol. 481, pp. 314-320, 2018.

[71] E. R. Shaaban, M. Y. Hassaan, M. G. Moustafa, A. Qasem, G. A. M. Ali, and E. S. Yousef., "Investigation of Structural and Optical Properties of Amorphous-Crystalline Phase Transition of $As_{40}S_{45}Se_{15}$ Thin Films", Acta Phys. Pol. A, vol. 136, no. 3, 2019.

[72] K. A. Aly, H. H. Hegazy, A. Dahshan, S. Shaaban, Y. Saddeek, S. R. Alharbi, A. M. Ali and S. A. Amin., "Study of the optical properties of amorphous As–Se–S thin films", Appl. Phys. A, vol. 124, no. 12, pp.1-8, 2018.

[73] D. C. Sati, S.C. Katyal & P. Sharma., "Role of Composition and Substrate Temperature on Nonlinear Optical Properties of GeSeTe Thin Films in 0.4–2.4μm Wavelength Range", IEEE Trans Electron Devices, vol. 63, no. 2, pp. 698-703, 2015.

[74] P. Sharma, V. S. Rangra, P. Sharma & S. C. Katyal., " Effect of antimony addition on the optical behaviour of germanium selenide thin films", J. Phys. D: Appl. Phys vol. 41, no. 22, pp. 225307, 2008.

[75] A. M. Farid, I. K. El-Zawawi & A. H. Ammar., "Compositional effects on the optical properties of $Ge_xSb_{40-x}Se_{60}$ thin films", Vacuum, vol. 86, no. 9, pp. 1255-1261, 2012.

[76] A. Kumar, V. Singh, P. Sharma & N. Goyal., "Optical properties of $(Se_{80}Te_{20})_{100-x}Zn_x$ ($2 \leq x \leq 6$) amorphous thin films", J Non Cryst Solids, vol. 531, pp. 119848 2020.

[77] A. S. Hassanien & I. Sharma., "Optical properties of quaternary a-$Ge_{15-x}Sb_xSe_{50}Te_{35}$ thermally evaporated thin-films: refractive index dispersion and single oscillator parameters", Optik, vol. 200, pp.163415, 2020.

[78] C. Das, M. G.Mahesha, G. M. Rao, & S. Asokan., "Electrical switching and optical studies on amorphous $Ge_xSe_{35-x}Te_{65}$ thin films", Thin Solid Films, vol. 520, no. 6, 2278-2282, 2012.

[79] S. Singh & S. Kumar., "Investigation of optical constants and optical band gap for amorphous $Se_{40-x}Te_{60}Ag_x$ thin films", Chalcogenide Lett, vol. 14, no. 4, pp. 139-146, 2017.

[80] S. Mishra, P. Lohia, & D. K. Dwivedi., "Structural and optical properties of $(Ge_{11.5}Se_{67.5}Te_{12.5})_{100-x}Sb_x$ ($0 \leq x \leq 30$) chalcogenide glasses: A material for IR devices", Infrared Phys. Technol, vol. 100, pp. 109-116, 2019.

[81] K. A. Aly., "Optical properties of Ge–Se–Te wedge-shaped films by using only transmission spectra", J Non Cryst Solids, vol. 355, no. 28-30, pp. 1489-1495, 2009.

[82] S. Sharma, N. Sharma, & A. Sarin., "Influence of compositional variations on optoelectrical properties of $Ge_{20}Sn_{10}Se_{70-x}Te_x$ glass system", Opt. Eng, vol. 57, no. 11, pp. 117110F, 2018.

[83] H. Singh., "Structural and optical study of nanostructured $Se_{80-x}Te_{20}Sb_x$ ($0 \leq x \leq 12$) thin films", Nano-Struct. Nano-Objects, vol. 10, pp. 192-197, 2017.

[84] R. H. Doremus., Glass Science 2nd ed. Wiley, New York, NY, 1994.

[85] Al-Agel, F. A., E. A. Al-Arfaj, F. M. Al-Marzouki, Shamshad A. Khan, and A. A. Al-Ghamdi., "Study of phase separation in $Ga_{25}Se_{75-x}Te_x$ chalcogenide thin films", Prog. Nat. Sci, vol. 23, no. 2, pp. 139-144, 2013.

[86] A. Kumar & N. Mehta., "Studies of dielectric relaxation and thermally activated ac conduction in Se_{78-x} $Te_{20}Sn_2Cd_x$ ($0 \leq x \leq 6$) chalcogenide glass", J. Mater. Sci.: Mater. Electron, vol. 28, no. 7, pp. 5634-5644, 2017.

[87] S. K. Pal, N. Chandel, & N. Mehta., "Synthesis and thermal characterization of novel phase change materials (PCMs) of the Se–Te–Sn–Ge (STSG) multi-component system: calorimetric studies of the glass / crystal phase transition, *Dalton Trans, vol. 48*, no. 14, pp. 4719-4729, 2019.

[88] R. Svoboda and D. Brandova., "Crystallization behavior of $(GeTe_4)_x(GaTe_3)_{100-x}$ glasses for far-infrared optics applications", J. Alloys Compd, vol. 770, pp. 564-571, 2019.

[89] P. Petkov, V. Ilcheva, T. Petkova, and P. Ilchev., "Thermal Studies of Ge-Te-Ga Glasses", AIP Conf. Proc, vol. 1203, no. 1, pp. 932-937, 2010.

[90] Abd - Elrahman, M. I., M. Sayed, A. Abu El-Fadl, A. A. Abu-Sehly, and M. M. Hafiz., "The activation energies at glass transition temperatures and dynamic

fragility of $(Se_{90}Te_{10})_{100-x} In_x$ glassy alloys", Thermochim. Acta, vol. 672, pp. 86-92, 2019.

[91]   R. Svoboda, D. Brandova, M. Chromcikova, & M. Liska., "Thermokinetic behavior of Ga-doped $GeTe_4$ glasses", J Non Cryst Solids, vol. 512, pp. 7-14, 2019.

[92]   B. J. Fernandes, N. Naresh, K. Ramesh, K. Sridharan, and N. K. Udayashankar., "Crystallization kinetics of Sn doped $Ge_{20}Te_{80-x}Sn_x$ $(0 \leq x \leq 4)$ chalcogenide glassy alloys", J. Alloys Compd, vol. 721, pp. 674-682, 2017.

[93]   V. Rao, N. Mehta, & D. K Dwivedi., "Investigations of crystallization kinetics of $Se_{82-x}Te_{18}Sb_x$ (x = 0, 4, 8, 12) glassy alloys by iso-conversional approach", Mater. Res. Innov, vol. 23, no. 3, pp.141-148, 2019.

[94]   V. Rao, N. Mehta, A. Kumar, & D. K. Dwivedi., "Effect of Sb incorporation on thermo-mechanical properties of amorphous Se-Te-Sn alloys", Mater. Res. Express, vol. 5, no. 6, pp. 065206, 2018.

[95]   A. M. Abd-Elnaiem & G. Abbady., "A thermal analysis study of melt-quenched Zn_5Se_{95} chalcogenide glass", J. Alloys Compd, vol. 818, pp. 152880, 2020.

[96]   N. Yin, J. Xu, F. E .Chang, Z. Jian, & C. Gao., "Effect of Te proportion on the properties of $Ge_{25}Sb_{10}Se_{65-x}Te_x$ chalcogenide glasses", Infrared Phys. Technol, vol. 96, pp. 361-365, 2019.

[97]   M. Mohamed & S. Moustafa., "Morphology, structure and thermal analysis of $(As_{50}Se_{50})_{100-x}Ag_x$ glasses., Appl. Phys. A: Mater. Sci. Process, vol. 126, no. 4, pp. 1-12, 2020.

[98]   A. Kumar, V. Singh, H. Singh, P. Sharma & N. Goyal., "Electronic transport properties of $(Se_{80}Te_{20})_{100-x}Zn_x$ $(2 \leq x \leq 6)$ chalcogenide alloys", Phys. B: Condens. Matter, vol. 555, pp. 41-46, 2019.

[99]   M. Mohamed, E.R. Shaaban, M. N. Abd-el Salam, A. Y. Abdel-Latief, S. A. Mahmoud & M. A. Abdel-Rahim., "Investigation of the optical and electrical parameters of $As_{47.5}Se_{47.5}Ag_5$ thin films with different thicknesses for optoelectronic applications", Optik, vol. 178, pp. 1302-1312, 2019.

[100] Abd-Elnaiem, Alaa M., M. A. Abdel-Rahim, and S. Moustafa., "Comparative investigation of electronic properties of As-70 at.% Te thin films:

Influence of Ga doping and annealing temperature", J. Non. Cryst. Solids, vol. 540, pp. 120062, 2020.

[101]   K. O. Cajko, D. L. Sekulic, S. Lukic-Petrovic, M. V. Siljegovic, & D. M, Petrovic., "Temperature-dependent electrical properties and impedance response of amorphous $Ag_x(As_{40}S_{30}Se_{30})_{100-x}$ chalcogenide glasses", J. Mater. Sci.: Mater. Electron, vol. 28, no. 1, pp.120-128, 2017.

[102]   Y. B. Saddeek, K. A. Aly, T. Alharbi, A. Dahshan, S. A. Issa, M. Ahmad & M. M. Soraya., "Mechanical and electrical parameters of a-Ge-Se-Sn glasses", Phys. B: Condens. Matter, vol. 583, pp. 412059, 2020.

[103]   P. Sharma & V. Sharma., "Temperature Dependent Electrical Study of $Ge_{17}Se_{74}Sb_9$ Thin Film", Int. J. New. Hor. Phys, vol. 2, no. 1, pp. 21-24, 2015.

[104]   K. A. Aly, A. Dahshan, Gh Abbady, and Y. Saddeek., "Electrical and thermoelectric properties of different compositions of Ge–Se–In thin films", Phys. B: Condens. Matter, vol. 497, pp. 1-5, 2016.

[105]   H. H. Hegazy., "Semiconducting chalcogenide Ge-Se-Sb-Cu as new prospective thermoelectric materials", Results Phys, vol. 14, pp. 102492, 2019.

[106]   K. O. Cajko, D. L. Sekulic, D. M. Petrovic, N. Celic, V. Labas, M. Kubliha & S. Lukic-Petrovic., " Behavior of Electrical Conductivity and Dielectric Study of Chalcogenide $Ag_{0.5}(As_{40}S_{30}Se_{30})_{99.5}$ Glass", J. Electron. Mater, vol. 48, no.10, pp. 6512-6520, 2019.

[107]   N. Bennaji, Y. Fadhli, I. Mellouki, R . Lahouli, M. Kanzari, N. Yacoubi, & K. Khirouni. Thermal., "Electrical and Dielectric Characteristics of SnSbS Thin Films for Solar Cell Applications", J. Electron. Mater, vol. 49, no. 2, pp. 1354-1361, 2020.

[108]   E. R. Shaaban, M.Y Hassaan, M. G. Moustafa & A. Qasem., "Sheet resistance – temperature dependence, thermal and electrical analysis of $As_{40}S_{60-x}Se_x$ thin films", Appl. Phys. A: Mater. Sci. Process, vol. 126, no. 1, pp. 1-10, 2020.

[109]   R. Neffati, K. Aly, & A. Dahshan., "Electric and thermoelectric properties of $(SbSn)_xSe_{100-x}$ chalcogenide glasses", Appl. Phys. A: Mater. Sci. Process, vol. 127, no. 8, pp. 1-8, 2021.

Experimental details

2. Experimental details

This chapter comprises of methods used to prepare amorphous chalcogenide glasses in powder as well as in thin film form. Also it includes various characterization techniques used to study different properties.

2.1 Bulk glass synthesis

There exist a dozen of different techniques used for the preparation of non-crystalline semiconducting materials. Out of these techniques melt quenching is the conventional used approach for the bulk sample preparation. The glasses produced by melt quenching approaches are more than 99% of the practical glasses. This technique is flexible as no stoichiometry is required among the composition. The flexibility in the variation of the composition is the most important feature of this technique as compared to other techniques. For example, for the production of glasses with unique properties, the doping of the transition metal or rare earth elements at a few percent or very less is possible. As chalcogen elements have a high vapour pressure, the melting of these materials has a high viscosity and is susceptible to hydrolysis and oxidation. Quenching can be done by liquid nitrogen, dry ice-alcohol and ice water. It is necessary for the proper glass formation that the cooling rate must be fastened to avoid crystallization, nucleation, and growth. Fischer and Krebs [1,2] discussed the following facts for the synthesis of chalcogenide materials.

1) The frequent agitation of melt is required for the homogeneity of the melt.

2) The step heating of temperature should be preferred as the vapour pressure of chalcogens Se and Te increases quickly at higher temperature.

3) It is well known that chalcogens are prone to oxidation, so ampoules should be sealed at high vacuum. The heating rate should depend upon the vapour pressure and melting point of the constituent elements. The heating rate should be slow *i.e.* $3 - 4^{o}C/min$. At higher heating rates, the vapour pressure of the chalcogens increases quickly and it may break the ampoule. To surmount these problems, conventional melt quenching technique was utilized for the preparation of $Ge_{10}Te_{80}Se_{10-z}Ga_z(z = 0$ to $10)$ bulk glassy system. During higher temperature the chalcogenide glasses are reactive with oxygen, so melting is preferred in

the cleaned quartz ampoules. The ampoules are precleaned by reducing the oxide and hydroxide impurities which may affect the transmission window of glass. The cleaning process of quartz tubes was performed with Chromic acid, ethanol, distilled water and dried in a oven at temperature 100°C. The material of 5N purity of Ge, Te, Se and Ga was weighed according to their weight % with the single pan balance. The weighed materials was placed into quartz ampoules and sealed under the vacuum of 10^{-4} pa. Figures 2.1 (a & b) represent the sealing unit and the sealed ampoules. After that, the sealed ampoules were put into the muffle furnace at a temperature of 1000°C. The temperature of furnace is increased in the step heating of 3°C/min. The maximum temperature of the furnace is kept constant for atleast 12 hours for the homogeneity of the melt [3]. The flow diagram of melt quenching process is depicted in figure 2.2.
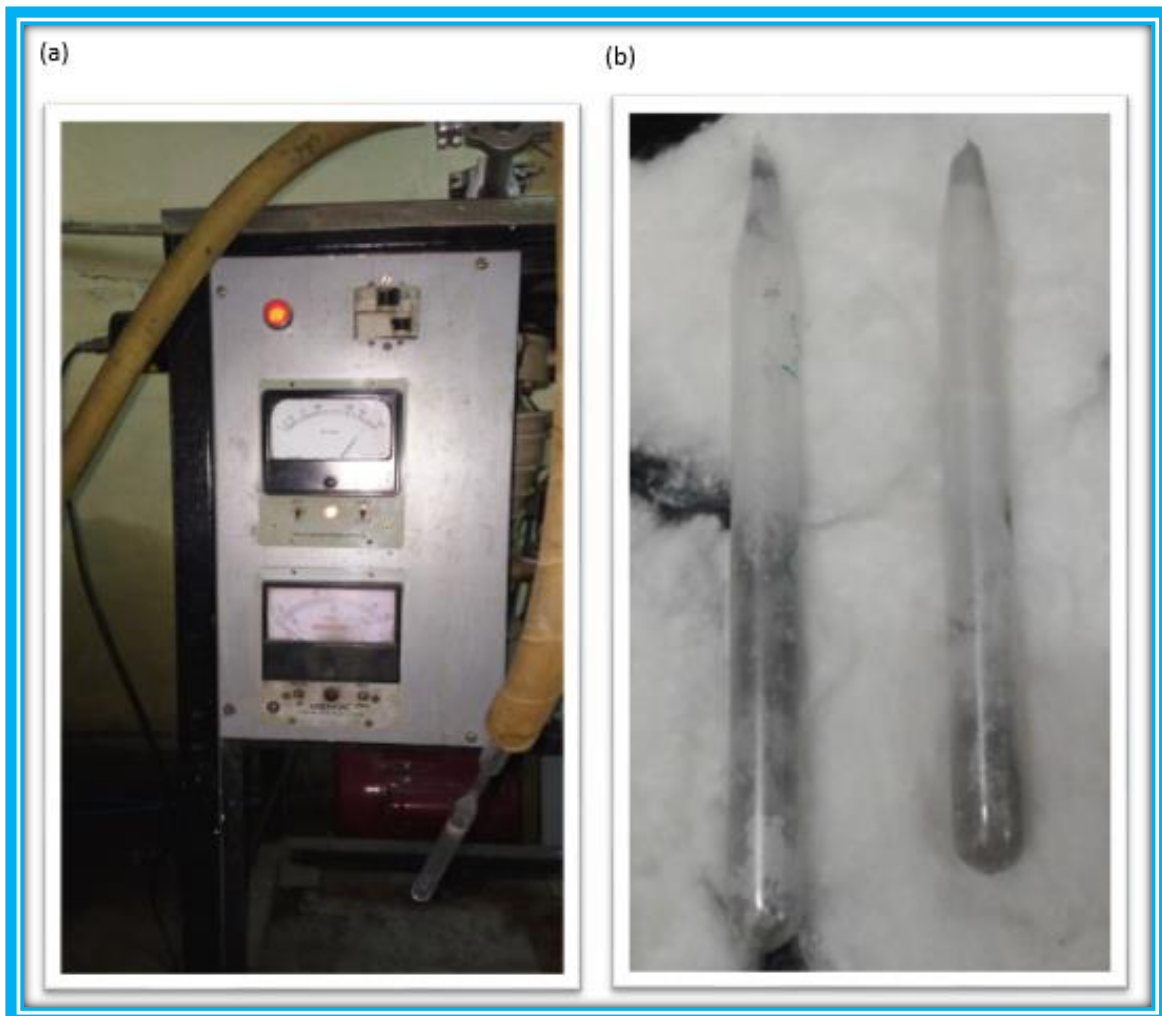
Figure 2.1: (a) Represents the ampoules sealing unit　(b) Sealed ampoules
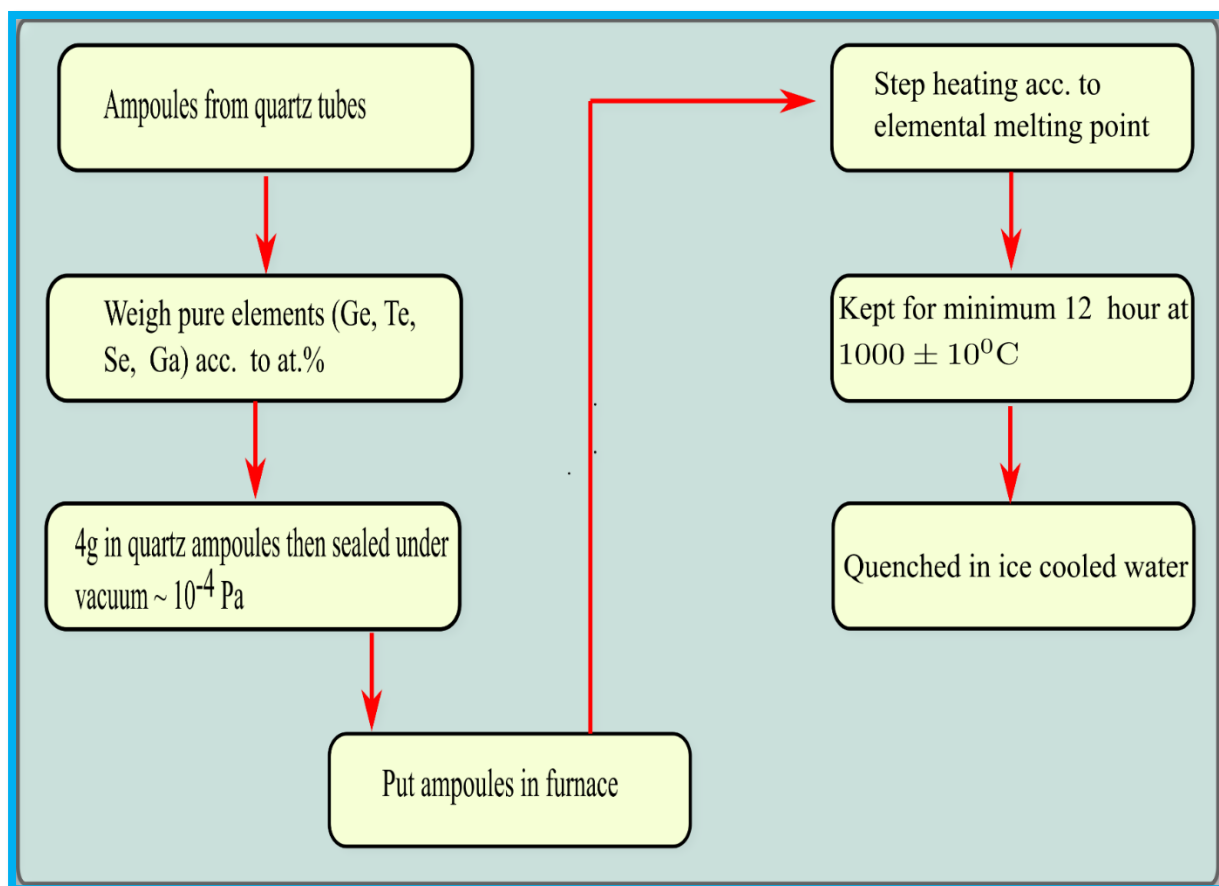
Figure 2.2: The flow chart of melt quenching process

The temperature program for the $Ge_{10}Te_{80}Se_{10}$ and $Ge_{10}Te_{80}Se_8Ga_2$ composition has been shown in figures 2.3 (a & b). The heating rate curve used for heating elements according to their melting point. For the proper melting of a particular element, the temperature has been kept constant for 1 hour. The ampoule has adequately been shaken to melt properly at this constant temperature. After this, the melt is quenched in ice cooling water. The quenched ampoules were put in $HF+H_2O_2$ solution for 24 hours for the etching of the material from the tube. The materials were removed from the ampoules and kept in a desiccator.
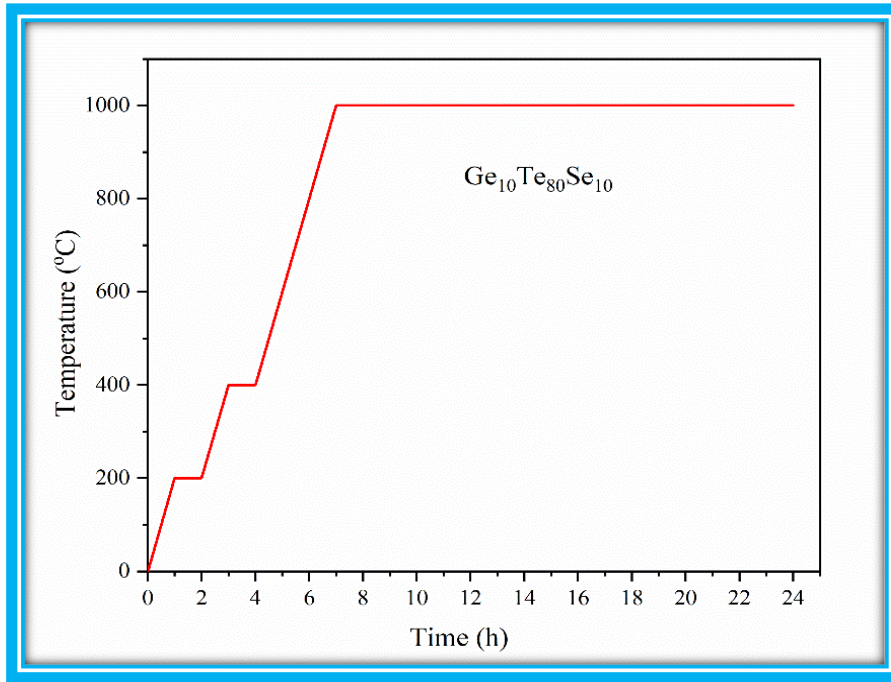
Figure 2.3 (a): Time-Temperature profile program for $Ge_{10}Te_{80}Se_{10}$
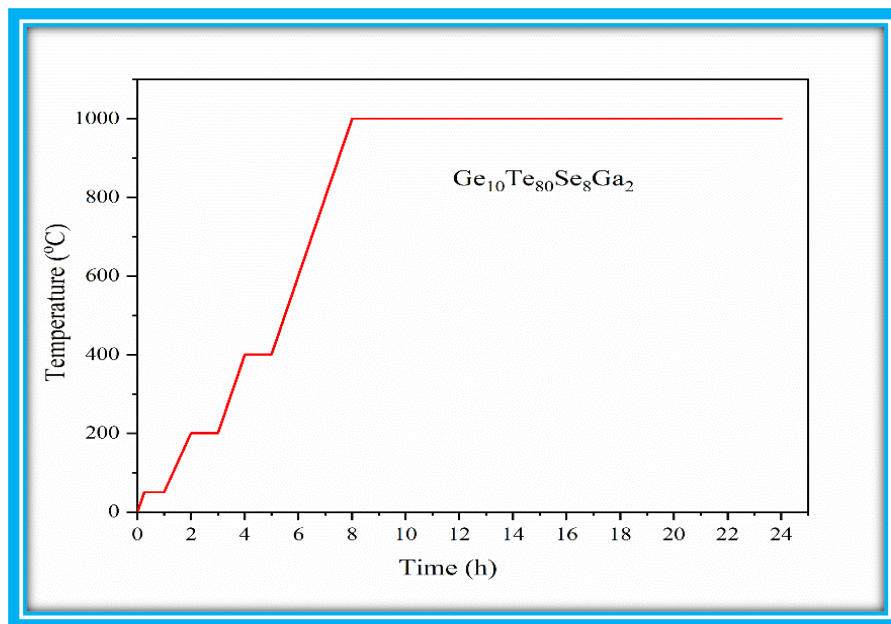
Figure 2.3 (b): Time-Temperature profile program for $Ge_{10}Te_{80}Se_8Ga_2$

2.2 Preparation of thin films

The thin films can be prepared by variety of approaches like thermal evaporation, sputtering, e- beam and chemical vapour deposition (figure 2.4).
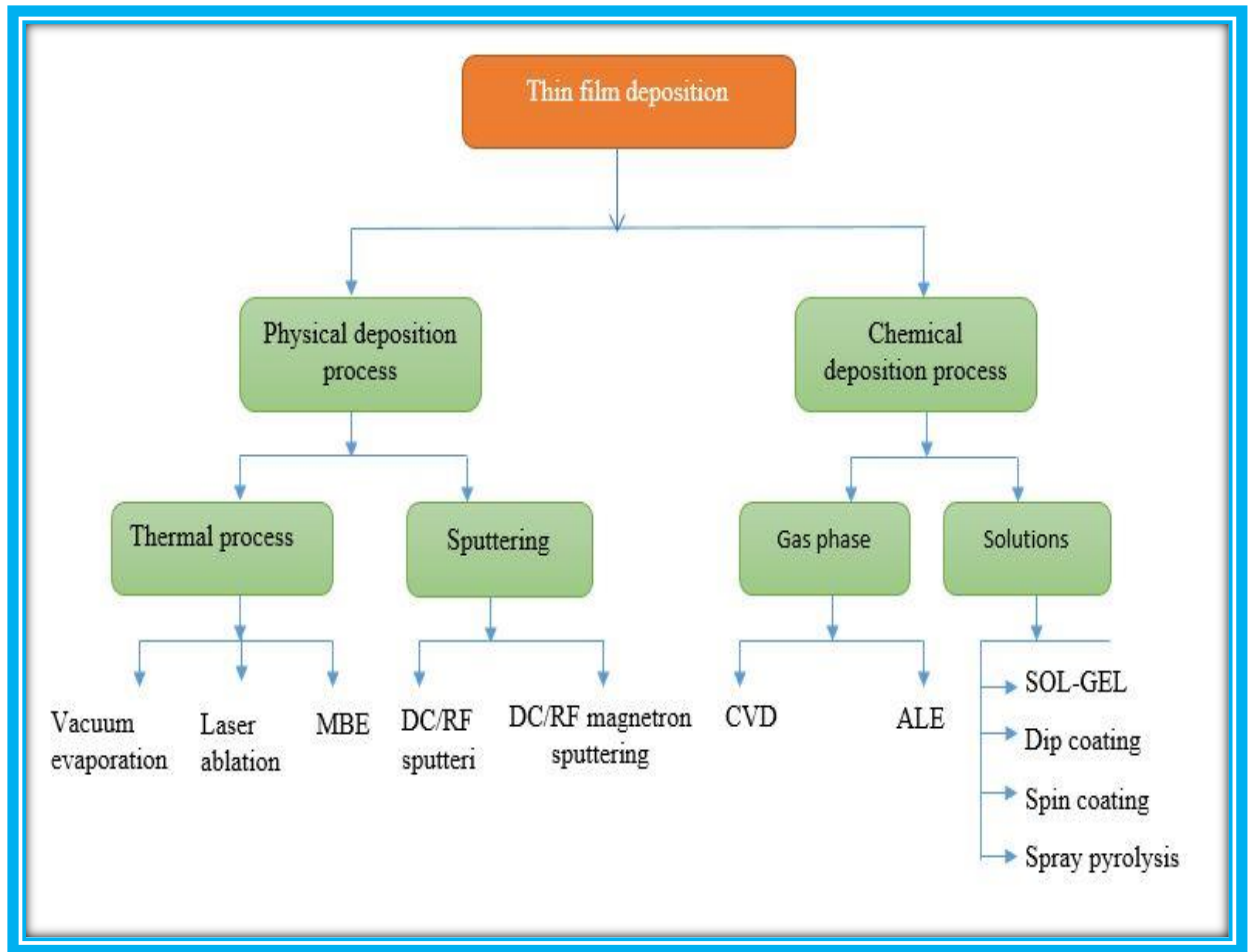
Figure 2.4: Techniques for film deposition

The thin films of the synthesized bulk samples were prepared by "thermal evaporation technique". The films were deposited in the vacuum coating unit "HINDHIVAC model 12A4D" India (figure 2.5). The thin films were deposited on the clean glass substrates [4]. The cleaning of the glass substrate involved three steps:

1). The glass slides were rubbed by the soap solution continuously for 3-4 times. Then, the glass slides were rinsed in the distilled water. The step was performed to remove extra dust, grease and oil impurities.

2). After that the substrate was cleaned ultrasonically with ethanol for 10 - 15 minutes. This process was repeated 2-3 times.

3). The vapour cleaning of the substrate was performed for the removal of organic impurities.

Figure 2.5: Vacuum coating unit HINDHIVAC

The boat of different material like molybdenum, tungsten and tantalum may be used for the deposition process. In the present work a molybdenum boat has been used for the process. The boat was cleaned properly by passing the high current through it until it become red hot. The precleaning of the boat is known as boat firing. This process is performed under high vacuum of 10^{-5}mbar. The bulk sample of ~200 mg was crushed in the mortar pestle for making it fine. The bulk powder sample was kept in the boat. The whole process was performed at the room temperature at pressure of 10^{-6} mbar. The thickness of the evaporated thin films was controlled by the "thickness monitor DTM-101" using a quartz crystal. The deposited films were kept in the deposition chamber in the dark for 12 hours to attain the thermodynamic equilibrium [5]. The prepared thin films have been depicted in figure 2.6.

54
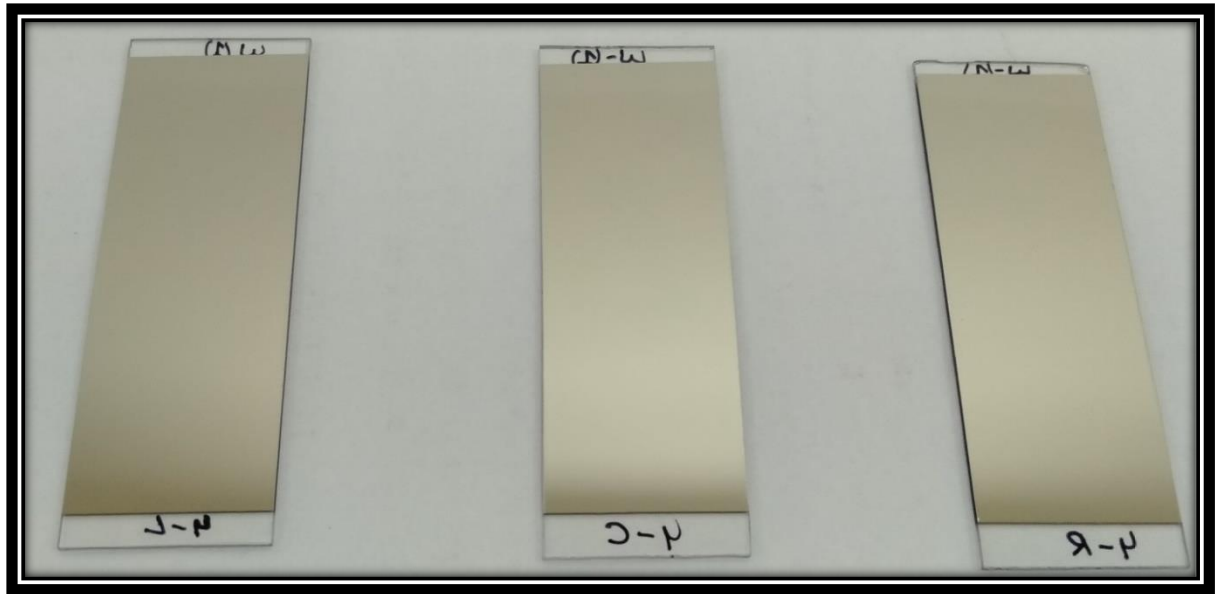
Figure 2.6: The picture of prepared thin films

2.3 Characterization of bulk samples and thin films

2.3.1 "X-ray diffraction (XRD)"

On the microscopic level, crystalline and amorphous solids can be easily identified. Crystalline materials have regular periodic atomic arrangement like common salt have cube faces, while the glasses have curved surfaces. On a microscopic level, the "x-ray diffraction technique" can be used to differentiate between the two. The amorphous nature of the prepared glassy thin films has affirmed through "x-ray diffraction. X-ray diffraction (XRD)" discovered in 1912 by Max Von Laue and it was applied by W. L. Brag and W. H. Bragg for the determination of structure. This technique is a combination of interference and scattering [6].

In the present study, the XRD of thin films has been obtained by using the Shimadzu 6000 diffractometer having CuKα source (λ= 1.54056Å) over the range 10°-80° at 2°/min scan speed (figure 2.7) and the results are discussed elsewhere.

Figure 2.7: "SHIMADZU analytical: XRD 6000 diffractometer"

2.3.2 "Energy dispersive x- ray spectroscopy"

The "Energy dispersive X-ray spectroscopy (EDS)" is used to find the elemental composition of the bulk or film sample. In the current investigation, the presence of elements and the surface morphology of the materials have been analyzed with the help of "FEI-Quanta FEG 200F high resolution Scanning Electron Microscope (HRSEM)" (figure 2.8).

Figure 2.8: "FEI-Quanta FEG 200 HRSEM and EDX"

2.3.3 Transmission Spectroscopy

Several phenomena occur with the passage of light into a solid, such as absorption, transmission, reflection *etc*. There is always some reflection and absorption in some portion of the spectra, so no material is completely transparent in all optical frequencies. It is possible to measure the amount of light transmitted, reflected and absorbed by the technique UV-Vis-NIR spectrophotometer. Intensity of light through the sample is I and I_o represents the intensity of light before the light travels through the sample. The I/I_o is known as transmittance. Spectrometer can be a single or double beam.

In the present study, the normal incidence transmittance spectra in the spectral range 1 - 2.6µm of thin films have been measured by a "double beam Ultraviolet- visible- near infrared spectrophotometer (Perkin Elmer Lambda-750)" (figure 2.9) at "room temperature (300 K)". The spectrophotometer is set with a "slit width of 1 nm" in the given spectral range. (Slit width correction is not needed due to its small value in comparison with different line widths) [7].

Figure 2.9: "Perkin Elmer Lambda 750 UV-visible-NIR spectrophotometer"

2.3.4 Fourier-Transform infrared spectroscopy

There exist different regions of electromagnetic spectrum. The infrared (IR) region exist between the visible and microwave region. Infrared region mainly consists of three regions, NIR, mid-IR, far-IR region. The Fourier transform infrared spectroscopy is a combination of IR spectroscopy and the Fourier transform, which identify the functional group and

detect the impurities present in the sample [8]. The block diagram of FTIR spectroscopy is shown in figure 2.10.
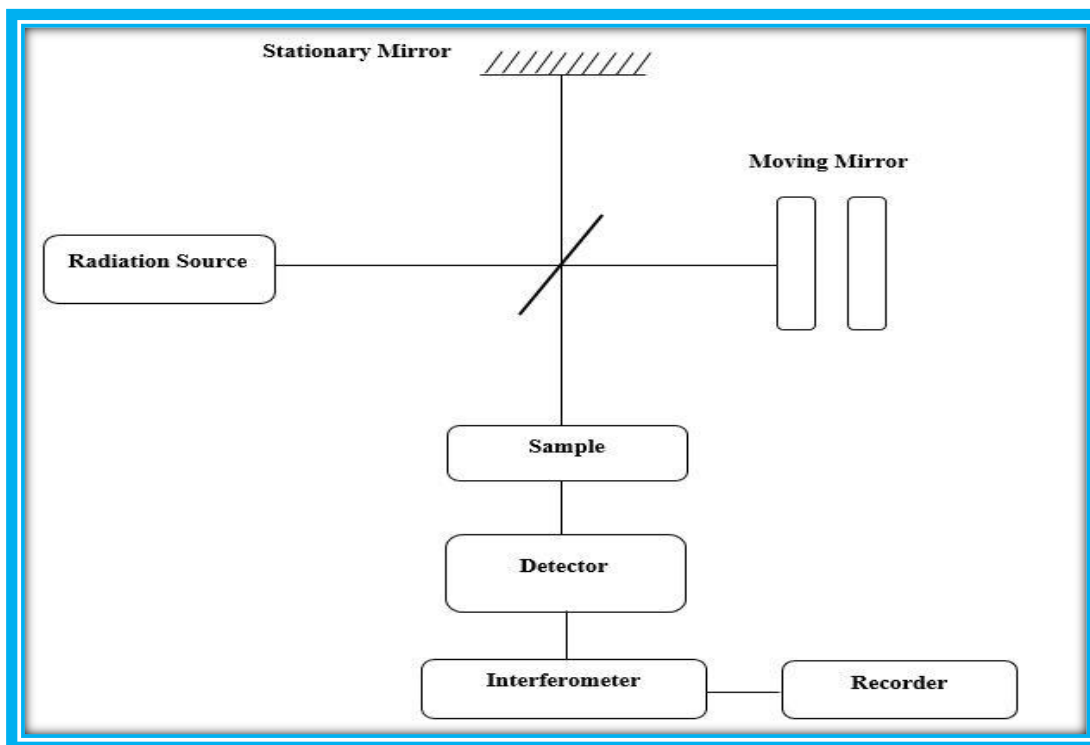
Figure 2.10: Block diagram of Fourier Transform Infrared spectra

In the present study the "far–IR transmission" measurements of powdered materials are recorded in the range 30 -300cm^{-1} with the help of FTIR spectrometer ("Bruker, Germany 3000 Hyperion Microscope with Vertex 80") at the spectral resolution of 0.2 cm^{-1} (figure 2.11).

Figure 2.11: Bruker FTIR – Imaging system

2.3.5 "Differential scanning calorimetry (DSC)"

"Differential scanning calorimetry (DSC)" is a technique used to determine the variation in heat flow given out or taken in by a sample during temperature scanning in a controlled environment. Any transformation that occurs in a material, whether heating or cooling, is accompanied by a heat exchange; DSC allows the temperature of this transformation to be assessed and the heat from it to be quantified [9]. Generally, it may be defined as when a substance undergoes a physical or chemical change under continuous pressure, the exchange of heat energy is obtained using thermal analysis by DSC. In the present study, the thermal analysis of powdered samples is performed in the range of room temperature to 450°C with the help of a Differential Scanning Calorimeter (Perkin Elmer) in N_2 environment (figure 2.12). The sample of 5 to 10 mg has been measured in Nickel-Chromium sample plate using nitrogen gas at 20.0 ml/min.

Figure 2.12: Perkin Elmer DSC system

References

[1] M. Fischer and H. Krebs., "Amorphous Materials", London & New York: Wiely-Interscience, 1972.

[2] M. A. Popescu., "Non-Crystalline Chalcogenicides" , Springer Science & Business Media, vol. 8, 2001.

[3] K. Tanaka and K. Shimakawa, "Amorphous chalcogenide semiconductors and related materials", 2001.

[4] S. K. Pandey, E. Ramya, J. K. S. Gangwar, P. Kaur, S. Kumar, D. N. Rao and S. M. Rao., "Structure and optical properties of MoS_2 films deposited by different methods on glass and silicon substrates", In AIP Conference Proceedings , vol. 1675 (1), pp. 020040, 2015.

[5] V. Sharma., "Phase transition in a-$Se_{85}Te_{15}$ thin film on thermal annealing", Journal of Physics: Condensed Matter, vol. 18(45), pp.10279, 2006.

[6] C. Suryanarayana and M. G. Norton., "X-rays and Diffraction. In X-ray Diffraction A Practical approach, Springer, Boston, MA, pp. 3-19, 1998.

[7] E. Marquez, J. Ramirez-Malo, P. Villares, R. Jimenez-Garay, P. J. S. Ewen and A. E. Owen., "Calculation of the thickness and optical constants of amorphous arsenic sulphide films from their transmission spectra", Journal of Physics D: Applied Physics, vol. 25(3), pp.535, 1992.

[8] J. W. Goodman., "Introduction to Fourier optics", 3rd. Roberts and Company Publishers, 2005.

[9] P. Gill, T. T. Moghadam and B. Ranjbar., "Differential scanning calorimetry techniques: applications in biology and nanoscience," Journal of biomolecular techniques: JBT, vol. 21(4), pp.167, 2010.

Physical and Structural properties of GeTeSeGa Chalcogenide system

➢ **Ekta Sharma**, H.H. Hegazy, Vineet Sharma, Pankaj Sharma, Topological behavior and glassy framework of GeTeSeGa chalcogenide glasses, **Phys. B Phys. Condens. Matter.** 562 (2019) 100–106.

➢ **Ekta Sharma**, Rajan Sharma, Vineet Sharma, Pankaj Sharma, Cohesive Energy Calculation of Quaternary Ge-Te-Se-Ga Chalcogenide Glasses using Chemical Bond Approach, **AIP Conf. Proceeding.** 020008 (2018) (Vol. 2050, No. 1, p. 020008). AIP Publishing.

➢ **Ekta Sharma,** P.B. Barman, Pankaj Sharma, Structural correlation of GeTeSeGa system by XRD and far-infrared spectroscopy. **Appl. Phys. A** (2021). Vol. 127, p. 1-10.

3. Physical and Structural properties of GeTeSeGa system

3.1 Physical Properties

This chapter consists of numerous physical parameters *viz.* "average coordination number ($<r>$), cohesive energy (CE), theoretical energy gap (E_g^{th}) and glass transition temperature (T_g)" which have been determined for $Ge_{10}Te_{80}Se_{10-z}Ga_z$(z =0 at.% to 10 at.%) quaternary chalcogenide glasses.

Chalcogenide glasses are becoming the area of research for their high transmittance in the mid to far-IR region. Due to their good optical and thermal properties, these glasses are becoming an attractive candidate for several applications. These glasses can be used in optical fibers, biosensors, phase change memory devices, holography and infrared detectors [1-4]. The determination of physical or theoretical parameters is important to explore the best features of a system for scientific and practical applications. The addition of Ga to the GeTeSe system causes the configurational disorder in the system. The bonding state among the constituents' elements vary with the ratio of composition.

3.1.1 Experimental details

"Melt quenching technique" is adopted to prepare bulk glassy GeTeSeGa quaternary chalcogenide alloys. The details of the synthesis have been discussed in chapter 2.

3.1.2 "Results and Discussion"

3.1.2.1 "Mean coordination number and counts of constraints"

Phillips Thorpe [5] model originally proposed for non-oxide covalent materials such as chalcogenide glasses which adopt more microscopic approach by taking into account the connectivity of individual atoms in the glassy network. The mean coordination number $<r>$ plays a significant role in interpreting the physical, thermal, optical and chemical properties of chalcogenide glasses. For the glasses family, there are two coordination numbers "$< r > = 2.4$ and $< r > = 2.67$", which are known as topological thresholds. Phillips proposed the constraint theory [5-6] according to which the chalcogenide glasses are comprised of floppy or under coordinated and over coordinated regions. According to this model the characteristics of the glassy network is divided into three categories as mentioned below:

> ➢ "For $< r > < 2.4$ and $N_c < 3$; under coordinated, loosely connected and floppy mode (Polymeric glass) where N_c represent the total number of constraints".

> ➤ "For $<r> = 2.4$ and $N_c = 3$; optimum glass composition. The transformation from floppy to rigid structure (rigidity percolation)".

> ➤ "For $<r> > 2.4$ and $N_c > 3$; network is over coordinated or over-constrained, rigid. (Amorphous Solids)".

The electronic features of the semiconductor system can be expressed by their bonding response, *i.e.* "average or mean coordination number". The value of <r> for GeTeSeGa system is evaluated by using the relationship [5]:

$$<r> = \frac{(aN_{Ge} + bN_{Te} + cN_{Se} + dN_{Ga})}{100} \qquad (1)$$

Where *a, b, c, & d* represent the atomic percentage of elements and $N_{Ge} = 4$, $N_{Te} = 3$ [7-8], $N_{Se} = 2$, $N_{Ga} = 4$ [9, 10] (table 3.1) are coordination numbers of Ge, Te, Se and Ga respectively.

Table 3.1: Standard values of specific parameters of Ge, Te, Se & Ga [7-12]

Parameters	Ge	Te	Se	Ga
Density (ρ) (g cm^{-3})	5.323	6.24	4.819	5.91
Coordination number (N)	4	3	2	4
Electronegativities (χ)	2.01	2.1	2.55	1.81
Atomic mass (u)	72.59	127.6	78.96	69.72
Heat of atomization ($\bar{H}_S$) (kJ/mol)	377	196	227	277
Band gap (E_g) (eV)	0.67	0.335	1.95	0

According to this theory [5, 6], the glass-forming ability of a system is estimated by the comparison of a number of interaction force field constraints with the count of the degree of freedom. For the 3-D space system, each atom consists of three translational degrees of freedom. Due to the presence of constraints, these degrees of freedom can be ignored. In the covalent solids, there exist two kinds of near-neighbour bonding forces; "bond

64

stretching (N_s) and bond bending (N_b)" representing "two-body radial bond-stretching and three-body angular bond-bending".The stretching bond constraint per atom is described as [6] "$N_s =< r >/2$" and "bond bending constraint" is expressed as : "$N_b = 2 < r > -3$"

The mean counts of total constraints (N_c) per atom is given by

$$N_c = N_b + N_s \tag{2}$$

The estimated obtained values are tabulated in table 3.2.

The mean counts of total constraints (N_c) are associated with the "effective coordination number $<r_{eff}>$" and the bonding of atoms. For all compositions of *GeTeSeGa* system, effective coordination number $<r_{eff}>$ is estimated as [6]:

$$< r >= \left(\frac{2}{5}\right) \times (N_c+3) \tag{3}$$

The count of floppy modes (M_f) is given by;

$$M_f = 2 - 5\frac{< r >}{6} \tag{4}$$

and "cross-linking density (D_{CL})"; $D_{CL} = N_c - 2$ are also estimated. The value of floppy modes decreases by the increment of both the Ga concentration and $< r >$ (table 3.2). It clarifies that the material acquires more rigidity with the enhancement of Ga concentration.

Table 3.2: Calculated values "$<r>$, N_b, N_s, N_c, $<r_{eff}>$, D_{CL}, and M_f".

z	$<r>$	N_b	N_s	N_c	$<r_{eff}>$	D_{CL}	M_f
0	3	1.5	3	4.5	3	2.5	-0.5
2	3.04	1.52	3.08	4.6	3.04	2.6	-0.53
4	3.08	1.54	3.16	4.7	3.08	2.7	-0.57
6	3.12	1.56	3.24	4.8	3.12	2.8	-0.6
8	3.16	1.58	3.32	4.9	3.16	2.9	-0.63
10	3.2	1.6	3.4	5	3.2	3	-0.67

The "lone pair" of electrons play a interguing role in the formation of glasses. Deforming a bond with "lone pair electrons (L)" is easier than deforming a bond having no sharing electrons. The "lone pair of electrons" can be estimated as [11]

$$L = V - <r>$$

(5)

V refers to the count of valence electrons. Figure 3.1 clearly depicts that by adding Ga in the system, L values decreased from 2.8 to 2.3. This effect may be because of contact of Ga with bridged Te atom lone pair electrons. This decrease may also be attributed to the reduction in the flexibility of the network. It may also be linked with the increment in $<r>$ values which clarifies that the system is shifting towards the rigid state.
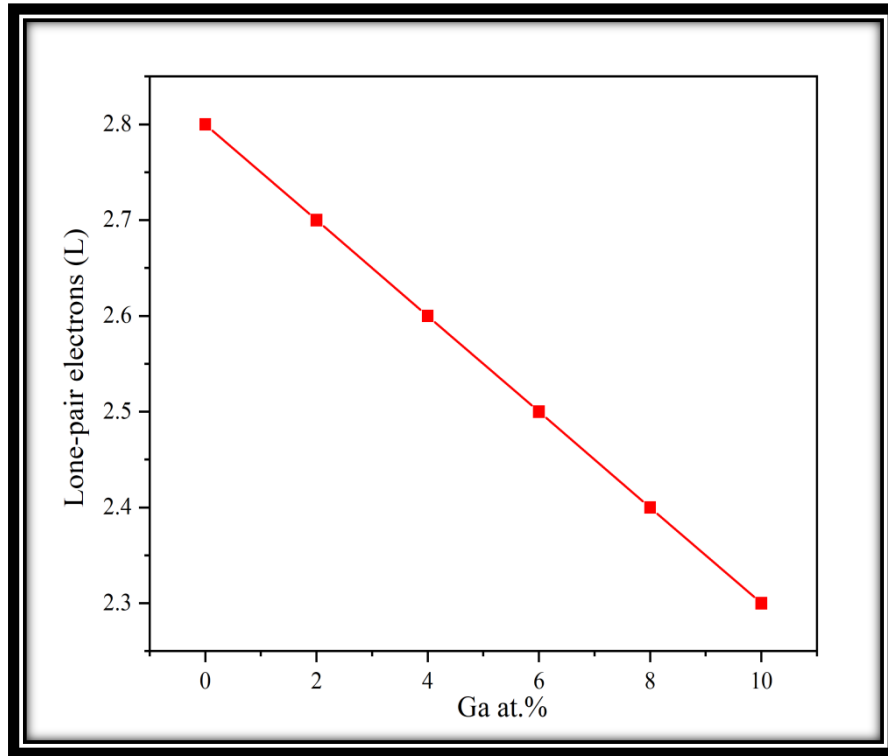
Figure 3.1: Variation of Lone pair electrons with gallium concentration

Zhenhua [12] introduced the simple criteria for analysing glass-forming ability in chalcogenide system, *i.e* for "L > 2.6 for binary and L > 1 for ternary composition respectively". In the present investigated system although lone pair electrons decrease with Ga addition but L>2 for whole system. Consequently, all the compositions of GeTeSeGa may be acknowledged as good glass former.

3.1.2.2 Density, Molar volume, Compactness and free volume
"Density (ρ), molar volume (V_m) and compactness (δ)" are considered the most important factors that influence material's physical properties. The rigidity of the material can be connected with the density. Theoretically, density (ρ) values of the system are obtained by [13].

$$\rho = \left(\Sigma \frac{X_i}{d_i} \right)^{-1} \tag{6}$$

Where X_i and d_i refers to the atomic fraction and density of i^{ih} element of the glass. Theoretical values of the sample densities help to determine the "packing density (P.D)" estimated as:

$$P.D = \frac{\rho N_A}{M_i} \tag{7}$$

where M_i and N_A represent the molecular weight and Avogadro number. The rise in packing density values (table 3.3) may be due to the increase in density with the enhancement of Ga concentration. Ga (5.91gcm^{-3}) is much denser than Se (4.819gcm^{-3}), thus substitution of Se by Ga give rise in the enahancement of "density" and may be attributed to the more compactness of the system. Increasing Ga in the material leads to rise in density values (figure 3.2), so the values of refractive index are also expected to increase. The higher refractive index values of the samples make them suitable for use in IR filters and mirrors. With the increase in <r> values, density values increase (figure 3.2).
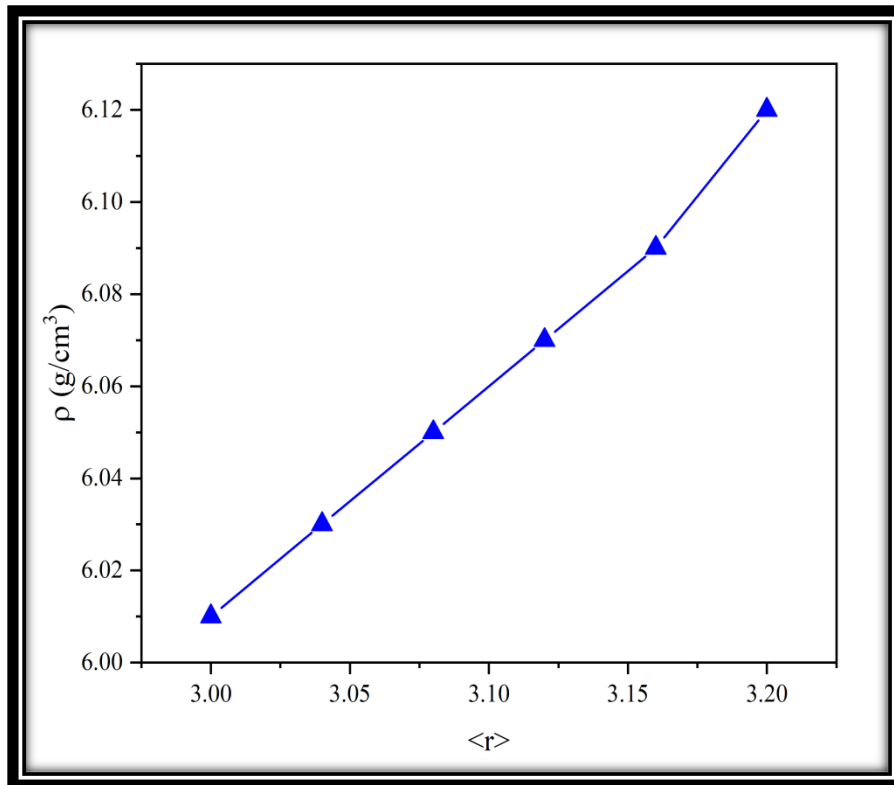
Figure 3.2: Variation of density with mean coordination number for GeTeSeGa glasses

Molar volume has been evaluated by using the density values by the following relation:

$$V_m = \left(\sum X_i m_i\right)/\rho \tag{8}$$

where m_i represents the molecular weight of ith element. It is noted from table 3.3 that the value of molar volume decreases with the increment of Ga concentration. This may be attributed to the replacement of Se by Ga (At. wt. Se > At. wt. Ga) leads to diminishing in V_m with raise of Ga content.

Compactness (δ) is defined as the estimation of the normalized mean volume of atoms. It is obtained by the formula:

$$\delta = \frac{\sum_i \frac{X_i A_i}{\rho_i} - \sum_i \frac{X_i A_i}{\rho}}{\sum_i \frac{X_i A_i}{\rho}} \tag{9}$$

Where X_i, ρ_i, A_i refer to the atomic fraction, density and atomic weight of the particular elements [14].

Table 3.3: "Values of packing density (P.D), molar volume (V_m), cohesive energy (CE), theoretical band gap (E_g^{th}), heat of atomization ($\overline{H}_S$), and degree of ionicity & covalency

(I$_c$ & C$_c$)."

z	P.D.($\times10^{22}$ atom/cm^3)	V_m (cm^3/mol)	(CE) (kJ/mol)	E_g^{th}	$\overline{H}_S$ (kJ/mol)	Bonds	C$_c$	I$_c$
0	3.08	19.52	263.1	0.495	218	Se-Ge	92.9	7.03
2	3.1	19.42	259.5	0.464	219	Te-Ga	97.9	2.08
4	3.11	19.32	248.7	0.433	220	Te-Ge	99.8	0.20
6	3.13	19.22	251.8	0.401	221	-	-	-
8	3.14	19.12	247.7	0.370	222	-	-	-
10	3.16	19.02	243.4	0.338	223	-	-	-

With the increment of Ga concentration (0 to 10 at. %) in the pure composition, the compactness of the material enhances. The variation of compactness and "free volume percentage (FVP)" with $<r>$ is plotted in figure 3.3. "FVP" for all composition has been determined from the relation [15]:

$$FVP = [(V_m - V_T)/V_m] \times 100 \tag{10}$$

where V_m represents the molar volume as determined in table 3.3. The values of theoretical volume V_T are calculated as:

$$V_T = 10V(Ge) + 80V(Te) + (10 - z)V(Se) + zV(Ga) \tag{10(a)}$$

The variation in FVP are because of change in the composition structure caused by a variation in interatomic spacing, that may be linked to variation in the number of bonds per unit volume of the material. The values of FVP decrease with the enhancement of Ga, indicating the increase in rigidity of the material.
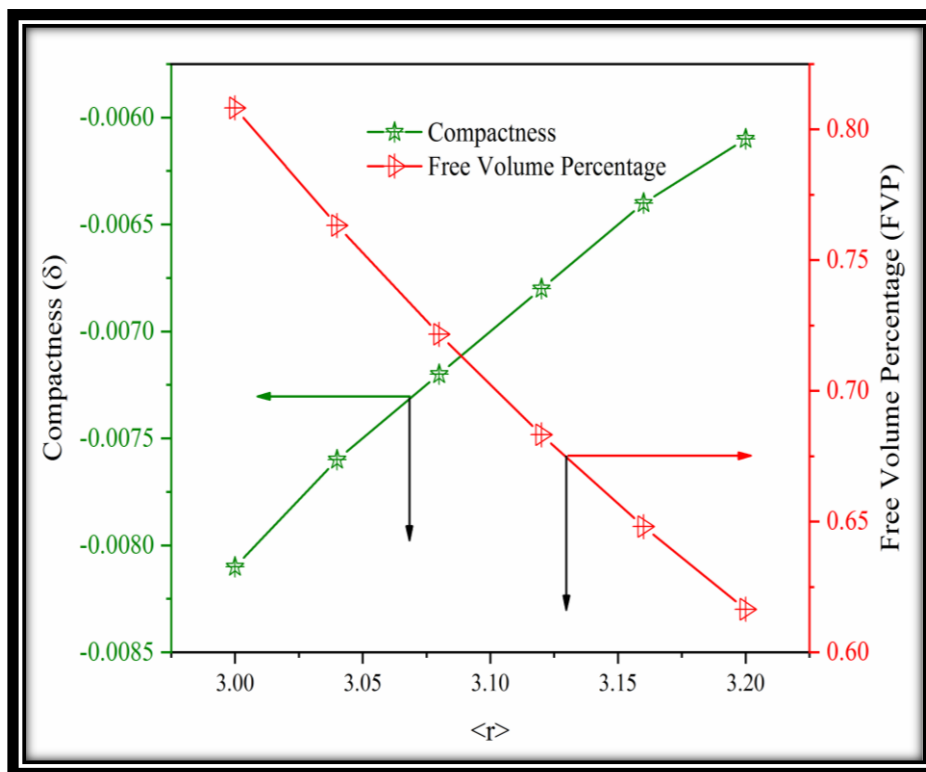
Figure 3.3: Plot of compactness and FVP with mean coordination number

70

3.1.2.3 *Estimation of "field strength (F) and polaron radius (R_p)"*

"Polaron" is defined as the "quasi-particle", which is utilized to realize the connection of atoms and electrons in materials. It may be calculated for ordered and disordered systems. The development of polaron drops the mobility of electrons in a semiconducting material. The size of the polaron should reduce with the enhancement of the number of atoms. Polaron radius (R_p) has been obtained using the formula [16]:

$$R_p = 0.5 \left(\pi \big/ 6N \right)^{\frac{1}{3}} \tag{11}$$

where N is the number of tellurium atoms per unit volume and is calculated by using the relation [16]:

$$N = \left(\frac{\rho W_P N_A}{AW \times 100} \right) \tag{12}$$

where ρ, W_P and AW denote the sample density, at. wt % of Te in *GeTeSeGa* material and atomic weight of Te. The interatomic distance (r) of all the compositions is estimated from the formula:

$$r = \left(\frac{1}{N} \right)^{\frac{1}{3}} \tag{13}$$

Field strength (F) is obtained by relationship:

$$F = V_{NO} \big/ R_P^2 \tag{14}$$

where V_{NO} denotes the valence number of the tellurium element. Figure 3.4 clearly depicts the decrement in the "polaron radius" and a concurrent increment in "field strength" and N values with the rise of Ga content. This outcome also advises a rise in compactness of the glassy network and consequent reduction in free space. The outcomes are in accordance with the outcome achieved for FVP and compactness.
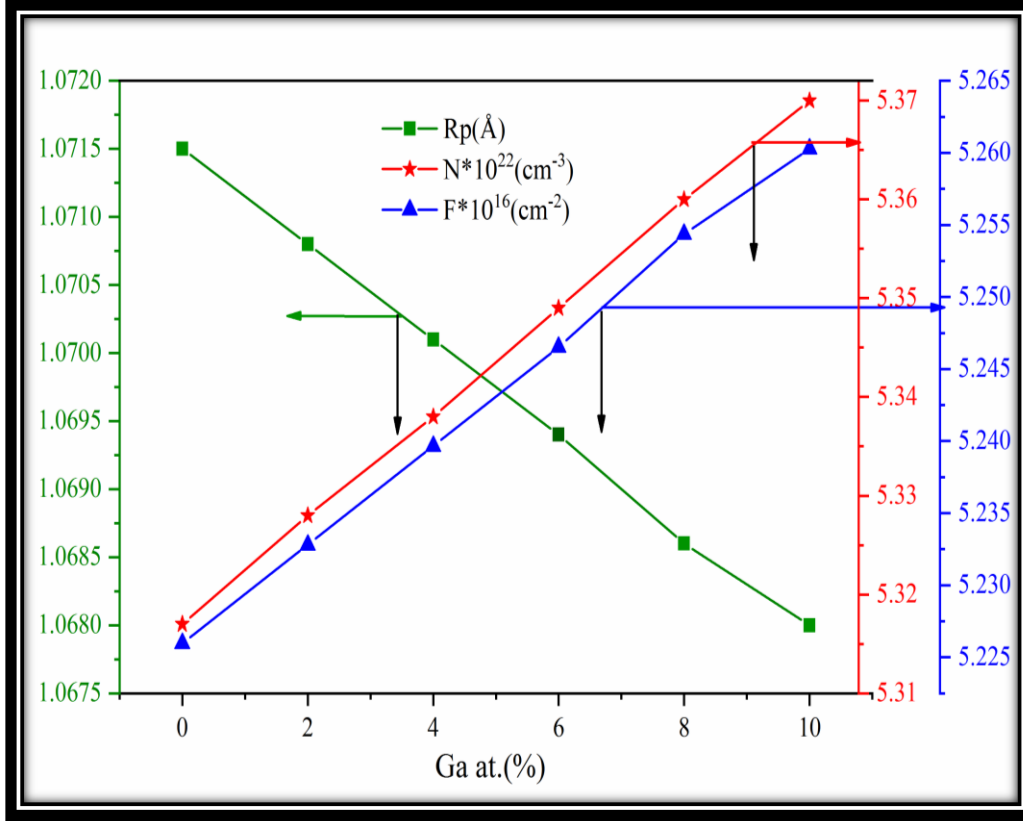
Figure 3.4: Variation of field strength, polaron radius and number of atoms with Ga content.

3.1.2.4 Distribution of bonds, assessment of cohesive energy

For the distribution of bonds, the "chemical bond approach (CBA)" [17] was applied for the estimation of counts of bonds and their types "(heteropolar and homopolar)". Based on this method, atoms associate more favourably with atoms of dissimilar type instead of similar type until the available valence of atoms are filled. Moreover, in comparison to homopolar bonds, the generation of heteropolar bonds is relatively simple in the order of reducing bond energy that is supposed to be additive in nature. The "heteropolar bond energy" (E_{A-B}) has been obtained by Pauling's relationship [18]

$$\text{``}E_{A-B} = \left(E_{A-A} \times E_{B-B}\right)^{1/2} + 30\left(\chi_A - \chi_B\right)^2\text{''} \tag{15}$$

Here E_{A-A} and E_{B-B} refer to the bond energies for the homopolar bond between A-A & B-B and "χ_A and χ_B refer to the electronegativities" of the particular atoms. The standard electronegativities values of constituents atoms such as χ_{Ge}, χ_{Te}, χ_{Se}, χ_{Ga} are listed in table

72

3.1. The bond energies for homopolar bonds of the compositions of the material are "Ga-Ga (106.4 kJ/mol, Ge-Ge (264.4 KJ/mol), Se-Se (330.5 kJ/mol) and Te-Te (257.6 kJ/mol)" [20].The obtained energies for heteropolar bonds from equation (15) are;

- "Te-Se=297.8571 kJ/mol
- Se-Ge=304.356 kJ/mol
- Te-Ga =168.079 kJ/mol
- Te-Ge =261.221 kJ/mol"

All these bonds are produced in the sequence of diminishing bond energy. The bond energy for the bond Se-Ge is larger compared to other bonds formed, so they will form first, followed by Te-Ge and Te-Ga. It is clear from figure 3.5 the first bond formed is Se-Ge, where all the Se content is being consumed and the possibility of formation of this bond reduces with the enhancing Ga content. Then after Te-Ga and Te-Ge bonds are generated and their bond formation value rises with the addition of Ga concentration (0 to 10 at. %). At last, the Te-Te homopolar bond is formed with the decrement in energy.
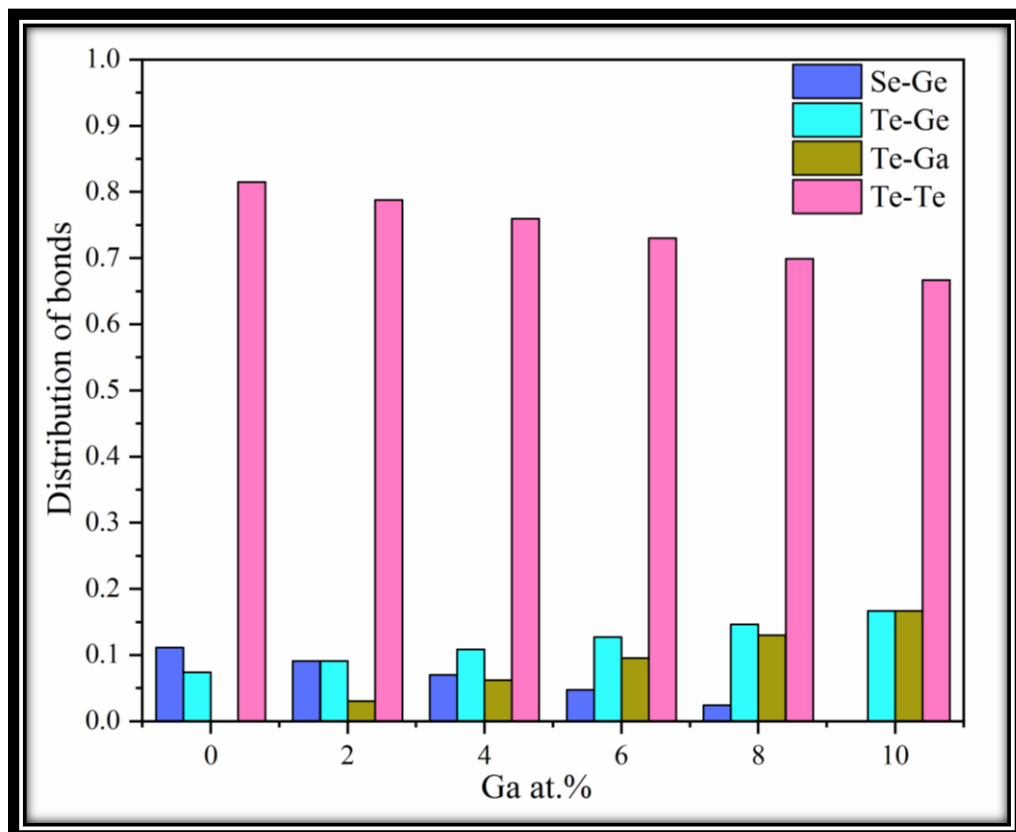
Figure 3.5: Distribution of bonds for the GeTeSeGa system

The optical behaviour of glasses can be interpreted on the basis of "cohesive energy" which is defined as the stabilization energy of an infinitely higher bunch of a system per atom. Cohesive energy (CE) determines the mean "bond strength" and is being computed by adding together and given by the relation $CE = \sum C_i E_i$ where C_i & E_i represent the chemical bond distribution and energy of bond present in the system. The computed values of CE are depicted in table 3.3. It is noticed from table 3.3 that by rising of Ga amount, CE decreases. The decrease in CE values is attributed to the weakening of bonds in the material and consequently lead to a reduction in the energy bandgap. The amount of Ge and Te in the GeTeSeGa system is fixed *i.e.* 10% and 80% respectively, thus the variation in CE is due to changes in Ga and Se concentration. The theoretical bandgap (E_g^{th}) of GeTeSeGa system has been computed from the relation [20]

$$E_g^{th} = eE_g(Ge) + fE_g(Te) + gE_g(Se) + hE_g(Ga) \qquad (16)$$

Here e, f, g & h refer to the volume fraction and the standard values of band gap E_g for constituent atoms are listed in table 3.1.The volume fraction has been obtained from the densities and atom weight fraction of constituent atoms.

The bandgap reduces with the raising Ga concentration and may be because of a drop in the average bond energy in the material. E_g^{th} changes from 0.495eV to 0.338eV for all compositions, as depicted in table 3.3.

3.1.2.5 "Heat of atomization"

The energy needed to detach one mole of a substance into its constituent atoms is known as the "heat of atomization $(\overline{H}_S)$". Several physical parameters of the semiconductors have a direct link with $(\overline{H}_S)$. Aigran *et al.* [21] reported the linear link between the "energy band gap (ΔE) and mean heat of atomization" as given by; "$\Delta E = a(H - b)$" where a & b represent the characteristics constants.

In the present study, the "lone pair electrons" states create the "valence band (σ state)" while "conduction band" arises from "anti bonding (σ*) states". So the bandgap can be correlated with the average bond strength. The decrement in the bond strength of the system leads to less splitting; and subsequently there is decrease in the band gap.

74

Pauling [19] stated that the heat of atomization for binary system at standard pressure and temperature for atoms is evaluated by the formula: $\overline{H}_s(A-B) = \Delta H + 0.5(H_s^A + H_s^B)$ where ΔH (change in heat of atomization) is proportional to $(\chi_A - \chi_B)^2$. For higher-order semiconductor materials (*viz* ternary, quaternary *etc.*) the average heat of atomization is computed by the relation [22, 23]:

$$\overline{H}_s = \frac{(aH_s^{Ge} + bH_s^{Te} + cH_s^{Se} + dH_s^{Ga})}{(a+b+c+d)} \quad (17)$$

where the symbols have their usual meaning. It can be seen from table 3.3 that with the decrease in Se concentration and increase of Ga content, the value of $\overline{H}_S$ increases. It may be due to the substitution of Ga having higher H_s value compared to Se. The average single bond energy is estimated by the formula : $\overline{H}_S / <r>$. The variation of $\overline{H}_S / <r>$ with Ga content (0 - 10 at. %) has been given in figure 3.6. From the figure it is noted that with the raising of Ga concentration, there is a fall in the values of $\overline{H}_S / <r>$. This behaviour may be correlated with the decrement in CE values that leads to the weakening of bond strength with enhancing Ga concentration.

The rise of Ga content and reduction of Se content leads to decrease in "average single bond energy $\overline{H}_S / <r>$" and energy bandgap. A similar trend has been previously stated by Fouad [24] for SeSb system and there is linear relation between $\overline{H}_S / <r>$ and E_g.
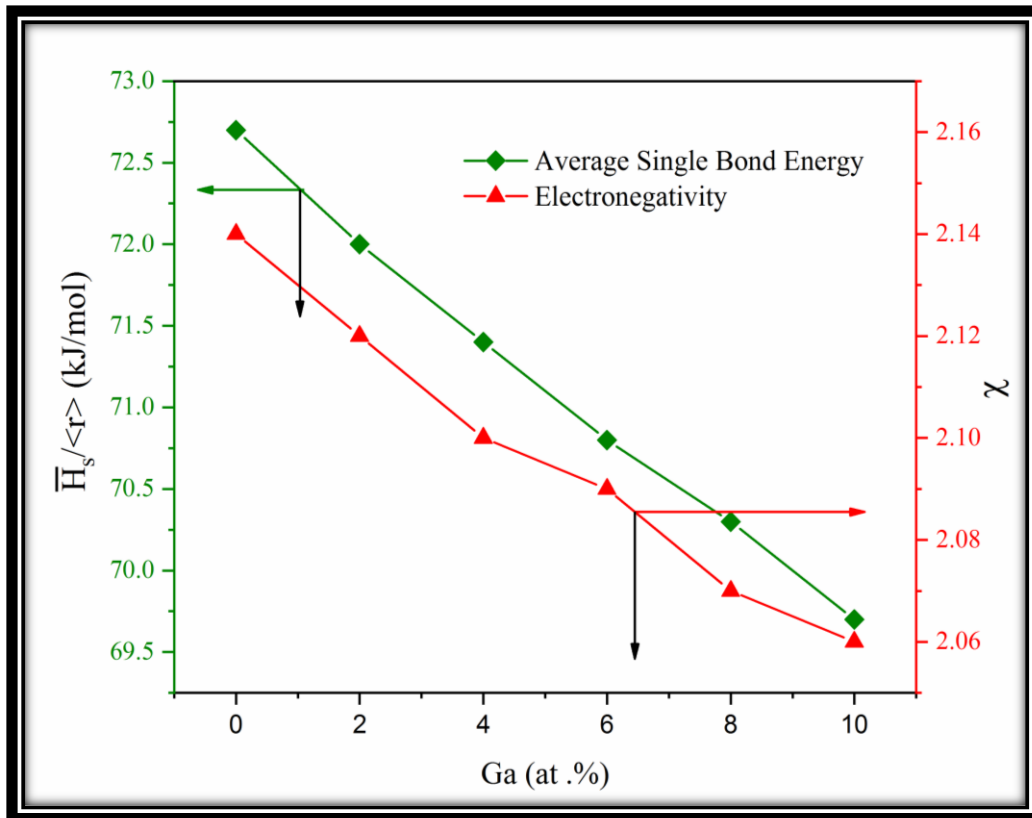
Figure 3.6: Plot of electronegativities and average single bond energy with Ga content

Electronegativity of the material is estimated from the principle stated by Sanderson [25]. Conferring to this, the geometric mean of the electronegativity of an alloy's individual constituents is the alloy's net electronegativity. It is clear from figure 3.6 that the electronegativity also reduces with the addition of Ga content.

3.1.2.6 Covalent and Ionic nature of bonds

According to the "bond constraint theory of Phillips-Thorpe" [6], for "<r> = 2.4, all bonds are absolutely covalent", however for another value of <r> greater than or less than 2.4, the material may show ionic nature along with the covalent character. The Pauling formula has been applied for the computation of the ionicity of a bond. Pauling ionic character (I_c) and degree of covalency (C_c)is given by the relation [26]:

$$ \text{``} C_c = 100 \times \left(\exp\left(-\frac{(\chi_A - \chi_B)^2}{4} \right) \right) \quad\quad (18) $$

$$ I_c = 100 \times \left(1 - \exp\left(-\frac{(\chi_A - \chi_B)^2}{4} \right) \right) \text{''} \quad\quad (19) $$

The difference in electronegativity of elements is inversely proportional to the degree of covalency of the material.All compositions under study have covalent character *i.e.*>90% (table 3.3).

3.1.2.7 Estimation of "stoichiometry deviation (R)" and prediction of "glass transition temperature (T_g)"

R value decides the content of chalcogen in the system. It can be defined as the ratio of covalent bonding of chalcogens element *viz* (Se & Te) to the anti- chalcogens *viz* (Ga & Ge). For the GeTeSeGa system, the R value is being obtained from the relation [27, 28].

$$ R = \frac{bNTe + cNSe}{aNGe + dNGa} \quad\quad (20) $$

According to R values, the chalcogenides can be categorized into three groups
- ➤ For R>1, then the material is considered as chalcogens rich having chalcogens-chalcogens bonds along with heteropolar bonds.
- ➤ For R<1, then the materaisl is considered as chalcogens poor, having only heteropolar bonds.
- ➤ For R=1, then the system has only heteropolar bonds.

The variation of R with Ga concentration is depicted in figure 3.7.
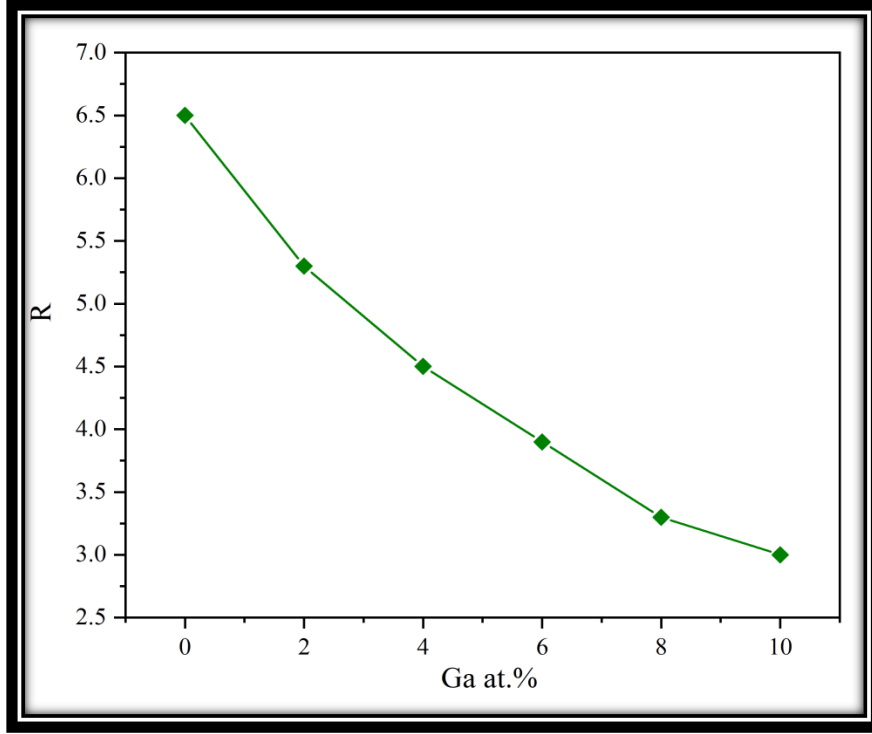
Figure 3.7: Plot of dependence of R with Ga content

In the present study, R>1 (figure 3.7) indicates that the material under study is regarded as chalcogens rich, having both chalcogens–chalcogens (homopolar) bonds and heteropolar bond.

The supercooled liquid becomes solid at some temperature known as "glass transition temperature T_g". It is an essential parameter which deals with the rigidity and strength of the glassy system. The optical characteristics of chalcogenide glasses are linked to the average bond energy that strongly depends on the value of <r>, the kind of bonds, bond energy and degree of cross-linking per atom. "The mean bond energy (<E>)" has been obtained according to "Tichy and Ticha" [27, 29] given by the relation:

$$\text{``} < E >= E_c + E_{rm} \text{''}$$ (21)

where E_c represent contribution originating from the stronger "heteropolar bonds" and E_{rm} represent contribution originating from the remaining weak "homopolar bonds". The value of both the parameters E_c and E_{rm} show dependency on the value of R. For the present system <E_c> is given by

$$E_c = aN(Ge)E_{Se-Ge} + aN(Ge)E_{Te-Ge} + dN(Ga)E_{Te-Ga}$$ 21(a)

where *a, b, c, & d* represent the atomic percentage of elements, N represent the coordination number of Ge, Te, Se and Ga respectively. The bond energies of the homopolar bonds are given by the relation;

$$E_{rm} = \frac{bN(Te) + cN(Se) - aN(Ge) - dN(Ga)}{<r>}$$ 21(b)

Tichy and Ticha proposed the equation for the estimation of "glass transition temperature (T_g)" as

$$"T_g = 311\left[\langle E\rangle - 0.9\right]"$$ (22)

where $<E>$ represents the mean bond energy of thesystem. It is noticed from figure 3.8 that with the raising of Ga concentration, the values of $<E>$ increases. As $<E>$ values are used in glass transition temperature calculation, same trend in T_g have also been observed. Saiter *et al.* [30] suggested that if the doped element shows a coordination number higher than 2, then T_g and $<r>$ are linked by the relation; $T_g = f(<r>)$. Hence an increment in T_g with the *Ga* concentration possess coordination number 4 signifies enhancement in the connectivity in the glassy system.
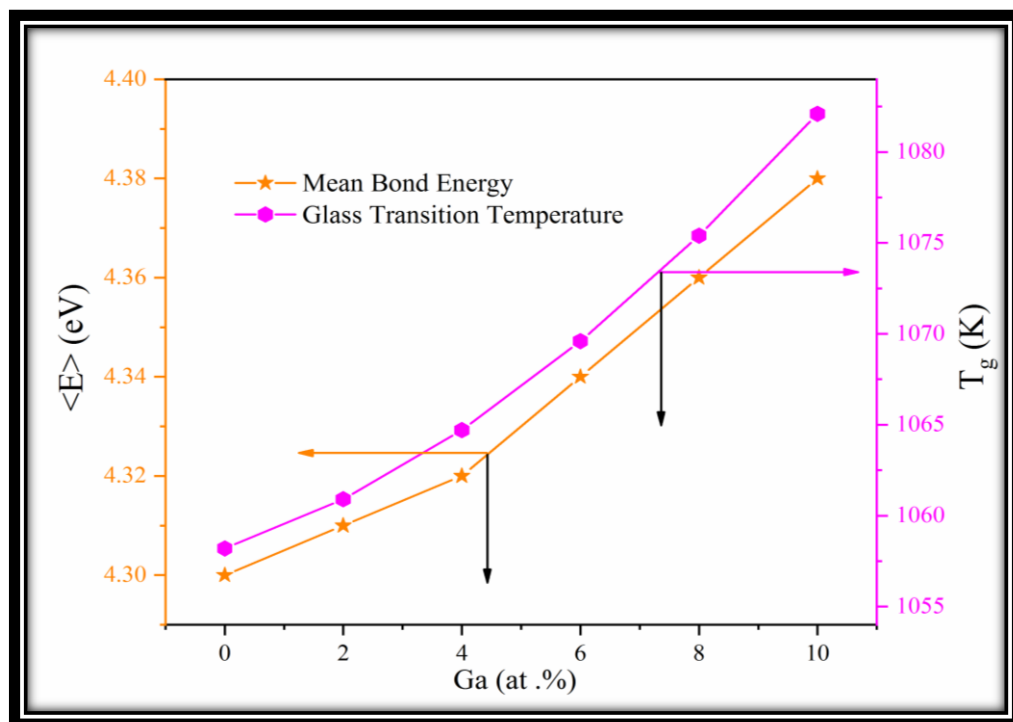
Figure 3.8: Plot of transition temperature and mean bond energy with Ga concentration

3.2 Structural Properties

This part of the chapter comprises of structural properties of GeTeSeGa quaternary chalcogenide glasses by the various characterization techniques such as "XRD, HRSEM and FTIR spectroscopy" up to far-IR region. The outcomes are discussed based on bond energies of distinct bonds, their probabilities and "chain crossing model, random–covalent network model and the chemical bond approach" in the investigated system. "X-ray diffraction and HRSEM" techniques have been used for the confirmation of the amorphous nature of the material.

3.2.1 Structural Studies of GeTeSeGa chalcogenide glasses

The XRD analysis of the GeTeSeGa thin films with various compositions has been depicted in figures 3.9 & 3.10. The absence of sharp peaks reveal the amorphous behaviour of the system.
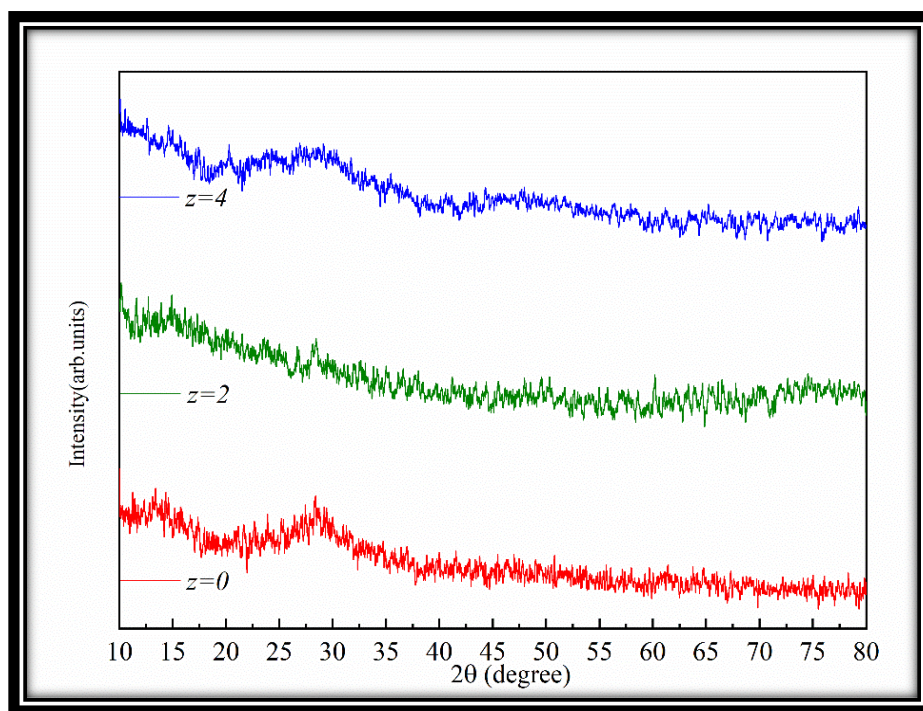
Figure 3.9: XRD pattern of $Ge_{10}Te_{80}Se_{10-z}Ga_z$(z = 0 at. % to 4 at. %*)* thin films
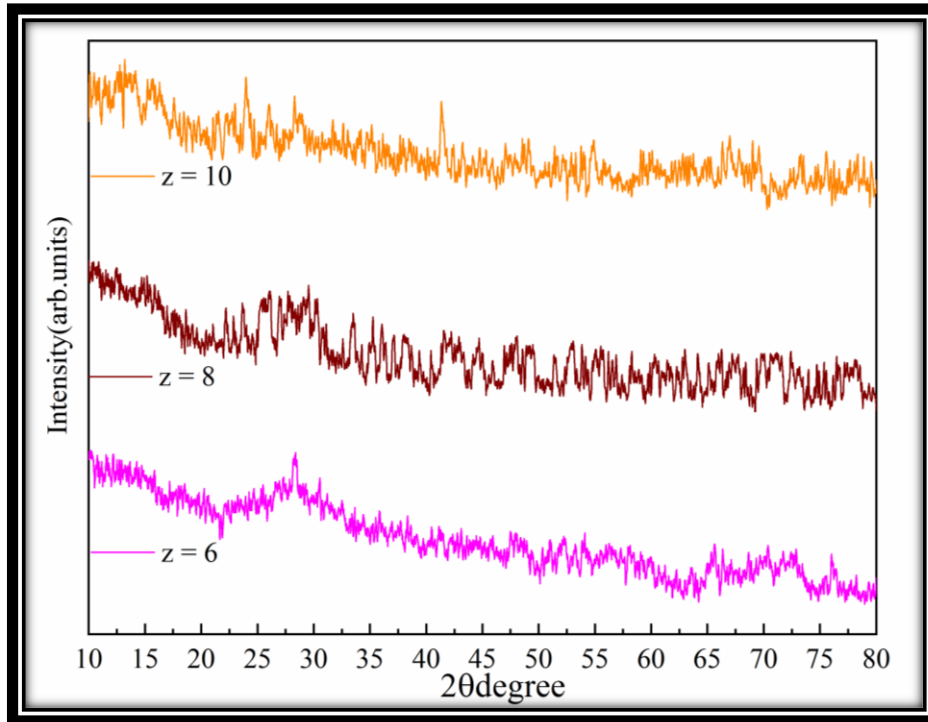
Figure 3.10: XRD pattern of $Ge_{10}Te_{80}Se_{10-z}Ga_z$($z = 6$ at. % to 10 at. %) thin films

3.2.2 EDS and HRSEM data analysis

The energy-dispersive X-ray spectroscopy (EDS) images provide idea about the presence of elements in the sytem and the spectral distribution of the constituent elements are shown in figure 3.11. The EDS outcomes signify the presence of peaks corresponding to Ge, Te, Se and Ga elements; which confirms the existence of these elements in the prepared alloys. The images of HRSEM defines the surface microstructure of the GeTeSeGa glassy system. The HRSEM figure 3.12 shows the irregular morphology, shape and position of the grains.
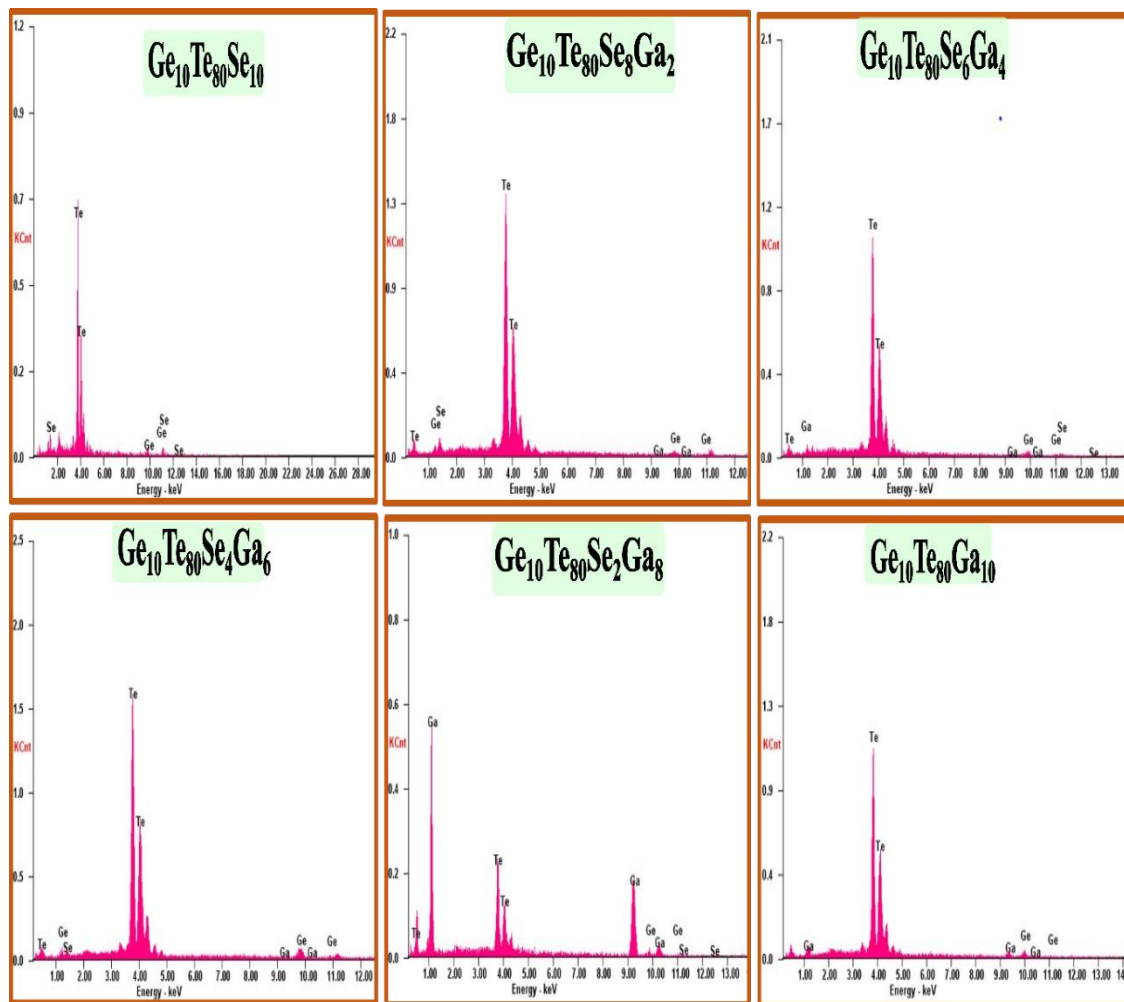
Figure 3.11 : EDS images for the GeTeSeGa glasses
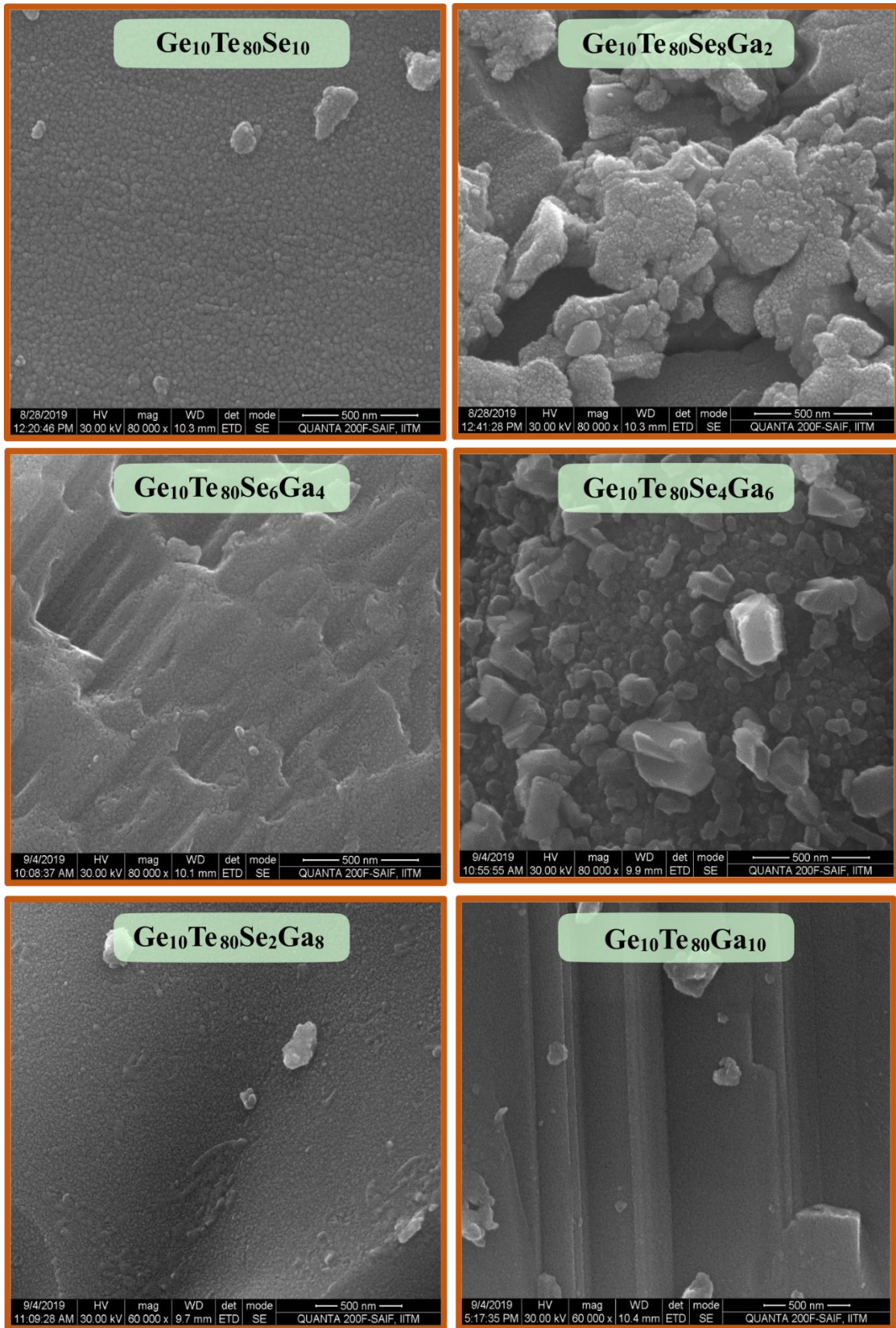
Figure 3.12 : HRSEM images for GeTeSeGa glassy system

3.2.3 Far- Infrared spectroscopy

3.2.3.1 A quantitative explanation of absorption bands

In this technique, absorption is a consequence of bending and stretching vibrations in the molecular system. The bonds energy of heteropolar bonds (E_{A-B}) like Te-Ga, Ge-Te, Ge-Se and Se-Te in the system under investigation is determined by the Pauling relation given in equation 15 [18]:

$$“E_{A-B} = (E_{A-A} \times E_{B-B})^{\frac{1}{2}} + 30(\chi_A - \chi_B)^2”$$ (15)

The "relative probability" of various bond formations has been obtained with the help of the probability function [31] $\exp\left(\dfrac{E}{k_B T}\right)$ at 300K and 1273 K respectively, where k_B represents the "Boltzmann constant". The obtained values of relative probabilities and the bond energies for different bonds are shown in table 3.5.

Table 3.4: Distribution of bonds, energies of bonds and relative Probability

Bonds	Bond Energies (kcal/mol)	Relative Probability of bond formation	
		at 300K	at 1273K
Ge-Se	49.42	1	1
Se-Ga	46.09	3.75×10^{-3}	2.68×10^{-1}
Te-Se	44.18	1.52×10^{-4}	1.26×10^{-1}
Se-Se	44.00	1.13×10^{-4}	1.17×10^{-1}
Ge-Ge	37.60	2.45×10^{-9}	9.35×10^{-3}
Ge-Te	35.46	6.76×10^{-11}	4.01×10^{-3}
Te-Te	33.00	1.093×10^{-12}	1.52×10^{-3}
Ge-Ga	28.62	7.04×10^{-16}	2.7×10^{-4}
Te-Ga	28.21	3.54×10^{-16}	2.3×10^{-4}
Ga-Ga	20.00	3.70×10^{-22}	8.9×10^{-6}

The Far-infrared transmission assessment of the GeTeSeGa glassy system has explained under the rules as follow:

i. "Valence field Theory (VFF): This theory is based on the assumption that there is a strong restoring force in the line of every valence bond if the distance between the two atoms bound by this bond is varied" [32].

ii. "The position of the intrinsic IR features is influenced mainly by stretching force constants of the corresponding chemical bonds" [32].

The wavenumber (v) of the vibration modes in the infrared spectrum is estimated by the weight of an atom and interatomic force in the group of atoms in the system. The relation is as [33, 34]:

$$v = \frac{1}{2\pi c}\left(\frac{K}{\mu}\right)^{0.5} \tag{23}$$

K represent the "force constant" and "μ refers to the reduced masses" of formed bonds and can be estimated by $\mu = \dfrac{M_1 M_2}{M_1 + M_2}$ here M_1, M_2 represent the atomic mass of the particular atoms.

The relation formulated by Gordy [35] for the estimation of force constant (K_r) value is as follows:

$$K_r = aN\left(\frac{\chi_A \chi_B}{d^2}\right)^{0.75} + b \tag{24}$$

The constant a and b have values 1.67 and 0.30, also d represent the bond length in nm obtained by the addition of the covalent radius of the atoms. N is the bond order given by the formula [35] "$N = \dfrac{d + 2r_1 - 3r_2}{2d + r_1 - 3r_2}$ where r_1, r_2 represent the covalent radius for a single and double bond".

The relation in (equation 32) is applicable to hold accurately for many simple polyatomic molecules and diatomic molecules respectively.

Somayayulu [36] formulated a relation to determine the "polyatomic force constants by covalent force constants and electronegativities" as follow:

$$K_{AB} = \left(K_{AA}K_{BB}\right)^{1/2} + \left(\chi_A - \chi_B\right)^2 \qquad (25)$$

K_{AB} denotes the force constant for heteropolar bond A-B, K_{AA} & K_{BB} represent the "force constants" for homopolar bonds "A–A & B–B". The values of force constants for Te-Te, Ga-Ga Se–Se and Ge–Ge are 1.25 eV, 0.24 eV, 1.91 eV, 1.29 eV [36, 37]. The manually estimated theoretically values of wavenumber (ν) along with reduced mass and force constant are depicted in table 3.6.

Table 3.5: Types of bond formation, d, K_{AB} by Somayayulu, μ, ν by Gordy and Somayayulu.

Bonds	d(nm)	K_{AB} (eV)	$\mu \times (10^{-26})$ (kg U^{-1})	ν (cm^{-1}) Gordy	ν (cm^{-1}) Somayayulu
Ge-Ge	0.244	1.29	6.05	268.5	246
Ge-Te	0.265	1.27	7.71	229.3	217
Ge-Se	0.239	1.86	6.30	267.9	289
Ge-Ga	0.245	0.59	5.92	231.4	167.4
Te-Te	0.286	1.25	1.06	189	182
Te-Se	0.26	1.75	8.13	228.9	246.2
Te-Ga	0.268	0.63	7.51	233.8	153.6
Se-Se	0.234	1.91	6.58	302.9	287
Se-Ga	0.247	1.22	6.17	271	235.9
Ga-Ga	0.25	0.24	5.81	253.8	107.8

3.2.3.1 Qualitative explanation of absorption bands

Sometimes the small frequency vibrations may not detected by Raman spectroscopy due to prohibition of selection rules. For that case, far IR spectrum is the only means for detecting

the data. The absorption in the "FTIR spectroscopy" is a consequence of bending and stretching vibrations in the material.

Numerous approaches have been followed to discuss the structural and physical charcteristics of chalcogenide materials. In the Te based glassy materials, two approaches, such as "random covalent network model (RCNM) and chain crossing model (CCM)" plays a significant role in managing two and four-fold coordination in the material. For a Ge-Se binary system, Tronc [38] investigated the Raman scattering spectra and their optical properties. CCM describes the cross-linkage of two-fold coordination in Se with four-fold coordination Ge. Every Ge atom in the molecules makes the "heteropolar bond" with Se and Te. So the probability of Ge - Ge "homopolar bond" is forbidden [39]. The RCNM states that the sharing of all existing bonds in GeTeSe system such that Se-Ge, Te-Se, Te-Te, Ge-Ge, Se-Se, are affected by the compositional and "two and four-fold coordination" and not by any other factor *viz.* bond strength *etc.* The structure of materials has been described by "CBA proposed by Bicerno and Ovshinsky" [17] which states that atoms assemble preferably with the atoms of a dissimilar type instead of a similar one.

The far IR spectra of GeTeSeGa powdered samples have been shown in figures 3.13 & 3.14. For z =0, pure glassy alloy, *i.e.* having no Ga, comprises peaks at (89, 112, 151, 229 and 280) cm^{-1} respectively. A peak located at 280 cm^{-1} is allocated to the Raman mode of $GeSe_2$, which agrees with "Ball *et al*." [40]. The peak situated at 229 cm^{-1} is allotted to $GeTe_4$ tetrahedral, which agrees with the earlier results [41]. While the peak located at 151 cm^{-1}has been labelled to the homopolar Te-Te bond [42], the peak at 85 cm^{-1} -90 cm^{-1} resembles V_2 (E) bending modes of $GeTe_4$ tetrahedra according to the literature data [43]. The fragile absorption peaks in the infrared spectrum can be because of Raman permitted modes of small crystal-like vestige [44].
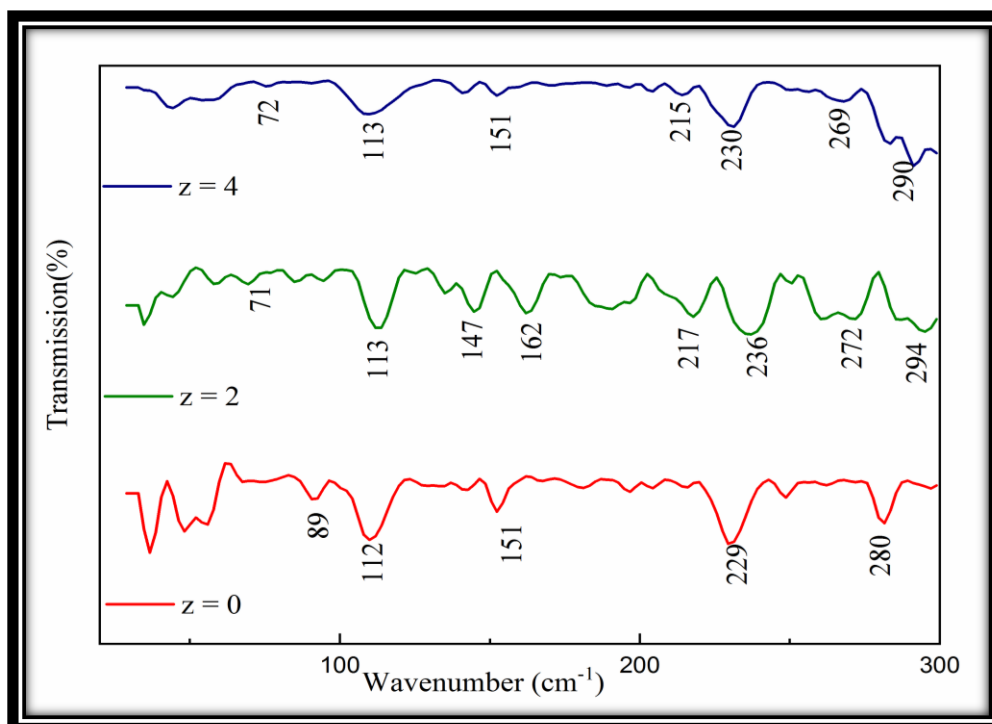
Figure 3.13: Far-IR spectra of $Ge_{10}Te_{80}Se_{10-z}Ga_z$ (z = 0 to 4) samples
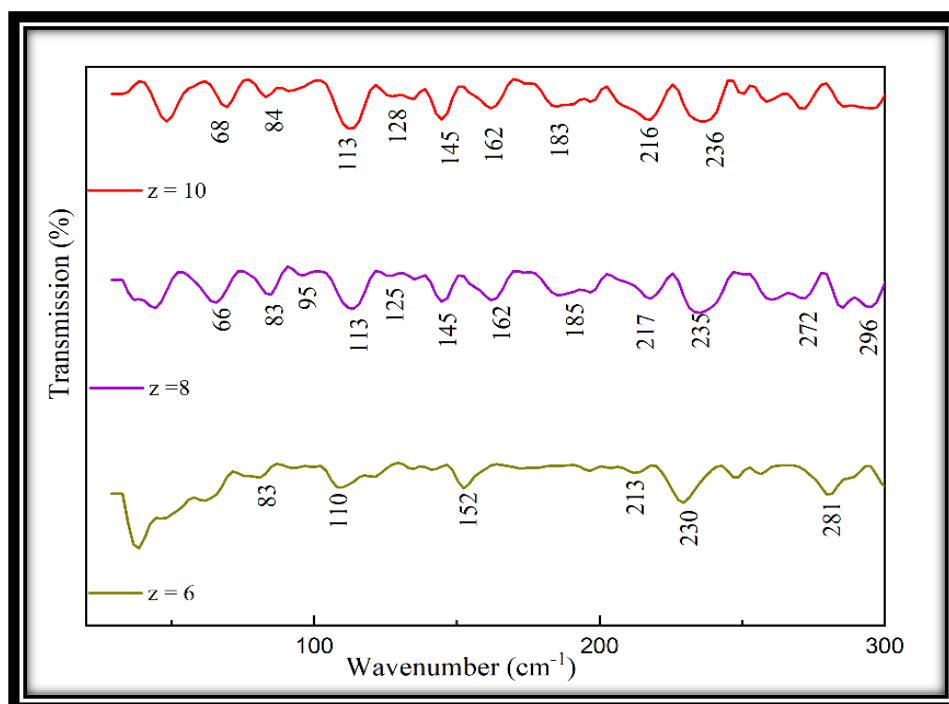
Figure 3.14: Far-IR spectra of $Ge_{10}Te_{80}Se_{10-z}Ga_z$ (z = 6 to 10) samples

With the incorporation of Ga in the $Ge_{10}Te_{80}Se_8$ system, the peak at (71, 113, 147 ,162, 217, 236, 272 , 294) cm^{-1} has been detected (figure 3.14). The bonding configuration of Ga in the GeTeSe material is still unclear. Some researchers [45] revealed that Ga possesses three-fold coordination that concerns the covalent bonds with the antibonding p electrons of Te; *i.e.* Ga atom does not form covalent network with GeTe alloy. However, several researchers reported [46] four-fold coordination of Ga which binds immediately into Ge-Ga-Te tetrahedral system. The peak situated at 272 cm^{-1} and 294 cm^{-1} has been assigned to the $GeSe_2$ mode. The band originated at 236 cm^{-1} represents $GeTe_4$ tetrahedral in which is in agreement with the previously stated data by [41]. With the incorporation of Ga within the GeTeSe system, Ga chooses to get into the tetrahedra outrigger site of Te and causes decrease in stress. It occurs merely because of the higher atomic radius of Ga (1.35Å) compared to Se (1.17Å). The incorporation of Ga leads to the existence of new peak at 217 cm^{-1}, which may be linked to the antisymmetric stretching of $GeTe_4$ tetrahedral [41, 47]. The peak detected at 147 cm^{-1} (z =2) maybe designated to the vibrations of Te-Te bonds [44, 42, 48]. However the same peaks are obtained at (151, 152, 145) cm^{-1} for z = 4 at.% to 10 at. % respectively. Similarly, the band recognized at 113 cm^{-1} is assigned to the tetrahedron $GeTe_4$ [47]. The peaks at 110 cm^{-1}, 113 cm^{-1} isalso being acknowledged in other compositions respectively. The peaks at 85 to 90 cm^{-1} are ascribed to the V_2 (E) bending modes of $GeTe_4$ tetrahedra for all compositions (table 3.7)[43]. The composition is chalcogens rich, consequently, the existence of a Ge-Ge homopolar bond is forbidden.

Table 3.6: Several absorption peaks positions in amorphous GeTeSeGa system

S.No	Peak position	Assignment (From Literature)
1.	269 cm^{-1} to 296 cm^{-1}	GeSe$_2$ [40]
2.	229 cm^{-1} to 236 cm^{-1}	GeTe$_4$ [41]
3.	213 cm^{-1} to 217 cm^{-1}	GaTe$_4$ (anti symmetric stretching mode) [41,42,47]
4.	183 cm^{-1} to 185 cm^{-1}	Ga-Ga [50]
5.	162 cm^{-1}	GeTe$_2$ [47]
6.	145cm^{-1} to 151 cm^{-1}	Symmetric stretching vibration of Te-Te bond [41,42]
7.	125 cm^{-1} to 128 cm^{-1}	V$_1$(A1) Symmetric stretching mode of GeTe$_4$, GaTe$_4$ [47]
8.	112 cm^{-1} to 113 cm^{-1}	Existence of Tetrahedron of GeTe$_4$ [42]
9.	83 cm^{-1} to 95 cm^{-1}	Assigned to tetrahedral bending modes of GeTe$_4$ [43]
10.	66 cm^{-1} to 68 cm^{-1}	Assigned to tetrahedral bending modes of GeTe$_4$ [43]

Amin *et al.* stated [8] that the chalcogens elements among Se and Te, Te has three-fold coordination hence excess Te in the system implies the formation of unsatisfied Te-Te bonds because of symmetric stretching of homopolar Te-Te bond.

It is revealed that the Raman signals of GaTe$_4$ and GeTe$_4$ tetrahedra overlap atleast in glassy systems, where the peaks or bands are broad and coinciding [49]. The absorption peak at 162cm^{-1} is assigned to GeTe$_2$ [44]. For z = 8 &10 the band arises in the range ~ 125 cm^{-1} to 128 cm^{-1}. This band is being ascribed to the V$_1$ (A$_1$) symmetric stretching mode of GeTe$_4$ and finally GaTe$_4$ tetrahedra. For z = 8 &10, the peak at 185cm^{-1} to 183 cm^{-1} has been

detected, which corresponds to Ga–Ga vibration as reported by "V. Nazabal *et al*." at 180 cm^{-1} [50]. By the substitution of Ga in Ge-Te-Se material, Te–Te chains were divided and new Ga-Te bonds are formed.

It is known that Ga and Ge are local neighbours in the modern periodic table and have the equivalent size and electro-negativities [49]. Ga may build up the Te chain and frame a new glassy structure relating to Ga-(Te-Te)$_{3/2}$ triangles and Ge-(Te-Te)$_{4/2}$ tetrahedra. Thus, the appearance of homopolar Te-Te bonds is reduced in present glassy network [49].

"The optical band gap (E_g^{opt})" of the studied material reduces with Ga percentage. The reduction in optical bandgap may be attributed to the generation of Te-Ga bonds possessing lower bond energy compared to Ge-Se bonds (table 5). Additionally, the reduction in the E_g^{opt} may be because of the generation of Te-Te bonds. By the replacement of Se with Ga, the far-infrared investigation predicts that new Te-Ga bonds formed along with former bonds *viz* Te-Te, Ge-Te and Ge-Se. Te-Ga bond possesses smaller bond energy compared to other bonds. The lower bond energy corresponds to reduction in the values of the mean bond strength of the material.

Consequently, calculated energy gap (E_g^{th}) and optical bandgap (E_g^{opt}) of the material reduces. Moreover, the defects state increases with the increment in Ga concentration which further reduces the optical bandgap. Therefore, far-infrared outcomes support a decline in E_g^{opt}.

3.3 Conclusion

Theoretical investigation indicates that with the addition of Ga, the mean coordination number, density and counts of constraints of the material increase. The system behaves as overcoordinated and rigid. The values of the "lone pair of electrons" decrease with the enhancement of Ga addition. Transition temperature and mean bond energy enhances with the rise of Ga amount. Theoretical energy gap, electronegativity and cohesive energy shows decreasing behaviour with the rise of Ga content.

XRD study indicates the amorphous character of the prepared thin films. Far - IR study indicate that the inclusion of Ga leads to the formation of Te-Te bonds and Te-Ga bonds. The lower bond energy corresponds to reduction in the values of the mean bond strength

of the material. Consequently, the calculated energy gap and "optical bandgap" of the material reduces.

References

[1] J. S. Sanghera and I. D. Aggarwal., "Active and passive chalcogenide glass optical fibers for IR applications: a review," J. Non-Cryst. Solids, vol. 256, pp. 6-16, 1999.

[2] P. Sharma, N. Sharma, S. Sharda, S. C. Katyal, and V. Sharma., "Recent developments on the optical properties of thin films of chalcogenide glasses", Prog. Solid. State Ch, vol. 44, no. 4, pp. 131-141, 2016.

[3] X. H. Zhang, Y. Guimond, and Y. Bellec., "Production of complex chalcogenide glass optics by molding for thermal imaging", J. Non. Cryst. Solids, vol. 326–327, pp. 519–523, 2003.

[4] K. Singh, S. Kumari, H. Singh, N. Bala, P. Singh, A. Kumar and A. Thakur., " A review on GeTe thin film-based phase-change materials," Appl. Nanosci, pp.1-16, 2021.

[5] J. C. Phillips., "Topology of covalent non-crystalline solids: Short-range order In Chalcogenide Alloys", J. Non. Cryst. Solids, vol. 34, no. 2, pp. 153–181, 1979.

[6] J. C. Phillips., "Constraint Theory, vector Percolation and Glass formation", Solid State Commun, vol. 53, no. 8, pp. 699–702, 1985.

[7] P. Sharma, S. C. Katyal., "Effect of tellurium addition on the optical and physical properties of germanium selenide glassy semiconductors", Phys. B Condens. Matter, vol. 403, pp.3667–3671, 2008.

[8] G. A. M. Amin, A. F. Maged., "Compositional Dependence of the Physical Properties of $Ge_1Se_{9-x}Te_x$ Amorphous System," Mater. Chem. Phys, vol. 97, pp. 420–424, 2006.

[9] R. Golovchak, L. Calvez, B. Bureau, H. Jain, R. Golovchak, L. Calvez, B. Bureau, H. Jain., "Structural evolution of Ga–Ge–Te glasses by combined EXAFS and XPS analysis", J. Chem. Phys, vol. 139, 2013.

[10] T. Petkova, Y. Nedeva, P. Petkov., "Compositional trends of the properties in chalcogenide Ge–Se–Ga glasses", J. Optoelectron. Adv. Mater, vol. 3, pp. 855–860 2001.

[11]   P. Sharma., "Glass-forming ability and rigidity percolation in SeTePb lone-pair semiconductors", Appl. Phys. A, vol. 122, pp. 1–8, 2016.

[12]   L. Zhenhua., "Chemical bond approach to the chalcogenide glass forming tendency", J. Non-Cryst. Solids, vol. 127, pp. 298–305, 1991.

[13]   S. A. Fayek, M. R . Balboul, K. H. Marzouk., "Optical, electrical and thermal studies on $(As_2Se_3)_{3-x}(As_2Te_3)_x$ glasses", Thin Solid Films, vol. 515, pp. 7281, 2007.

[14]   M.F. M Vlcek., "Model of photoinduced changes of optical properties in amorphous layers and glasses of Ge–Sb–S, Ge–S, As–S and As–Se systems", J. Non-Cryst. Solids, vol. 98, pp. 1223–1226, 1987.

[15]   S.S. Fouad, M.S. El-Bana, P. Sharma, V. Sharma., "Analysis of chemical ordering and fragility for Ge–Se–In glasses", Appl. Phys. Mater. Sci. Process, vol. 120, pp. 137–143, 2015.

[16]   F. M. Peeters, J. T. Devreese., "Radius, self-induced potential, and number of virtual optical phonons of a polaron", Phys. Rev. B, vol. 31, pp. 4890–4899, 1985.

[17]   J. Bicerano, S.R. Ovshinsky., "Chemical bond approach to the structures of chalcogenide glasses with reversible switching properties, J.Non. Cryst. Solids, vol. 74, pp. 75–84, 1985.

[18]   L. Pauling., "The Nature of the Chemical Bond and the Structure of Molecules and Crystals", Cornell University Press, London, 1960.

[19]   D. R. Lide., "CRC Handbook of Chemistry and Physics", CRC Press, Florida, pp. 1415-1419, 2009.

[20]   S. S. Fouad., "A theoretical investigation of the correlation between the arbitrarily defined optical gap energy and the chemical bond in $Te_{46-x}As_{32+x}Ge_{10}Si_{12}$ system", Vacuum, vol. 52, pp. 505-508, 1999.

[21]   C. Benoit, P. Aigrain, M. Balkanski., "Selected constants relative to semiconductors", Pergamon Press, New York, 1961.

[22]   P. Jovari, A. Piarristeguy, R. Escalier, I. Kaban, J. Bednarcik, A. Pradel., "Short Range Orderand Stability of Amorphous Ge_xTe_{100-x} Alloys", J. Phys. Condens. Matter, vol. 25, no.19, pp. 195401, 2013.

[23]   V. Sadagopan, H.C. Gatos., "On the relationship of semiconductor compound propertiesand the average heats of atomization", Solid State Electron, vol. 8, pp. 529–534, 1965.

[24]   S. S. Fouad, A.H. Ammar, M.A. Ghazala., "The relationship between optical gap andchemical composition in Sb_xSe_{1-x} system", Phys. B, vol. 229, 1997.

[25]   R. T. Sanderson., "Principles of electronegativity Part I. General nature", J. Chem. Educ, vol. 65, pp. 112, 1988.

[26]   Y. Luo, J. Kerr., "Bond dissociation energies", CRC Handb. Chem. Phys, pp. 65–98, 2007.

[27]   L. Tichy and H. Ticha., "On the chemical threshold in chalcogenide glasses", Mater. Lett, vol. 21, pp. 313, 1994.

[28]   L. Tichy and H. Ticha., "Covalent bond approach to the glass-transition temperature of chalcogenide glasses", J. Non- Cryst. Solids, vol. 189, pp. 141, 1995.

[29]   S. S. Fouad, A. H. Ammar, M. A. Ghazala., "The relationship between optical gap and chemical composition in Sb_xSe_{1-x} system", Phys. B, pp. 229, 1997.

[30]   J. M. Saiter, J. Ledru, G. Saffarini, S. Benazeth., " About the Coordination Number of Indium in $Ge_xSe_{1-x-y}In_y$ Glasses", Mater. Lett, vol. 28, no.- 4-6, pp. 451-455, 1996.

[31]   N. Sharma, S. Sharda, V. Sharma, P. Sharma., "Far-infrared investigation of ternary Ge-Se-Sb and quaternary Ge-Se-Sb-Te chalcogenide glasses", J. Non. Cryst. Solids, vol. 375, pp. 114–118, 2013.

[32]   I. Quiroga, C. Corredor, F. Bellido, J. Vkzquez, P. Villares, R. J. Garay, " Infrared studies of a $Ge_{0.20}Sb_{0.05}Se_{0.75}$glassy semiconductor", J. Non-Cryst. Solids, vol. 196, pp. 183–186, 1996.

[33]   H. Singh, B. Raina and K. K. Bamzai., "Structural, spectroscopic, thermal, electrical and mechanical properties of lanthanum chloride coordinated with salicylic acid and lanthanum chloride coordinated with glycine and salicylic acid complexes", J. Mater. Sci.: Mater. Electron, vol. 32, no. 7, pp. 9044-90642021, 2021.

[34]   R. Verma, A. Chauhan, K. M . Batoo, M. Hadi, E. H . Raslan, R . Kumar, M. F. Ijaz and A. K. Assaifan., "Structural, optical, and electrical properties of

vanadium-doped, lead-free BCZT ceramics", J. Alloys Compd, vol. 869, pp.159520, 2021.

[35]   W. Gordy., "A relation between bond force constants, bond orders, bond lengths, and the electronegativities of the bonded atoms", J. Chem. Phys, vol. 14, pp. 305–320, 1946.

[36]   G. R. Somayajulu., "Dependence of force constant on electronegativity, bond strength and bond order. VII", J. Chem. Phys, vol. 28, pp. 814–821, 1958.

[37]   A. Rana, B. P. Singh, R. Sharma., "Structural and chemical changesin Ga doped Ge-S glassy alloy", J. Non. Cryst. Solids, vol. 523, pp. 119597, 2019.

[38]   P. Tronc, M. Bensoussan, A. Brenac and C. Sebenne., "Optical-absorption edge and Raman scattering in Ge_xSe_{1-x} glasses", Physical Review B, vol. 8, no. 12, pp. 5947 1973.

[39]   A. A. Wilhelm, C. Boussard Pledel, Q. Coulombier, J. Lucas, B. Bureau and P. Lucas., "Development of far- infrared transmitting Te based glasses suitable for carbon dioxide detection and space optics", Adv. Mater, vol. 19, no. 22, pp. 3796-3800, 2007.

[40]   G. J. Ball, J. M. Chamberlain., "Infrared structural studies of Ge_ySe_{1-y} glasses", J. Non. Cryst. Solids", vol. 29, pp. 239–248, 1978.

[41]   P. Nemec, V. Nazabal, M. Dussauze, H.L. Ma, Y. Bouyrie, X. H. Zhang., "Ga-Ge-Te amorphous thin films fabricated by pulsed laser deposition", Thin Solid Films, vol. 531, pp. 454–459, 2013.

[42]   P. Sharma, S.C. Katyal., "Far-infrared transmission and bondingarrangement in $Ge_{10}Se_{90-x}Te_x$ semiconducting glassy alloys", J. Non. Cryst. Solids, vol. 354, pp. 3836–3839, 2008.

[43]   E. M. Vinod, A. K. Singh, R. Ganesan, K. S. Sangunni., "Effect of selenium addition on the GeTe phase change memory alloys", J. Alloys Compd, vol. **537**, pp. 127–132, 2012.

[44]   D. R. Goyal, A.S. Maan., "Far-infrared absorption in amorphous $Sb_{15}Ge_xSe_{85-x}$ glasses", J. Non. Cryst. Solids, vol. 183, pp.182–185, 1995.

[45]   P. Jovari, I. Kaban, B. Bureau, A. Wilhelm, P. Lucas, B. Beuneu and D.A. Zajac., "Structure of Te-rich Te–Ge–X (X = I, Se, Ga) glasses", J. Phys. Condens. Matter, vol. 22, no. 40, pp. 404207, 2010.

[46]   I. Voleska, J. Akola, P. Jovari, J. Gutwirth, T. Wagner, T. Vasileiadis, R. O. Jones., "Structure, electronic, and vibrational properties of glassy $Ga_{11}Ge_{11}Te_{78}$: Experimentally constrained density functional study", Physical Review B, vol. 86, no. 9, pp. 094108 , 2012.

[47]   S. Sen, E.L Gjersing and B. G. Aitken., "Physical properties of $Ge_xAs_{2x}Te_{100-3x}$ glasses and Raman spectroscopic analysis of their short-range structure", J. Non. Cryst. Solids, vol. 356, no. 41-42, pp. 2083-2088, 2010.

[48]   N. Dong, Y. Chen, N. Wei, G. Wang, R. Wang, X. Shen and Q. Nie., "Optical and structural properties of Ge-Ga-Te amorphous thin films fabricated by magnetron sputtering", Infrared Phys. Technol, vol. 86, pp.181-186, 2017.

[49]   R. Svoboda and D. Brandova., "Crystallization behavior of $(GeTe_4)_x(GaTe_3)_{100-x}$ glasses for far-infrared optics applications", J. Alloys Compd, vol. 770, pp. 564-571, 2019.

[50]   A. Lecomte, V. Nazabal, & L. Calvez., " Ge-free chalcogenide glasses based on Ga-Sb-Se and their stabilization by iodine incorporation", J. Non. Cryst. Solids, vol. 481, pp. 543-547, 2018.

Optical Properties of GeTeSeGa chalcogenide thin films

➢ **Ekta Sharma**, P. B. Barman& Pankaj Sharma (2020). Evaluation of optical linear and non-linear parameters of thermally deposited GeTeSeGa thin films in NIR (1 µm -2.6 µm) wavelength range from their transmission spectra. **Optik: International Journal of Light and Electron Optics** (Volume 219, p.165181).SCI Indexed.

➢ **Ekta Sharma**, Pankaj Sharma (2020). Applicability of different models of energy bandgap and refractive index for chalcogenide thin films. **Materials Today: Proc**. (Volume 28, p.92-95). Scopus Indexed.

➢ **Ekta Sharma,** P.B.Barman & Pankaj Sharma (2022). On the structural and optical aspects of GeTeSeGa thermally evaporated semiconducting thin films for infrared applications. **The European Physical Journal Plus** (Volume 137, p. 358). SCI Indexed.

4. Optical properties

This chapter comprises of investigation of several optical constants *viz "*refractive index (n), absorption coefficient (α), optical band gap$\left(E_g^{opt}\right)$", optical density (D_{op}), extinction coefficient (k), penetration depth (ψ) and dispersion parameters (E_d and E_o) *etc*. "The non-linear parameters like non-linear refractive index (n_2) and non-linear susceptibility ($\chi^{(3)}$) have also been calculated". The two essential parameters like E_g^{opt} and n have been determined by the "Swanepoel approach and the Tauc extrapolation technique" [1, 2]. The influence of Ga on *Ge$_{10}$Te$_{80}$Se$_{10-z}$Ga$_z$ (z = 0 to 10)* chalcogenide thin films have been investigated to check the variation of "linear and non-linear optical properties". Due to low optical bandgap and high "linear and non-linear refractive index", the studied system may be used for optoelectronic applications. The optical properties have been realized by "UV-Vis-NIR spectroscopy" in the NIR range. Because of their applications in modern covalent, chalcogenide-based glasses have gained enormous attention. These glasses have several industrial uses due to its "thermal, optical and optoelectronic" properties. The properties of chalcogenides may be easily modified by adding various elements as well as the method of synthesis and film deposition on a substrate.

4.1. Experimental details

The bulk samples of GeTeSeGa chalcogenide system are prepared by the traditional "melt quenching technique". The thin films of the prepared samples are deposited by thermal evaporation method. The details of synthesis of bulk samples and thin films have already been discussed in chapter 2.

4.2 Results and discussions

4.2.1   Linear parameters

4.2.1.1 Determination of "thickness and index of refraction of the thin film"

"The refractive index (n)" of the thin films has been evaluated by Swanepoel approach [1]. Figure 4.1 illustrates the transmission spectrum of prepared chalcogenide thin films. It is observed from figure 4.1 that with the addition of Ga in the system, the absorption edge moved to high wavelength region (red-shifted).Presence of various interference fringes indicates that the films are uniform and smooth, *i.e.* no absorption or scattering occurs at the longer wavelength. The strong absorption occurs due to the electronic band transitions

of carriers. According to Swanepoel, [1] the minima and maxima of transmission spectra can be utilized to measure the optical properties. The study of chalcogenide glasses by this method is reported by several researchers [,4, 5]. By utilizing minima and maxima, the continuous envelope has been drawn using software (figure 4.2).
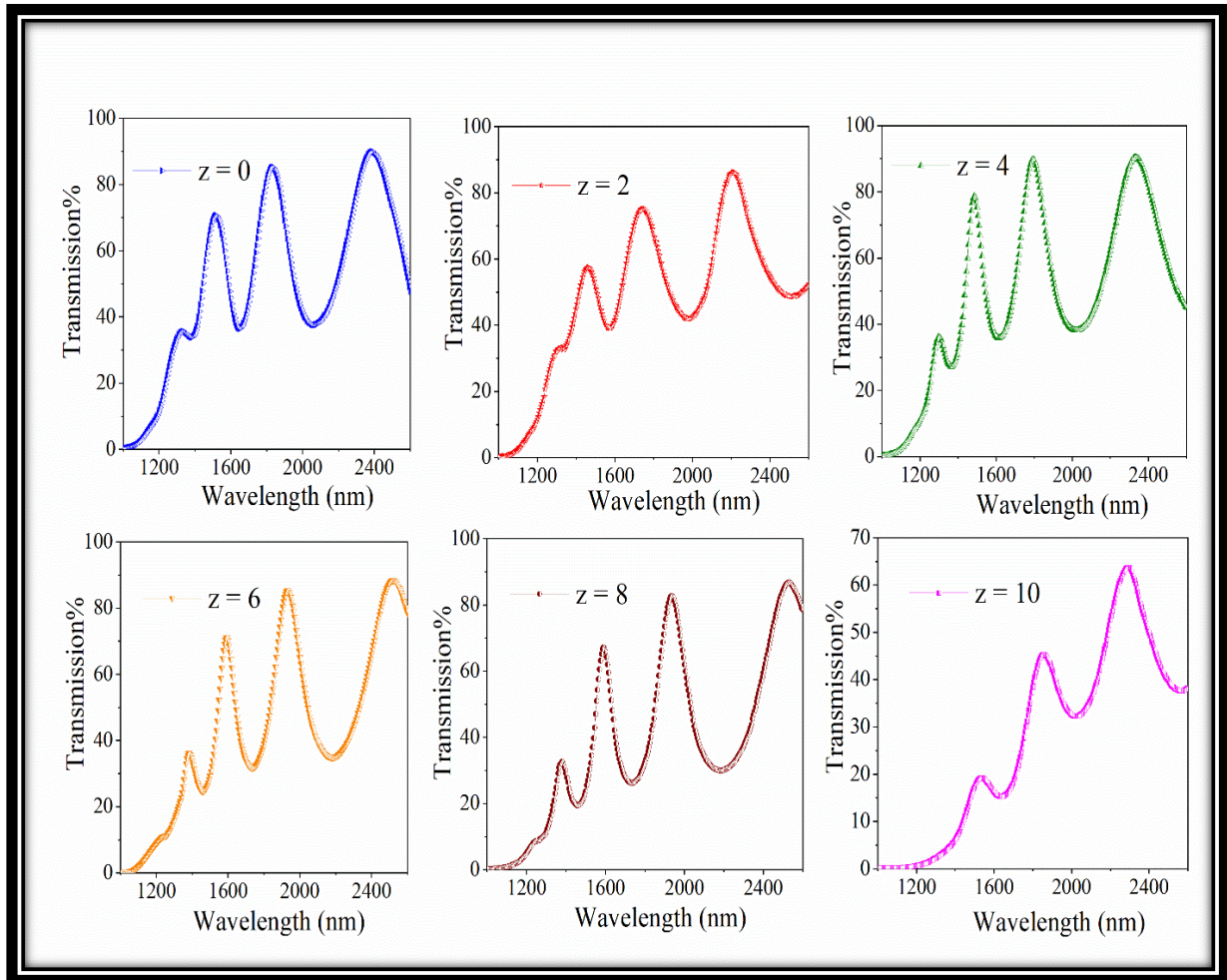
Figure 4.1: Transmission spectra of *Ge$_{10}$Te$_{80}$Se$_{10-z}$Ga$_z$ (z = 0 to 10)* chalcogenide thin films
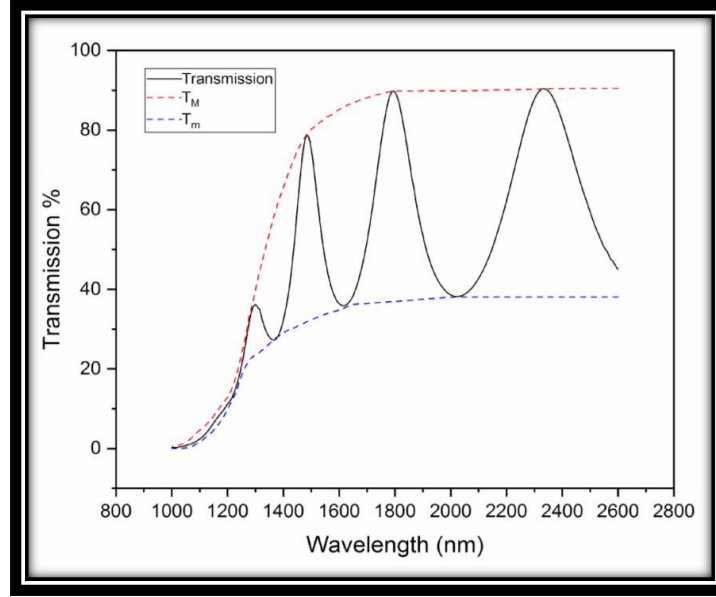
Figure 4.2: Graph of wavelength versus transmission showing upper and lower
envelope.

For all regions (transparent, medium and weak absorption region), the index of refraction
(n) is estimated by the relationship [1]:

$$n = [M + (M^2 - s^2)^{0.5}]^{1/2} \qquad (26)$$

$$M = 2s\frac{T_M - T_m}{T_M T_m} + \frac{(s^2 + 1)}{2} \qquad \text{for weak and medium absorption} \qquad 26(b)$$

$$\text{where } M = \frac{2s}{T_m} - \frac{(s^2 + 1)}{2} \text{ , for the transparent region and} \qquad 26(a)$$

T_m & T_M represent the minima & maxima of transmittance at particular wavelength (λ) and
s represent the indices of refraction of glass having a value of 1.51. The absorbance (*x*) has
been estimated by:

$$\text{``} x = \frac{E_M - [E_M{}^2 - (n^2 - 1)^3 (n^2 - s^4)]^{1/2}}{(n-1)^3 (n - s^2)} \qquad (27)$$

$$\text{where } E_M = \frac{8n^2 s}{T_M} + (n^2 - 1)(n^2 - s^2) \text{''} \qquad \qquad 27(a)$$

The basic interference equation is : $2nd = m_o \lambda$, where m_o denotes the integer for maxima & half-integer for minima. The film thickness is obtained using the relation [1]:

$$d = \frac{\lambda_1 \lambda_2}{2(\lambda_1 n_2 - \lambda_2 n_1)} \qquad \qquad (28)$$

where n_1 & n_2 are index of refraction of two nearby minima and maxima at "wavelengths λ_1 & λ_2" respectively. The values of d_1 and d_2 are calculated by substituting d_1 and d_2 in place of d in equation 28. The mean thickness (d_1) value has been employed to calculate the order number for distinct minima and maxima. Thereafter, corrected thickness (d_2) has estimated with the help of half-integer and exact integer value of m_o. The new values of d_2 and m_o have been utilized to determine final n values. The obtained values of thickness (d_1 and d_2) with Ga concentration have been tabulated in table 4.1.

Table 4.1: Values of thickness d_1 and d_2 for GeTeSeGa thin films

z	d_1(nm)	d_2(nm)
0	1031	1023
2	1092	972
4	950.5	989.8
6	1001	998
8	936.5	949.3
10	596	581

By the addition of Ga, the absorption edge is red shifted which leads in reduction of "band gap and also rise in refractive index". Further the variation in the film thickness values also changes with Ga content. The final n values are fitted using the "Cauchy dispersion equation ; $n = a + \frac{b}{\lambda^2}$" and the least square fitting approach is used to determine the values of a and b. The variation of n with λ is shown in figure 4.3.
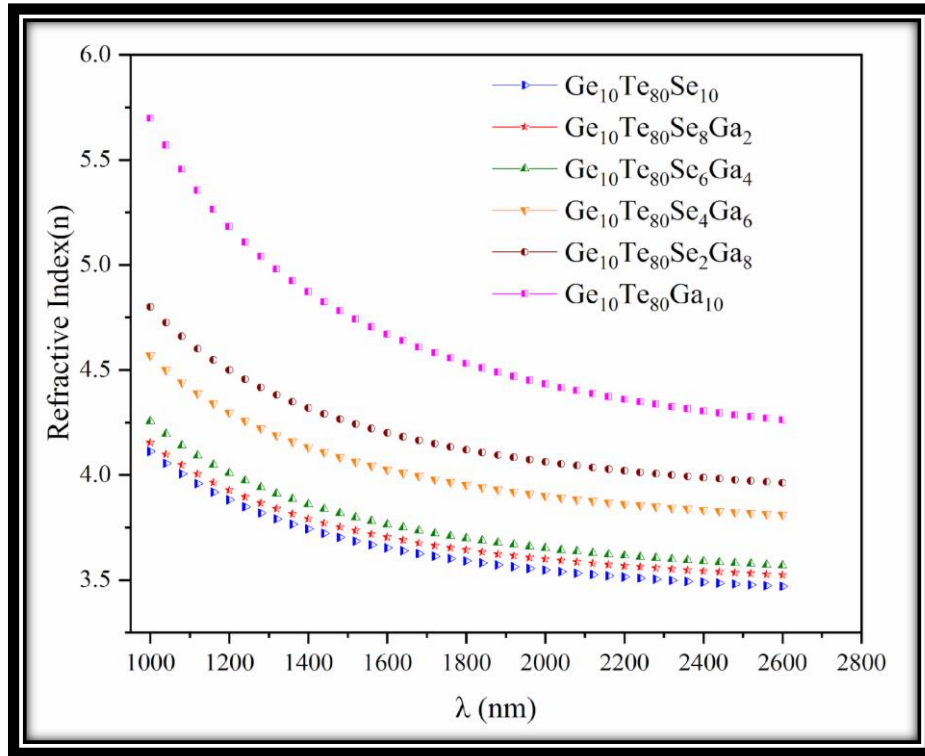
Figure 4.3: Dependence of n values with λ for GeTeSeGa thin films

It is noted from figure 4.3, that the "refractive index" values decrease as the wavelength increases. This decline may be ascribed as the "normal dispersion" response of the material. With the enhancement of Ga content, the refractive index of GeTeSeGa thin films increases. It may be attributed to the replacement of less dense element Se with the high denser element Ga. It has already been discussed in chapter 3 that by adding Ga in the system, the density values increases, hence the larger density values lead to enhancement in refractive index of the system. The Lorentz–Lorenz connection may account for the increase in refractive index [6]. The relation states that higher the atomic radii, greater is the polarization, thus greater is the refractive index [7]. Larger values of the index of refraction found for the samples are ideal for making IR mirrors and filters.

Absorption coefficient (α) is determined as follows [1,8]:

$$\alpha = \frac{1}{d}\ln\left(\frac{1}{x}\right) \qquad (29)$$

Where x and d denotes the absorbance and thickness of thin-film (cm). The dependence of α on the hν is depicted in figure 4.4.
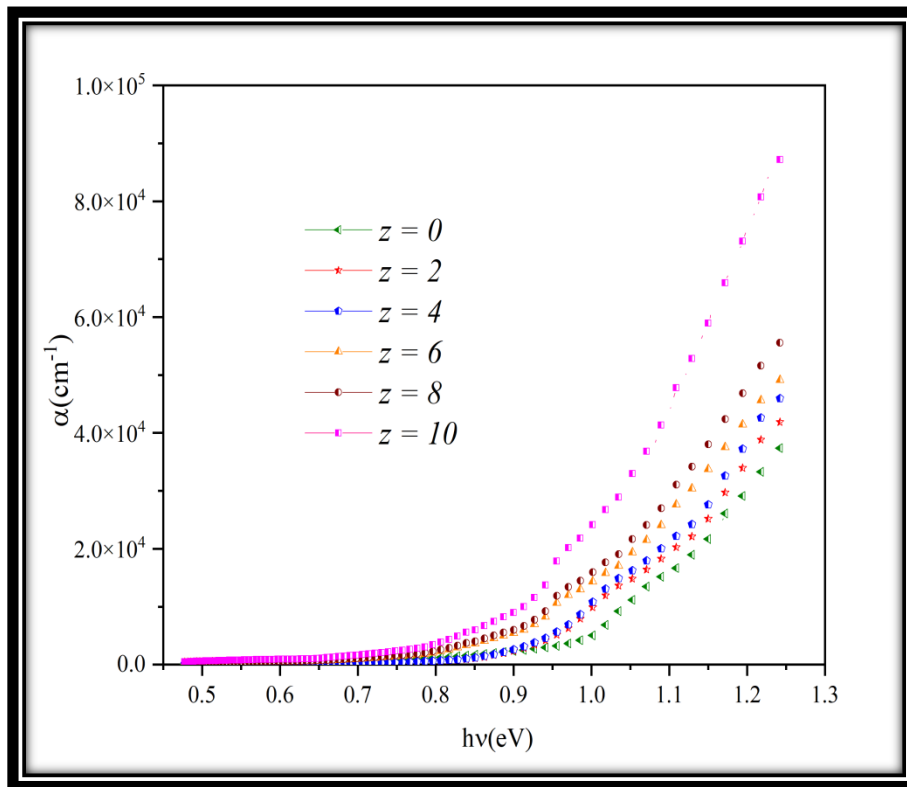
Figure 4.4: Variation of absorption coefficient with photon energy

Figure 4.1 clearly depicts that by increasing of Ga, the absorption edge is shifted towards higher wavelength region, *i.e.* red shift in the wavelength, which results in the rising of α value with Ga content.

The "extinction coefficient (k)" is described as the amount of em radiation lost per unit distance of the participating medium owing to scattering and absorption. The values of k have been obtained by the equation [1, 9]:

$$k = \frac{\alpha\lambda}{4\pi} \tag{30}$$

The values of the extinction coefficient of the investigated system rises as the concentration of Ga increases (figure 4.5).
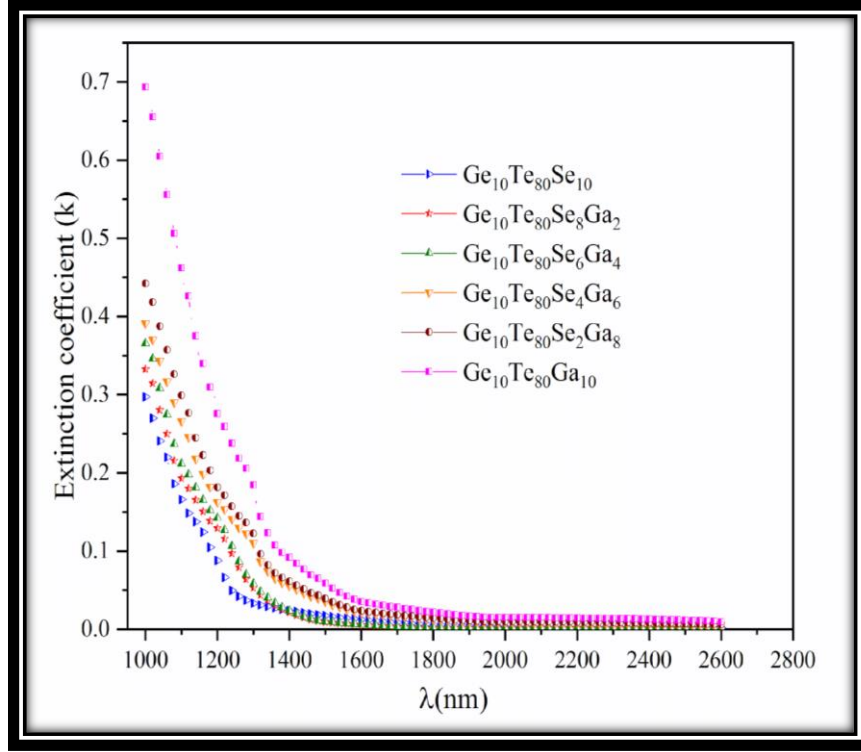
Figure 4.5: Plot of Wavelength and extinction coefficient for GeTeSeGa thin films

It is noted from equation 30 that k is proportional to α. Hence increase in α with Ga content leads to increment in k values.

"Dielectric constant (ε)" of the materials is related to the magnetic energies, dissipation energy and storage. The "real dielectric constant (ε_r)" determines how much it slows down the light propagation in materials whereas "imaginary part (ε_i)" of the "dielectric constant" describes a material's ability to completely absorb energy from a time-changing electric field. The dielectric constant (ε) is given by [10]:

$$\varepsilon = \varepsilon_r - \varepsilon_i = (n - ik)^2 \qquad (31)$$

$$\varepsilon_r = n^2 - k^2 \qquad 31(a)$$

$$\varepsilon_i = 2nk \qquad 31(b)$$

107

Figures 4.6 and 4.7 show how the "real and imaginary parts of the dielectric constant" vary with wavelength.
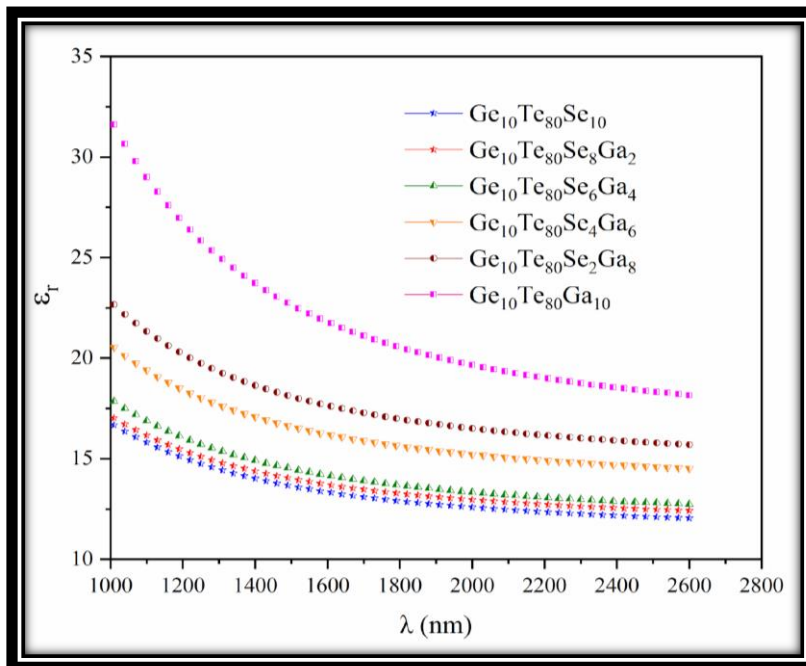
Figure 4.6: Plot of ε_r with λ for GeTeSeGa thin films
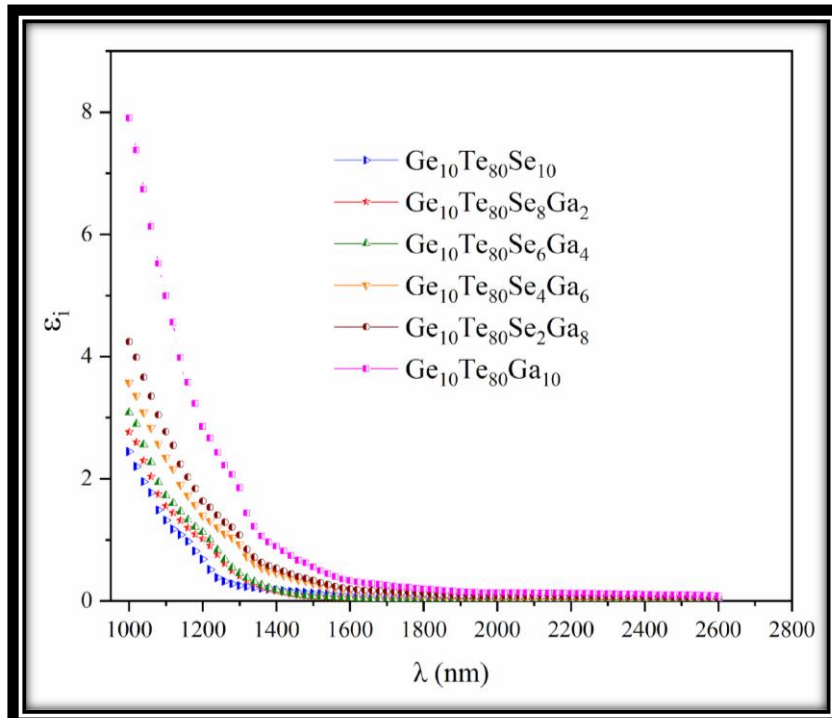
Figure 4.7: Plot between ε_i and λ for GeTeSeGa thin films

With increasing wavelength, ε_r & ε_i of the "dielectric constant" of examined thin films depict a comparable diminishing behaviour as that of n and k. It is already discussed in figure 4.3 and 4.5 that by increasing of Ga, the values of n and k enhances. Moreover, ε_r & ε_i are related to n and k (equations 31(a) and 31(b)). So increase in both the parameters (n and k) with the Ga content also results in the enhancement of ε_r & ε_i values.

4.2.1.2 Determination of WDD / Single oscillator parameters

Wemple - Di Domenico (WDD) [9, 10] suggested the single oscillator model to describe the dispersion energy parameters E_d and E_o. E_o and E_d denote the energy of a single oscillator and the energy of dispersion respectively. The dispersion in n of the studied films has been fitted by the WDD model.

The n value is determined by using the equation [11, 12]:

$$n^2 - 1 = \frac{E_o E_d}{E_o^2 - (h\upsilon)^2} \tag{32}$$

E_o also referred as "average energy gap ($E_g{}^{WDD}$)" has been observed to decline as the Ga increases. Tanaka [13] proposed the relation: $E_o = 2E_g{}^{WDD}$. The single oscillator parameters (E_d and E_o) are obtained from the linear graph of $(n^2-1)^{-1}$ with $(h\upsilon)^2$ as plotted in figure 4.8.
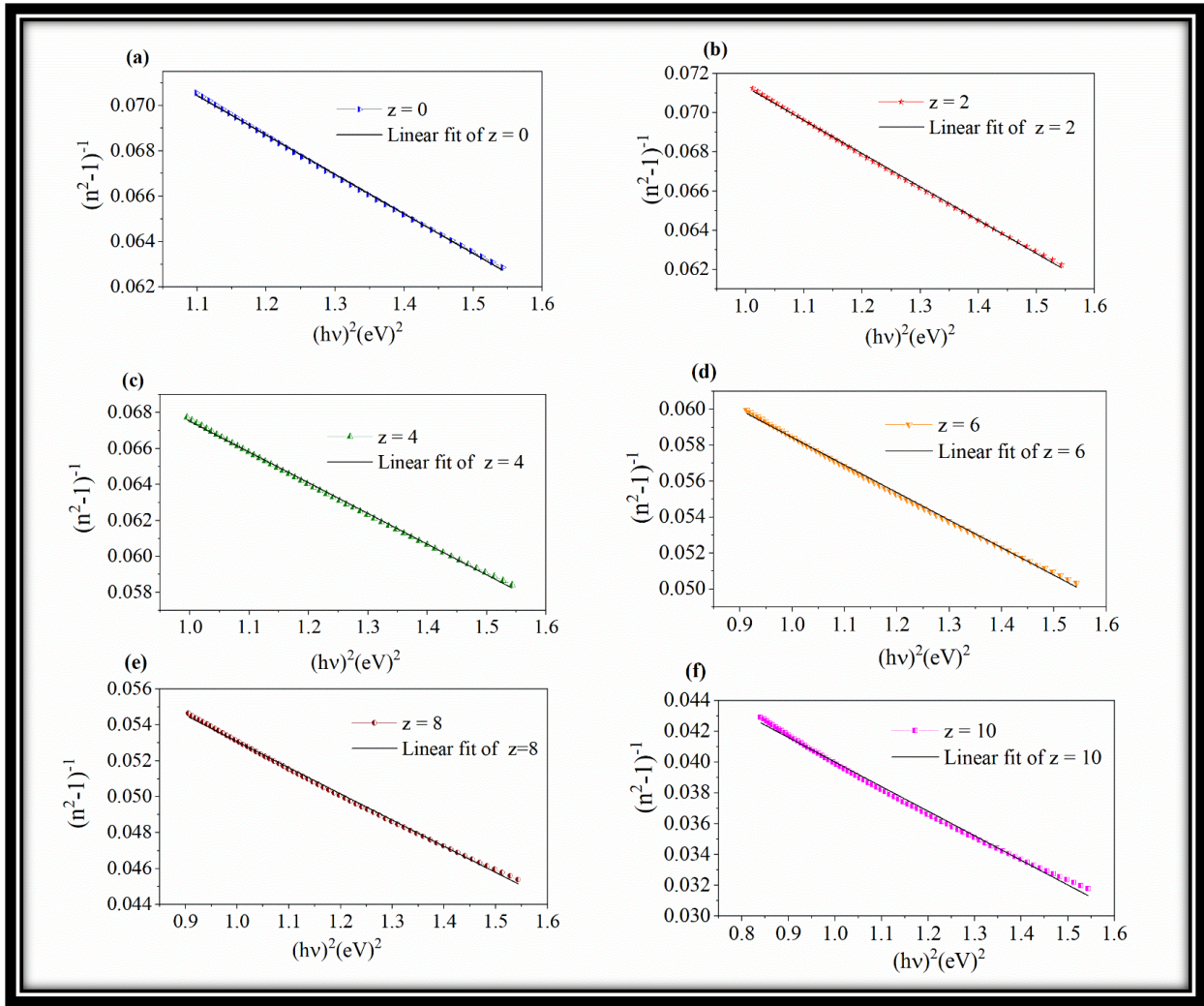
Figure 4.8: Dependence of "$(n^2-1)^{-1}$ with $(h\upsilon)^2$" for system

The values of E_o and E_d are estimated by linear fitting the plot and calculated with the help of intercepts E_o/E_d and slope $(E_o E_d)^{-1}$. The values of parameter E_o is observed to decrease while E_d increases (table 4.2). E_o is connected to the cohesive energy measures mean bond strength. It has been reported in chapter 3 that by adding Ga in the GeTeSeGa chalcogenide system, the mean bond strength reduces [14]. Table 4.2 clearly illustrates that with the enhancement of Ga, the WDD parameters (E_o and E_d) vary.

The dispersion parameter E_d exhibits the similar pattern as that of the film refractive index and both increase with Ga content. It is already discussed in chapter 3 that by adding Ga concentration, the values of <r> increases and so E_d increases.

Table 4.2: "Calculated values of dispersed energy (E_d), single oscillator energy (E_o), bandgap determined from single oscillator model (E_g), dielectric constant at a higher frequency (ε_∞) , static refractive index (n_o), moments of εi, (M_{-1}& M_{-3})".

z	E_d(eV)	E_o (eV)	E_g^{WDD} (eV)	n_o	ε_∞	M_{-1}	M_{-3}
0	25.22	2.26	1.13	3.48	11.917	10.92	2.19
2	25.44	2.24	1.12	3.50	12.31	11.31	2.23
4	25.71	2.22	1.11	3.54	12.567	11.57	2.33
6	29.72	2.19	1.09	3.81	14.55	13.55	2.81
8	31.84	2.15	1.07	3.97	15.673	14.67	3.04
10	36.49	1.95	0.98	4.43	18.86	18.64	4.86

The "static refractive index (n_o)" is obtained by the formula:

$$n_o = \left[1 + \frac{E_d}{E_o}\right]^{0.5} \tag{33}$$

The enhanced values of n_o with the rising Ga are listed in table 4.2. The increment in n_o values may also be attributed to the substitution of less dense Se (4.819gcm^{-3}) with more dense Ga (5.91gcm^{-3}) [14]. "Dielectric constant at a higher frequency (ε_∞)" is estimated by the relation $\varepsilon_\infty = (n_o)^2$. Table 4.2 shows that ε_∞ value enhances with Ga concentration. As ε_∞ is directly proportional to the square of n_o, hence increase in ε_∞ may be due to increase in n_o values.

The WDD parameters "E_o and E_d" are associated to "imaginary part of dielectric constant *i.e.*

ε_i =2nk". The optical moments "(M_{-1} and M_{-3})" has been determined as [11, 12]

$$\text{``} E_o^2 = \frac{M_{-1}}{M_{-3}} \qquad \text{and} \qquad E_d^2 = \frac{M_{-1}^3}{M_{-3}} \tag{34}$$

which may be written in revised form as:

$$M_{-1} = \frac{E_d}{E_o} \quad \text{and} \quad M_{-3} = \frac{M_{-1}}{E_o^2} \text{''} \tag{34(a)}$$

By raising of Ga content, the values of these parameters "(M_{-1} and M_{-3})" enhances (table 4.2). It is mentioned earlier that M_{-1} and M_{-3} are related with ε_i. Hence increase in ε_i values with Ga content (figure 4.7) led to increase in both the parameters (M_{-1} and M_{-3}).

The dispersion parameter (β) is given by [11, 12]:

$$E_d = \beta Z_a N_p N_e \tag{35}$$

where N_p represent the effective coordination number, N_e denotes to the "total count of valence electron per anion, and $Z_a=2$ refers to formal valency of the anion. The parameter β has two values $i.e.$"

$$0.37 \pm 0.04 eV \text{ for covalent (crystalline \& amorphous) solids, and} \tag{35 (a)}$$

$$0.26 \pm 0.03 eV \qquad \text{for ionic solids} \tag{35 (b)}$$

The values of above-mentioned parameter have been obtained by revising the base composition as $(Ge_1Ga_0)_{10}Te_{80}Se_{10}$. Now considering the hypothetical cation Ge_1Ga_0, $N_e = (10 \times 4 + 80 \times 6 + 10 * 6 + 0 * 3)/90 \approx 6.444$, $N_p = (1 \times 4) = 4$, $\beta=0.41$ and Za=2, the value of E_d has been calculated using equation 35 : E_d=21.14 eV. Similarly, the values of N_e, N_p and E_d for other compositions are listed in table 4.3. For all compositions, the values $\beta = 0.41$ and Za = 2 were used.

Table 4.3: Values of N_c, N_p and E_d and field strength (f) for different values of z

z	Proposed cation	N_e	N_p	E_d	f
0	Ge_1Ga_0	6.4	4	21.13	54.46
2	$Ge_{0.833}Ga_{0.166}$	6.5	4	21.39	57.20
4	$Ge_{0.714}Ga_{0.288}$	6.6	4	21.66	57.30
6	$Ge_{0.625}Ga_{0.375}$	6.7	4	21.94	65.18
8	$Ge_{0.55556}Ga_{0.4444}$	6.8	4	22.24	70.87
10	$Ge_{0.5}Ga_{0.5}$	6.9	4	22.55	71.42

The E_d values enhance with the rising concentration of Ga in the pure system. However, the value of cation's effective coordination number N_p remains constant. It is well known that if two atoms involved in the bond formation having large difference in their electronegativities (Pauling electronegativity), then the bond will be more ionic. With the rising amount of Ga in the system, E_d values rises as explained earlier. The value of N_p remains the same while N_e rises. The observed rise in values of E_d and N_e indicate the more interaction among structural layers and may be associated with the rise in compactness values in the system as discussed in chapter 3.

It is already mentioned in chapter 3 that the effective coordination number & average coordination number of the material enhance with the Ga concentration, so the E_d values also enhances [10]. Oscillator strength (f) has been obtained from relation [15]:

$$f = E_o E_d \qquad (36)$$

It is noted that as the gallium content rises, the value of oscillator strength rises substantially (table 4.3). Since the f values are related to E_d and E_o, variation in these parameters led to increase in f values with Ga content.

4.2.1.3 Optical density and depth of penetration

The absorption coefficient plays an essential role in defining other parameters *viz.* bandgap, skin depth (ψ), optical density (D_{op}) *etc.* Optical density may be described as the degree to which a refractive medium impedes the beam's transmitted rays. The parameter D_{op} in thin films results from scattering and refraction of light, which also implies the speed of the em wave in the system.

The optical density of the investigated thin films is obtained by the relation [16]:

$$D_{op} = \alpha d \tag{37}$$

Figure 4.9 displays the variation of D_{op} with $h\upsilon$. From the figure, it depicts that at lower photon energy, zero absorbance has been noted which indicates an enhancement in the transmittance of the electromagnetic spectrum in the lower photon energy region. This response indicates the high infrared transmittance window in GeTeSeGa chalcogenide thin films. With the rise in Ga content, the values of optical density also increased. It is already mentioned that α plays an important role to determine D_{op} values and also D_{op} is proportional to α. The increase in D_{op} values with the Ga content may be due to the increase in α (figure 4.4) with the addition of Ga content.

114
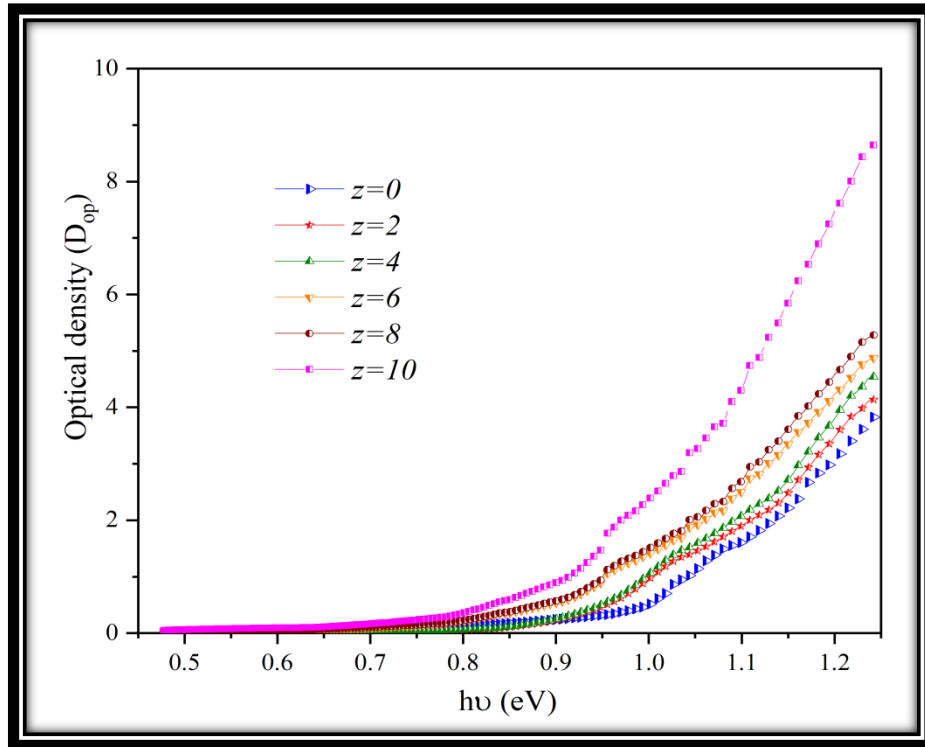
Figure 4.9: Variation of optical density with photon energy for GeTeSeGa system

Penetration depth or skin depth (ψ) is a measure of how deep the light or any em radiation can penetrate into a material. It is referred to as the depth at which the optical density of the incident light becomes 1/e of its value at the film's surface.

The penetration depth depicts its dependency on α as [16,17]:

$$\psi(cm) = \frac{1}{\alpha} \tag{38}$$

Figure 4.10 shows the dependency of ψ on the photon energy (hυ) for thin films
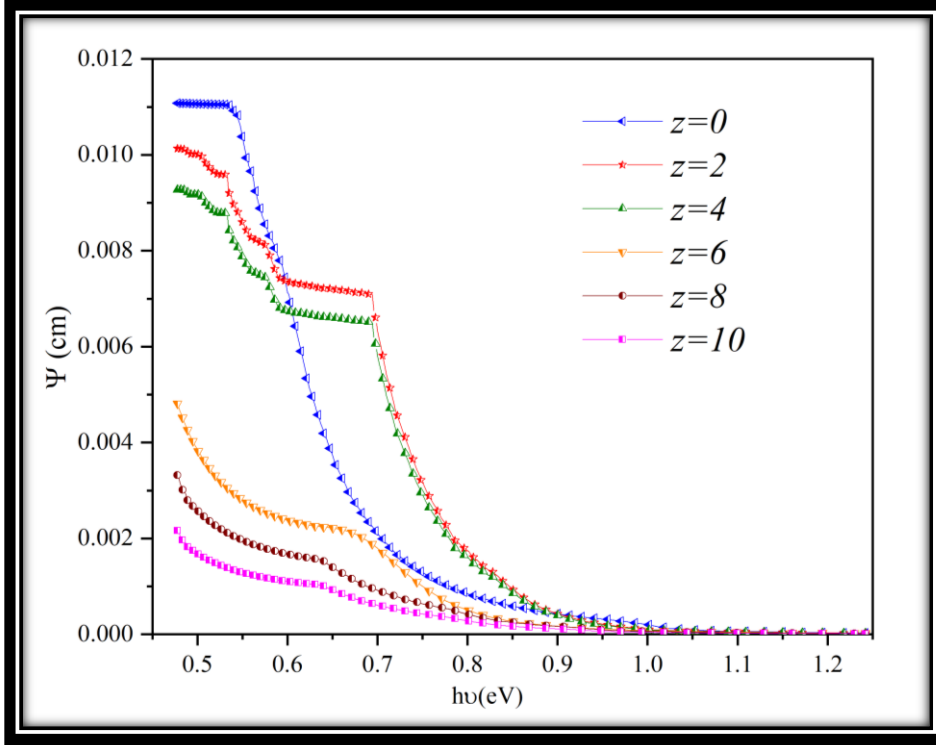
Figure 4.10: Plot of penetration or skin depth with photon energy

It is observed from figure 4.10 that with the rise of photon energy, the value of skin depth declines for all samples which may be due to increase in α value (equation 46) with the Ga content.

For the energy lesser than (hυ), the absorption effect disappears. The photon energy at which the skin depth depicts zero value is termed as cutoff energy. For all the investigated samples, $E_{cuttoff} = 0.93eV$ and the corresponding $\lambda_{cuttoff} = 1330nm$.Single mode optical fibre has cutoff wavelengths in the range 1300nm to 1550nm. The wavelength of the studied system also lies in the same range indicating the materials may be appropriate for single mode optical fibres.

The "optical conductivity (σ)" may be linked to the "imaginary and real part of dielectric constant (ε_i & ε_r)" by the correlation [18]:

$$\left.\begin{cases} \sigma = \sigma^{'} + i\sigma^{"} \\ \varepsilon = \varepsilon_r + i\varepsilon_i \\ \sigma^{'} = \omega\varepsilon_i\varepsilon_o \\ \sigma^{"} = \omega\varepsilon_r\varepsilon_o \end{cases}\right\}$$

$$(39)$$

116

where σ' and σ'' represent "real & imaginary parts of the optical conductivity, ω represents the angular frequency". Figures 4.11 & 4.12 illustrate the dependence of optical conductivity (σ' and σ'') with photon energy. It has been found from the figures that optical conductivity raises with the rise of photon energy. This response could be due to electron excitation as the incident energy increases.
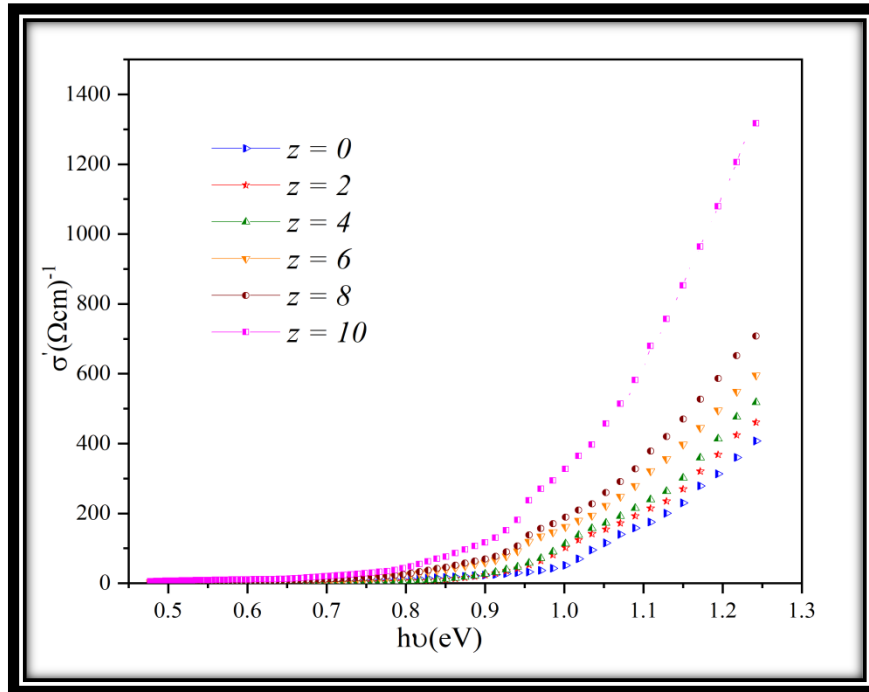
Figure 4.11: Plot of "real part of optical conductivity versus photon energy"
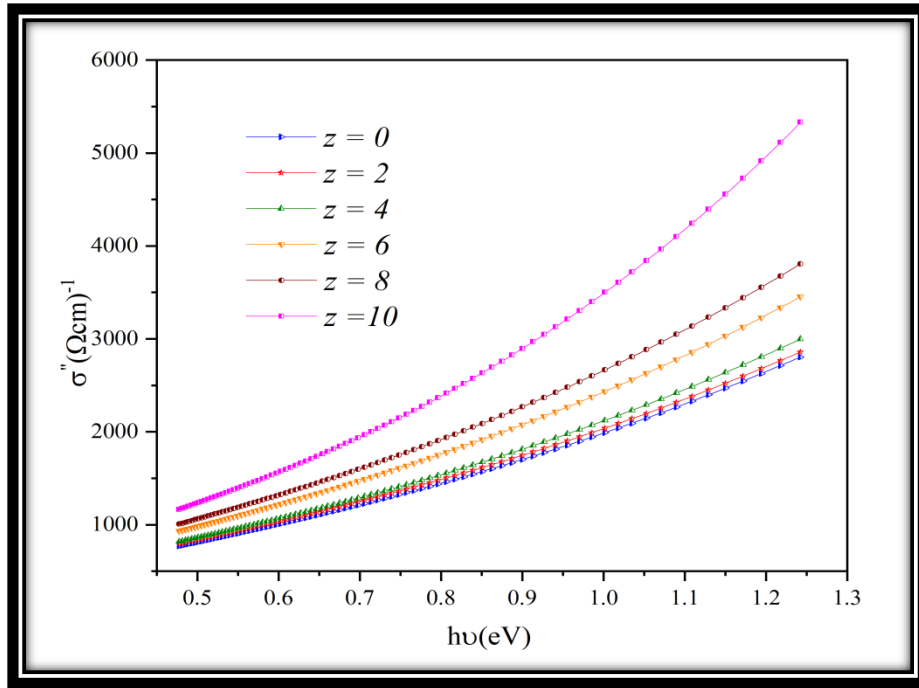
Figure 4.12: Graph of "imaginary part of optical conductivity vs photon energy"

It is known that σ ($\sigma^{'}$ and $\sigma^{''}$) parameter is related to ε_r and ε_i of dielectric constant. It is found that both ε_r & ε_i increases with the Ga amount. Also ε (ε_r & ε_i) are associated to n and k, so increase in all the four parameters led to increase in optical conductivity with the increase of Ga content.

4.2.1.4 "Optical band gap"

"The optical band gap (E_g^{opt})" for GeTeSeGa thin films in the high absorption region ($\alpha \geq 10^4 cm^{-1}$) is determined by the Tauc formula [2, 19-21]:

$$\alpha h\upsilon = B(h\upsilon - E_g^{opt})^m \tag{40}$$

where E_g^{opt} represents the "optical band gap" and B represents the tailing parameter. The values of m in the equation 40 have different values for allowed and non-allowed transitions, *i.e.* m = 2 for in-direct allowed and m = 1/2 for direct allowed transition [22, 23]. The response of $(\alpha h\upsilon)^{0.5}$ with $h\upsilon_{(ev)}$ has been plotted in figure 4.13. The value of E_g^{opt} is obtained by extrapolating $(\alpha h\upsilon)^{0.5} \to 0$. The obtained values of the "optical band gap" have been listed in table 4. It is found that with the rise in Ga concentration, the

118

absorption edge shifts towards the higher wavelength indicating the reduction in E_g^{opt}. Conferring to Mott and Davis [24], the E_g^{opt} is indirectly linked to the "width of localized states" and defects. The reduction in E_g^{opt} is in good agreement with the mean bond strength (CE) and E_g^{th} with the raise of Ga content. The shrinkage of E_g^{opt} of the system may be attributed to the presence of high localized states. The enhancement of defects and disorders in the network may be due to the generation of Ga-Te bonds with the rise in Ga concentration. This bandgap behaviour of the studied system is in consistent with the literature data [25, 26].
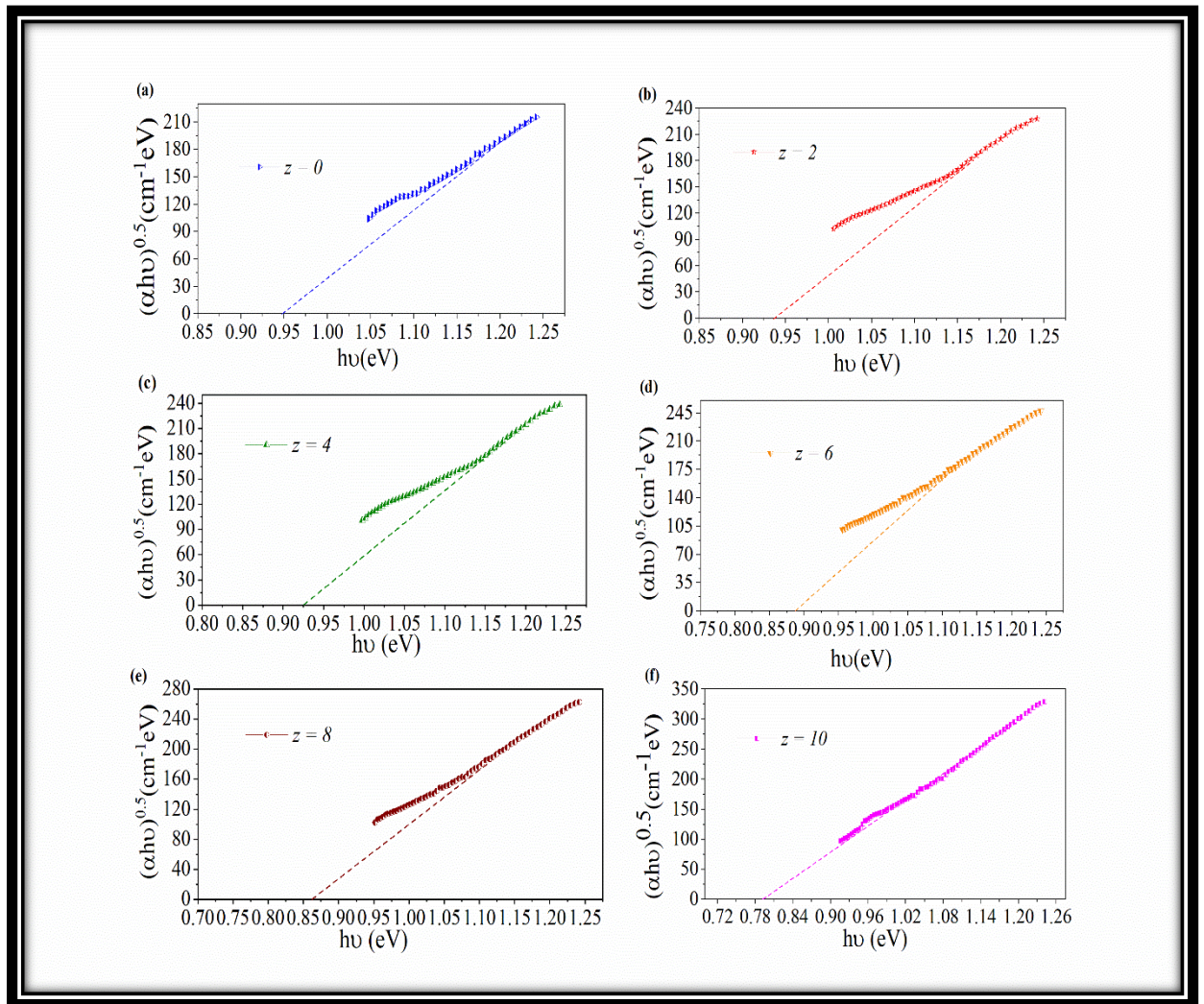
Figure 4.13: Dependence of $(\alpha h\upsilon)^{0.5}$ with hυ for prepared thin films

Again the bandgap is estimated by plotting $h\upsilon(\epsilon_i)^{0.5}$ against $h\upsilon$ (figure 4.14) and $E_g^{"opt}$ is obtained using the relation [18, 27]:

$$h^2\upsilon^2\varepsilon_i = \left(h\upsilon - E_g^{"opt}\right)^2 \tag{41}$$

The above relation can be rewritten as

$$h\upsilon\sqrt{\varepsilon_i} = \left(h\upsilon - E_g^{"opt}\right) \tag{41(a)}$$

The obtained values of $E_g^{"opt}$ show a good agreement with the E_g^{opt} values. The calculated values are tabulated in table 4.4. Optical band gap is very delicate property of the system and reflects its bond strength. The decrease in "optical band gap" values may be due to variation of bond angles and bond lengths.
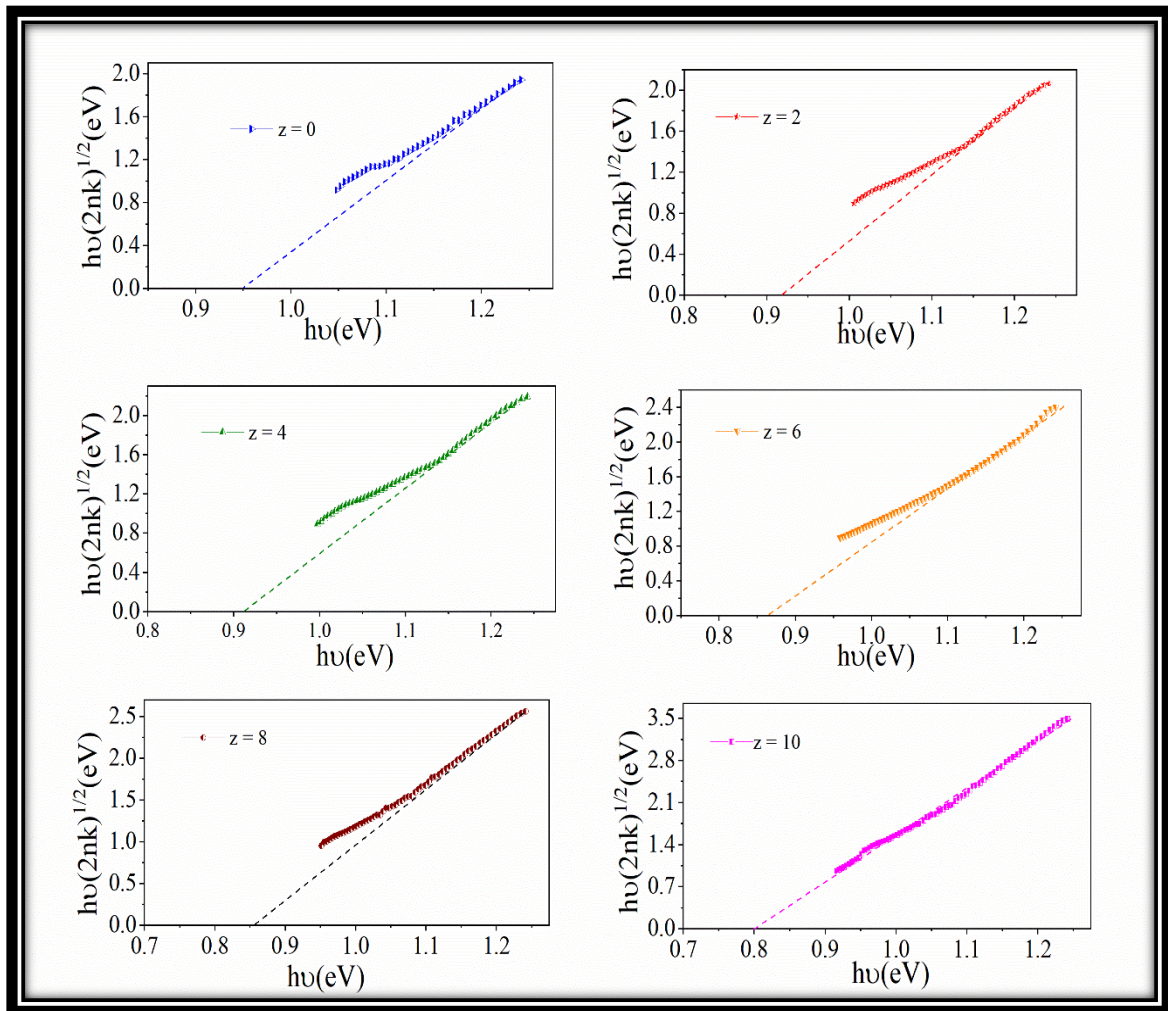
Figure 4.14: Dependence of $h\upsilon(\epsilon_i)^{0.5}$ with $h\upsilon$ for GeTeSeGa thin films

Additionally, it is observed that by adding Ga in GeTeSe system, it raises the density of defect states. However, the structural defect model argued that Ga has a lower electronegativity value than Se, so Ga generates the impurities with positive charge [28]. Furthermore, Ga is metal and possess zero band gap, which is less than that of Se (1.95 eV). As a result, "band gap" decreases with the Ga content (chapter 3).

Also, E_g^{opt} of the investigated samples reduces with Ga at.%. The reduction in optical bandgap may be attributed to the generation of Te-Ga bonds possessing lower bond energy compared to Ge-Se bonds as discussed in chapter 3. Additionally, the reduction in the E_g^{opt} may be because of the generation of Te-Te bonds. By the substitution of Se with Ga, the far-infrared investigation envisages that new Te-Ga bonds formed along with former bonds *viz* Te-Te, Ge-Te and Ge-Se. Te-Ga bond possesses smaller bond energy compared to other bonds [29]. The lower bond energy corresponds to reduction in the values of the mean bond strength of the material. Consequently, calculated theoretical energy gap (E_g^{th}) and optical bandgap (E_g^{opt}) of the material reduces. Moreover, the defects state increases with the increment in Ga concentration which further reduces the optical bandgap.

4.2.1.5 Estimation of frequency dependence dielectric constant

The large frequency dielectric constant can be estimated by realizing the obtained data of the refractive indices by two methods [30]. While the first method explains the contribution of modes of lattice vibration of dispersion and free carriers, second one is based on the dispersion produced by the bounded carriers in free space.

4.2.1.5.1 Ist method: Estimation of lattice constant and carrier concentration

The lattice constant arises mainly because of two factors partly due to free electrons and partially due to bound electrons. The relationship between the "wavelength, dielectric constant and refractive indices" is given by the equation [24, 31]:

$$n^2 = \varepsilon_L - \left[\frac{e^2}{4\pi c^2 \varepsilon_o} \frac{N^*}{m^*} \right] \lambda^2 \qquad (42)$$

ε_L represent the lattice dielectric constant, N^* denote the number of the carrier concentration and m* is the "effective mass" of the charge carriers. The graph between n^2 and λ^2 is shown in figure 4.15 which reveals very small dispersion for longer wavelengths.
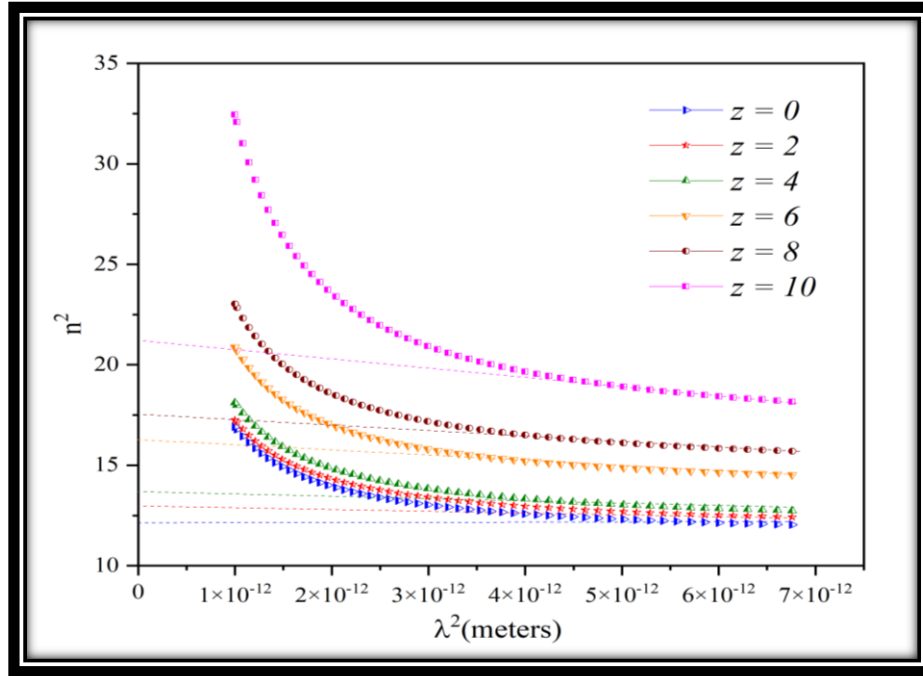
Figure 4.15: "Plot of n^2 vs λ^2" for GeTeSeGa thin films.

The values of N^*/m* and ε_L are obtained from the slope and intercept of the curve by extrapolating the plot (figure 4.15). The estimated values of ε_L and N^*/m* are tabulated in table 4.4. With the enhancement of the Ga concentration, ε_L increases from 13.44 to 21.33 and similarly, N^*/m* also increases from 2.66 to 5.89. It can be observed from the graph that at a higher energy region, the refractive index is maximum because of normal dispersion response of material. This behaviour is consistent with the response of "refractive index" with the Ga content.

In general, the "high frequency dielectric constant ε_L and the ratio N^*/m*" is linked to the internal microstructure of the thin film. Also thickness and band gap are related to the microstructure of the films. It is observed that ε_L and N^*/m* rise with the Ga which is most likely due to an enhancement in scattering of free carriers from ionized impurities and defects with rising Ga content and variation in thickness [32].

Additionally, it is found that $\varepsilon_L > \varepsilon_\infty$ (table 2) which corresponds to the participation of free carriers on the polarization process that take place within the material when the light is incident on it [33].

Table 4.4: Estimated values of λ_o & S_o, ε_L, N^*/m^*, E_g^{opt} and $E_g^{"opt}$

z	λ_o (nm)	$S_o \times 10^{13}$ (m^{-2})	ε_L	N/m* $\times 10^{56}$ (m^{-3}kg^{-1})	E_g^{opt} Tauc (eV)	$E_g^{"opt}$ (eV)
0	547.74	3.714	13.44	2.66	0.95	0.95
2	551.61	3.718	13.88	2.83	0.93	0.92
4	557.45	3.721	14.40	2.88	0.92	0.91
6	566.38	4.22	16.48	3.80	0.88	0.88
8	575.66	4.46	18.30	3.96	0.86	0.86
10	639.06	4.55	21.33	5.89	0.79	0.80

4.2.1.5.2 2nd method: Estimation of Sellmeier parameters

The refractive index executes the classical dispersion relation at the higher wavelength. The relation is given by [31]:

$$\frac{n_o^{2} - 1}{n^2 - 1} = 1 - \left(\frac{\lambda_o}{\lambda}\right)^2 \tag{43}$$

Here λ_o represent the oscillator wavelength. The λ_o and n_o values have been obtained from figure 4.16.

Again the average oscillator strength (S_o) is given by:

$$S_o = (n_o^{2} - 1)/\lambda_o^{2} \tag{43(a)}$$

and equation (43) can also be expressed as:

$$\frac{1}{(n^2 - 1)} = \frac{1}{\lambda_o^{2} S_o} - \frac{1}{\lambda^2 S_o} \tag{44}$$
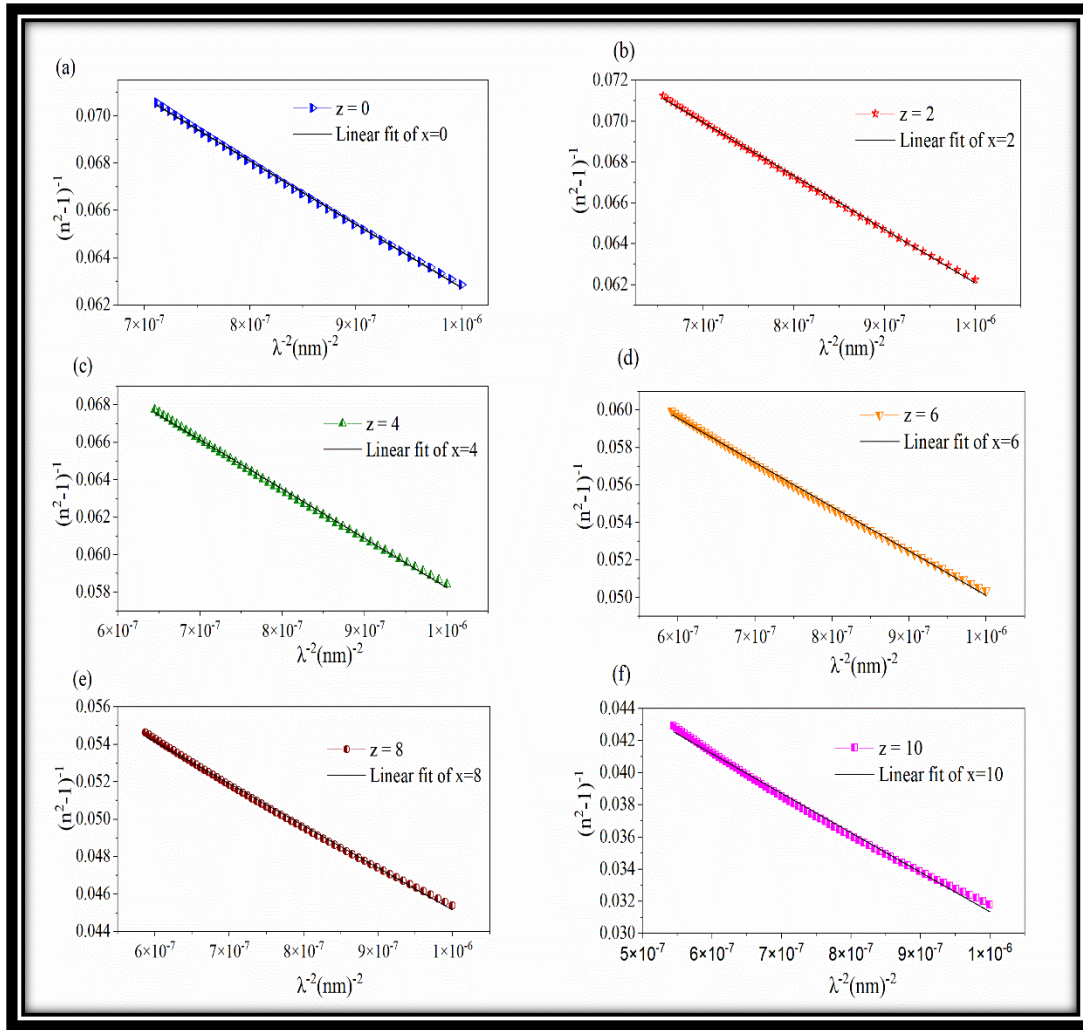
Figure 4.16: Dependence of $(n^2-1)^{-1}$ with λ^{-2} for GeTeSeGa thin films

The values of S_o & λ_o are estimated from the slope $(1/S_o)$ and intercept $(1/\lambda_o^2 S_o)$ of figure 4.16 using equation 44 and the obtained values are given in table 4.4. It is observed that the values of S_o and λ_o enhances with Ga content.

It is known that "oscillator wavelength (λ_o)" is inversely related to E_o and it depends on E_g^{opt}. Consequently $\lambda_o \propto \dfrac{1}{E_g^{opt}}$, so increase in λ_o values attributes to decrement in E_g^{opt} value. However S_o is related to E_d also thus increase in E_d values leads to increase in S_o values with the Ga content.

4.2.1.6 Assessment of plasma frequency and optical carrier concentration.

The optical carrier concentration for amorphous GeTeSeGa chalcogenide thin films is obtained by Drude's Theory [34]

$$n^2 - k^2 = \varepsilon_{opt} - \frac{(\hbar\omega_D)^2}{(\hbar\omega)^2} \qquad (45)$$

where $\hbar\omega$, ε_{opt} and $\hbar\omega_D$ denote the photon energy, residual dielectric constant and screened plasma energy respectively. Dependence of n^2-k^2 with $(\hbar\omega)^2$ for GeTeSeGa thin films have been shown in figure 4.17.
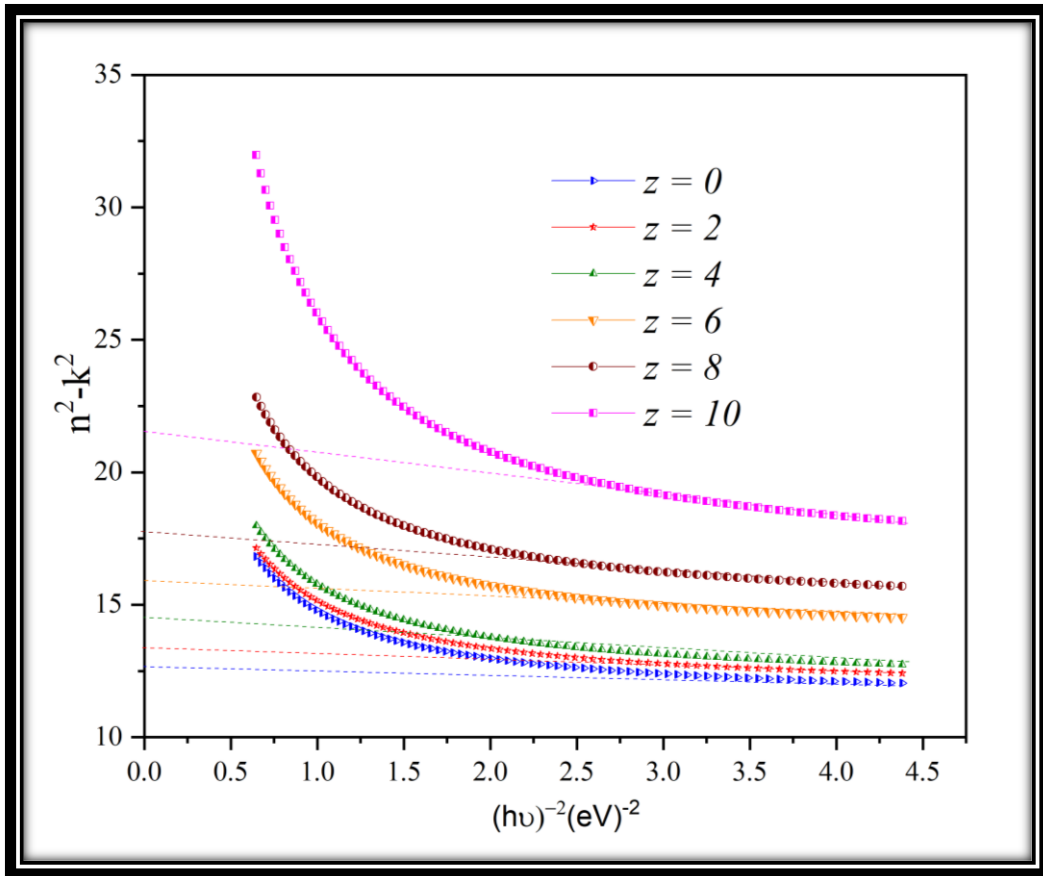
Figure 4.17: Dependence of n^2-k^2 on $(h\upsilon)^{-2}$ for GeTeSeGa thin films

The "optical dielectric constant (ε_{opt}) and screened plasma energy ($\hbar\omega_D$)" is estimated from the intercept and the slope of the graph (figure 4.17). The values of ε_{opt} for studied thin films have been found to be in the range of 13.75 to 21.68. Both the parameters $\hbar\omega_D$ and ε_{opt} is linked to the "plasma frequency (ω_p)" by the formula:

$$``\hbar\omega_p = \frac{\hbar\omega_D}{\sqrt{\varepsilon_{opt}}}\text{''}$$ (46)

The values of ω_p are $\in$ [2.66 Hz, 2.98 Hz] (table 4.5). The optical carrier concentration (N_{opt}) is determined by using two factors *viz* ω_p and ε_{opt} as follow:

$$N_{opt} = \frac{\varepsilon_o \varepsilon_{opt} m_c^* \omega_p^2}{e^2}$$ (47)

where m_c^* represents the "effective mass of the electron ($m_c^* = 0.4m_o$)" [35]. It is noticed from the table that both the parameters ω_p and ε_{opt} show a rising trend with the Ga amount. The estimated values of N_{opt} are $\in$ [1.23, 1.42$\times$ 10^{26} (m^{-3})]. (table4.5).

"By Drude's theory, the ratio N^*/m^* for a dielectric material can be related to the ω_p and the lattice dielectric constant ε_L through the formula [36]: $\frac{N^*}{m^*} = \frac{\varepsilon_o \varepsilon_L}{e^2}\omega_p^2$". The increase in N^*/m^* values (table 4.4) leads to increase in ω_p values. Also ω_p is related to N_{opt} (equation 47). Hence increase in N_{opt} value is observed with Ga content in the system. This is in good harmony with the semiconductor carrier concentration.

Table 4.5: Calculated values of ε_{opt}, ω_p, N_{opt}, $\chi^{(3)}$ and n_2

z	ε_{opt}	$\omega_p \times 10^{14}$ (Hz)	$N_{opt} \times 10^{26}$ (m^{-3})	$(\chi^{(3)}) \times 10^{-10}$ (esu)	$n_2 \times 10^{-9}$ (esu)
0	13.75	2.66	1.23	1.05	1.05
2	14.01	2.69	1.26	1.12	1.20
4	14.35	2.73	1.29	1.22	1.29
6	16.80	2.79	1.33	2.30	2.27
8	18.25	2.82	1.38	3.26	3.01
10	21.68	2.98	1.42	8.25	7.01

It is already been discussed that by increasing Ga, both the parameters n and k increases, while these parameters decrease with the rise of wavelength. This response may be linked to normal dispersion of the material. Additionally, it may be due to high polarizability rate and more density of Ga compared to Se.

4.2.1.7 Estimation of Electronic Polarizability

The "electronic polarizability (α_p)" is critical for estimating the relationship between the ionic/covalent character of solids and the other optical parameters. "Duffy and others" [37-38] correlated several independent linear optical constants with α_p. The average molar refraction (R_m) for amorphous semiconducting materials is determined by Lorentz-Lorenz equation [5]:

$$R_m = \left(\frac{n^2-1}{n^2+2}\right)\frac{M_w}{\rho} = \left(\frac{n^2-1}{n^2+2}\right)V_m \qquad (48)$$

where M_w, ρ and V_m denote the molecular weight, density and molar volume of the GeTeSeGa system.

α_p can be linked to the R_m of the solid by "Clausius – Mosotti equation" [5]:

$$R_m = \left(\frac{4\pi N}{3}\right)\alpha_p \qquad (49)$$

Conferring "Clausius – Mosotti equation and Lorentz-Lorenz relation", the relation between α_p, n and V_m is described as

$$\frac{n^2-1}{n^2+2} = \frac{4\pi N\rho}{3M_w}\alpha_p \qquad (50)$$

where 4/3 is a constant and "$(n^2-1)/(n^2+2)$ is the reflection loss" denoted by R_L. The values of R_L is obtained from the y-axis intercept at higher energies (figure 4.18(a)). Figure 4.18(b) illustrates that by enhancing Ga content, the value of α_p rises. This enhance response may be ascribed according to the Lorentz-Lorenz relationship & Clausius – Mosotti model. The correlation has been found by the generalization of these relation as: $r \propto n \propto \varepsilon_r \propto \alpha_p$, where r, ε_r, n, α_p denote the atomic radii, dielectric constant, refractive indices and

electronic polarizability. The replacement of Se with Ga, increases all these parameters in the investigated samples.
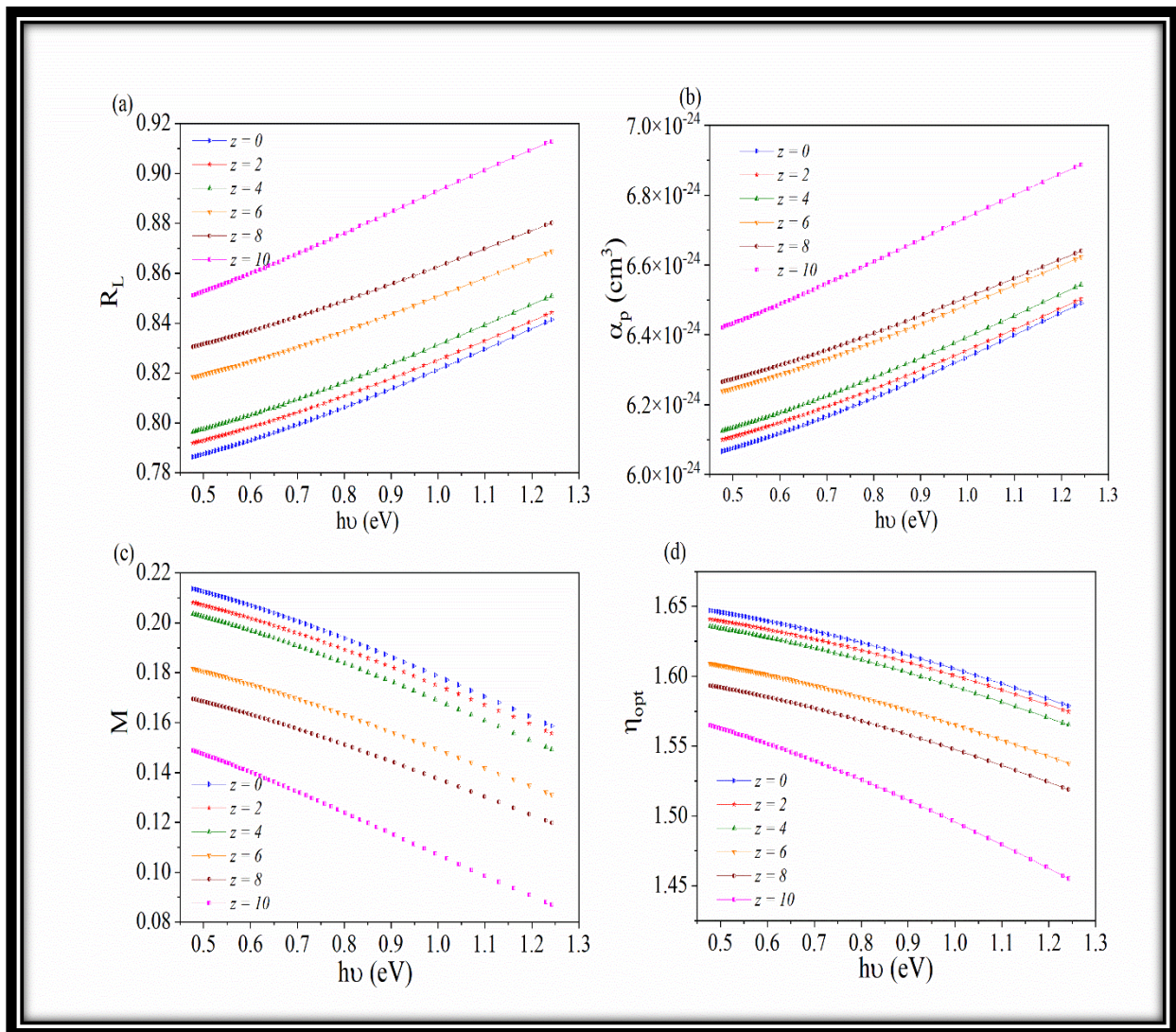
Figure 4.18: (a, b, c and d) Plot of "R_L, α_p, M, η_{opt}" with hυ.

4.2.1.8 Metallization criterion

Metallization (M) characteristics of a material is a parameter, which studies the metallic or insulating character of the material. The value of M is estimated from the equation [5]:

$$M = \left(1 - R_m / V_m\right) \qquad (51)$$

M values can be divided into two groups:

"$R_m < V_m$, M > 1; for metallic character

$R_m > V_m$, M < 1; for insulating or non-metallic character"

Figure 4.18 (c) shows the variation of M on hυ and its value is found to be less than 1 (0.21 to 0.15) for all the studied samples It is well known that among all the chalcogens (S, Se & Te), Te is more metallic than others which lead to easily crystallization. To surmount this problem Ga is added in Te based system. Hence it may be concluded that with the inclusion of Ga in the system, metallic character of system reduces. The consequences indicate the insulating character of thin films.

4.2.1.9 "Optical electronegativity"

"Optical electronegativity (η_{opt})" is a parameter recommended by "Duffy" [39, 40] predicts the possibility of ionic bond formation as of atoms or radicals to attract electrons. "Duffy" suggested a link between electronegativity and n as;

$$" \eta_{opt} = \left(\frac{C}{n} \right)^{0.25} "$$

(52)

where C denotes the unit less constant having the value of "25.54 for all materials". It is found that η_{opt} reduces with the raising of Ga concentration (figure 4.18(d)). It can be correlated with the decrease of electronegativity of GeTeSeGa system as discussed in chapter 3. With the substitution of Ga ($\chi_{Ga} < \chi_{Se}$), the covalency (C_c) also parameter increases and ultimately decrease in optical electronegativity is observed.

4.2.2 Non-linear optical parameters

Nonlinear optical (NLO) materials serve an important role in nonlinear optics, particularly in information technology and industrial applications. Non-linear optics deals with the branch of physics which explains the response of em wave in the non-linear media when a material is exposed to a strong electric field generated by an intense laser beam. So the polarization (P) and electric field (E) are represented as a power series [41]. $P = \chi^{(1)}E + \chi^{(2)}E^2 + \chi^{(3)}E^3 \cdots\cdots$ where "$\chi^{(1)}$ E is linked to the linear response and $\chi^{(2)}$ and $\chi^{(3)}$ denote the second and third-order non-linear susceptibility". The intensity-dependent refractive indices are the most intriguing phenomena among other non-linear

optical phenomena. Experimentally it has been obtained that under strong "electric fields"; the polarizability of a material is no longer proportional to the "linear electric field" but rather the square of the "electric field". The change in "refractive index (Δn)" follows the relationship:

$$\Delta n = n_2 |E|^2$$ (53)

where E stands for the electric field and n_2 represents the "non-linear refractive index". The non-linearity of chalcogenide glasses strongly depends on incident light [42].

Non-linear refractive index may be defined as when an intense beam travels through a solid; the electric field of the light may induce a variation in the index of refraction of the system, which is related to the intensity of beam. The chalcogenide glasses possess 1000 times greater non-linearities than silica [43, 44] and hence are good candidates for mid-infrared super continuum (MIR SC) generation [45]. Glasses that consist of polarizable atoms or ions, are likely to have large non-linear optical characteristics. In comparison to glasses, the crystals show non-linear effects. However, glasses lead due to more advantages *viz* low cost, large "refractive index" *etc*. The refractive index (n) may be described as n = n_o + n_2<E^2>. Here n_o >> n_2, and both parameters n_2 and n_o are not dependent on the intensity of em wave and <E^2> represent mean square electric field [42]. The second term of the "non-linear refractive index n_2" is related to the non-linear electron polarizability, P_{NL} as:

$$P = \chi^{(1)} E + P_{NL}$$ (54)

$$\text{Where } P_{NL} = \chi^{(2)} E^2 + \chi^{(3)} E^3$$ 54(a)

4.2.2.1 Tichy and Ticha relation

The non-linear index of refraction (n_2) has been deduced according to "Tichy and Ticha" approach [46]. "Tichy and Ticha" combined the single oscillator model and Miller generalization rule [47, 48] to evaluate n_2 as:

$$n^2 = 1 + \frac{E_o E_d}{E_o^2 - (h\upsilon)^2}$$ (55)

"Third order non-linear susceptibility $(\chi^{(3)})$" is calculated by the relation:

$$\chi^{(3)} = A(\chi^{1})^{4}$$ (56)

"where $\chi^{1} = (n^{2} - 1)/4\pi$ at ($h\upsilon \to 0$ and n = n$_o$)" to determine the refractive index (n$_2$) and $\chi^{(3)}$:

$$\chi^{(3)} = A\left[\frac{E_d}{4\pi E_o}\right]^{4}$$ 56(a)

where A= 1.7×10^{-10}esu. "The inordinate response of the material when it has been placed in the electric field is treated as the non-linear refractive index and is expressed as":

$$n_2 = \frac{12\pi\chi^{(3)}}{n_o}$$ (57)

where n$_o$ represents the "static refractive index". The obtained values of $\chi^{(3)}$ and n$_2$ are given in table 4.5. "Wang" [47] suggested the relation between $\chi^{(3)}$ and E_g^{opt}. With the incorporation of Ga in the material, the values of $\chi^{(3)}$ increases and the optical band gap E_g^{opt} decreases (figure 4.19). The values of composition-dependent $\chi^{(3)}$ are depicted in the table 4.5. In the investigated samples, the high susceptibility value is noted and is raising the enhancement of Ga content. Generally polarizability, optical band gap and density are considered as the vital parameters to determine third order susceptibility. In the present investigation $\chi^{(3)}$ increases monotonically with the decrement in the optical band gap (figure 4.19). It is further described by the increment in "refractive index" values with the Ga concentration.

Additionally, n and E_g^{opt} are inversely proportional to each other. Hence increase in n leads to increase in $\chi^{(3)}$ values and decrease in E_g^{opt}.
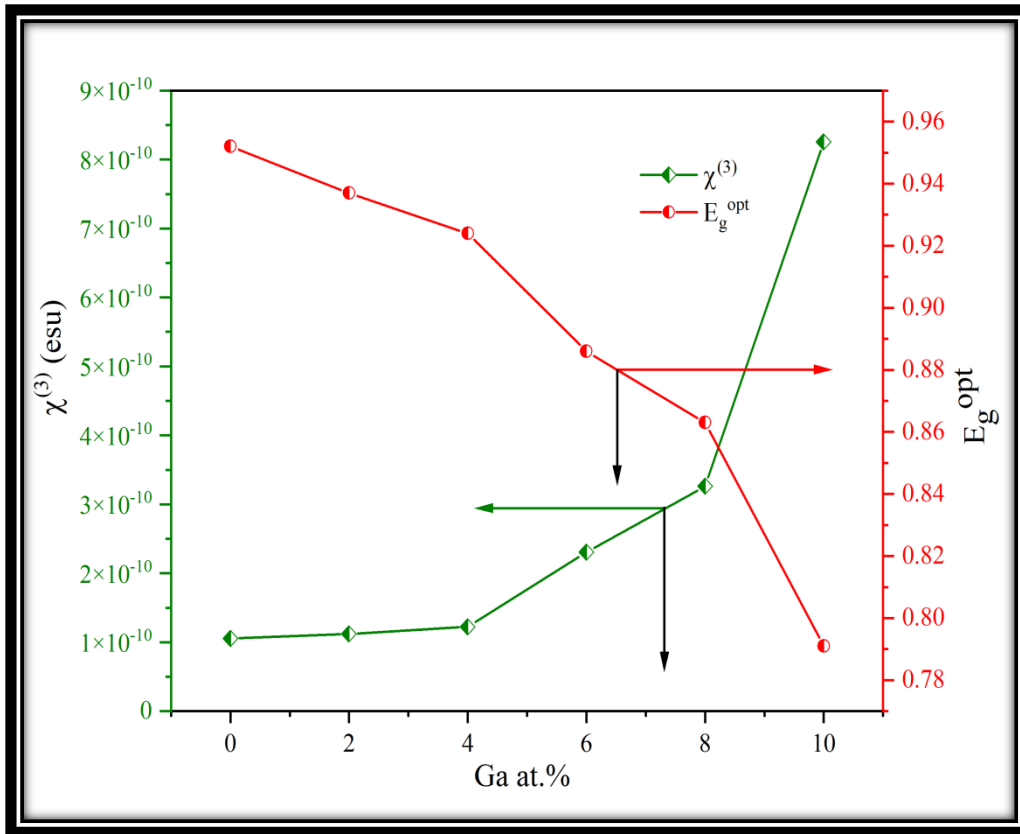
Figure 4.19: Variation of non-linear susceptibility and optical band gap with Ga concentration

4.2.2.2 "Fournier and Snitzer relationship"

"Fournier and Snitzer" [49] have suggested relation for estimating n_2 of the thin films which is stated as

$$n_2 = \frac{(n^2 + 2)^2 (n^2 - 1)}{150.72 Nn} \frac{E_d}{(E_o)^2} \left(\frac{x_{32}^2}{x_{2g}^2} - 1 \right) \qquad (58)$$

Here n, N denotes the refractive index and density of polarizable constituents. n_2 pursues a similar response as n follows with the wavelength. The values of n_2 also shows rising trend with the Ga content (figure 4.20).
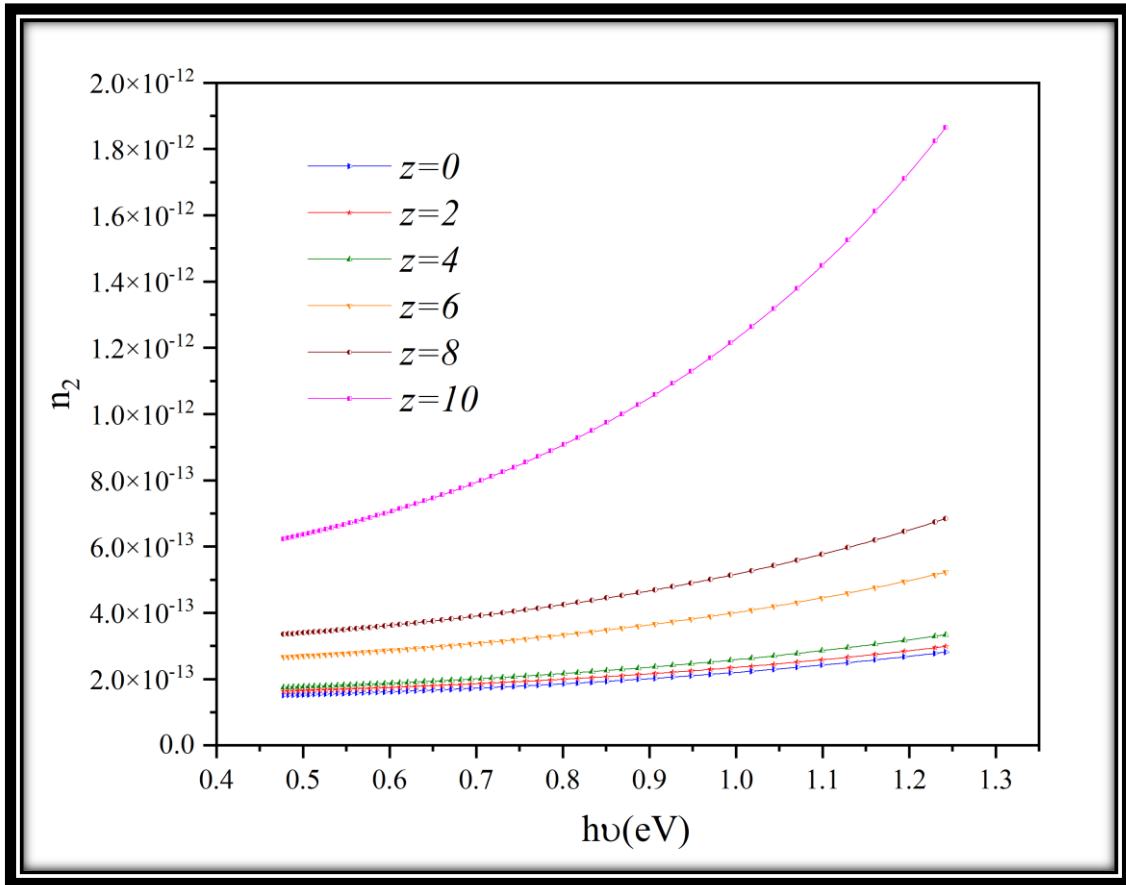
Figure 4.20: Photon energy and non-linear refractive index plot

The increase in n_2 values can be related to increase of n which may also be attributed to Lorentz- Lorentz relation. According to this relation greater is the atomic radii, more will be polarizability and larger will be refractive index. In the present case Ga has large atomic radii compared to Se ($r_{Ga}(1.35Å) > r_{Se}(1.15Å)$) and is also more denser. Thus both n and n_2 increases with increment of Ga amount in the system for all compositions.

The non-linearity of the glassy materials may be conferred on the basis of bandgap and defects states [50]. According to Moss model, the non-linearity may be obtained by the relation [51]:

$$n_2 \propto (E_g^{opt})^{-4} \tag{59}$$

It is already known that by adding Ga, E_g^{opt} reduces and subsequently n_2 enhances. The large non-linearity of the sample makes these materials appropriate for high speed and low power

devices for telecommunication. The studied thin films have n > 2 and have a higher transmittance window; therefore, suitable in NIR imaging and sensing applications.

4.2.3 Relationship between energy gap (E_g^{opt}) and refractive index (n)

Various efforts have been made to establish the relation between E_g^{opt} and n by different researchers. Moss [51] suggested the model which conferred that the energy levels of materials are scaled down by the factor $1/E_{eff}$, where E_{eff} denotes the "effective dielectric constant".

"Moss" proposed the relation is given by:

$$n_o{}^4 E_g^{opt} = k \tag{60}$$

The value of k = 95eV. "Ravindra *et al*." [52] revised the Moss relationship by providing a different value for k= 108eV and equation 68 can be rewritten as:

$$n_0{}^4 E_g^{opt} = 108 \tag{61}$$

The correlation suggested by "Moss" has limited the efficacy of relation 61. Hence "Ravindra and Gupta" [53] suggested another relationship between refractive indices and bandgap. The relation is as follow:

$$n = 4.084 - 0.62 E_g^{opt} \tag{62}$$

After investigation, "Moss" claimed that the above equation (62) is valid to bandgap < 4 eV. Thereafter "Reddy *et al.*" [54] suggested a new relation having an exponential response.

$$`` E_g^{opt} e^n = 36.3 " \tag{63}$$

"Herve – Vandamme [55] suggested the relation by using Penn's theory. This theory is based on the random phase". The equation is given by:

$$n^2 = 1 + \left(\frac{A}{E_g^{opt} + B} \right)^2 \tag{64}$$

where B=3.47 eV and A denote the ionization energy of hydrogen =13.6eV.

Kumar *et al*. [56] suggested a model to obtain the relation between the index of refraction and bandgap. They claimed that this method might be suitable to determine optoelectronic applications for specific semiconductors system.

$$n = KE_g^{opt\,c} \text{ where c= -0.32234 and K= 3.3668} \tag{65}$$

Annani *et al*. [57] suggested the relationship as

$$E_g^{opt} = (17 - 5n) \text{ eV} \tag{66}$$

$$\Rightarrow n = 3.4 - 0.2E_g^{opt} \tag{67}$$

Duffy [39] suggested the correlation between the "optical energy gap and the electronegativity"

$$\Delta\chi^* = 0.2688\,E_g^{opt} \tag{68}$$

Reddy *et al*. [58] obtained the relationship between refractive index and electronegativity as follow:

$$n = -\ln\left[0.1028\Delta\chi^*\right] \tag{69}$$

Combining equations (68) and (69), the new equation becomes:

$$n = -\ln\left[0.027\,E_g^{opt}\right] \tag{70}$$

Ahammed and Reddy [59] suggested a relation to surmount a few of the downsides of the Moss equation as

$$n^4\left(E_g^{opt} - 0.365\right) = 154 \tag{71}$$

However, this relationship does not hold for E_g^{opt} less than 0.365 eV.

It can be noted from Herve and Annani *et al*. (equations 62 & 67) that the relations are limited to n values of 3.4 & 4.084 only. For equation (62), when n = 0, then $E_g^{opt} = 6.587$. For $E_g^{opt} \geq 6.587\,eV$, the equation 62 provides negative refractive index values. In the studied system the refractive indices values change from 4.11 to 5.69 at 1µm and so these equations are suitable for GeTeSeGa thin films. It is found from figure 4.21 that the relations proposed by Reddy and Ahammad [59], Ravindra and Gupta [53], Kumar & Singh

[54], Reddy [55] and Reddy & Duffy [39, 58] are approximately similar to the experimentally observed values in the present system. However, the relations provided by Herve- Vandamme [55], Moss [51], Annani [57] and Ravindra [52] have depicted more variation from experimental values.
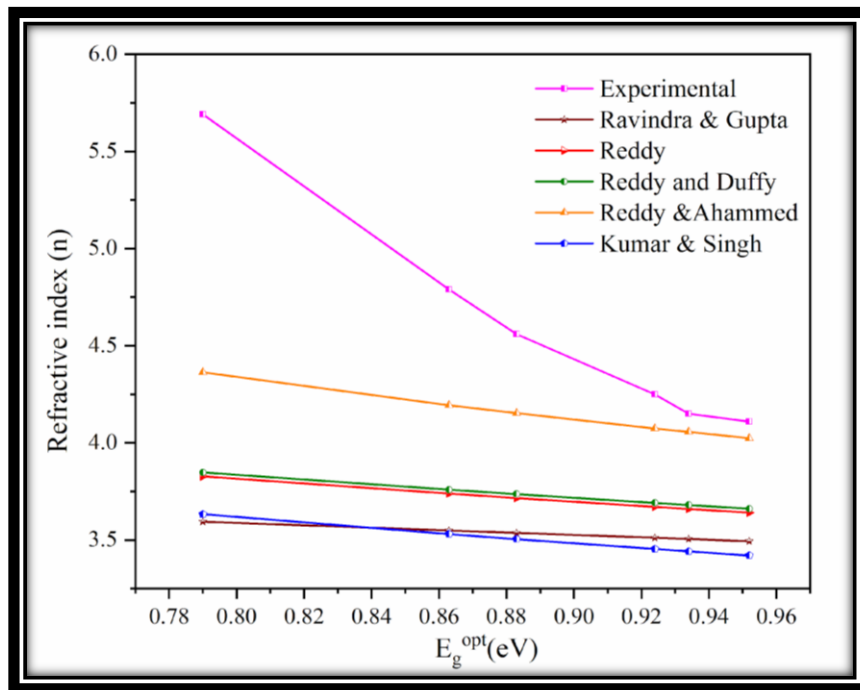
Figure 4.21: Graph of the index of refraction by various models with optical band gap
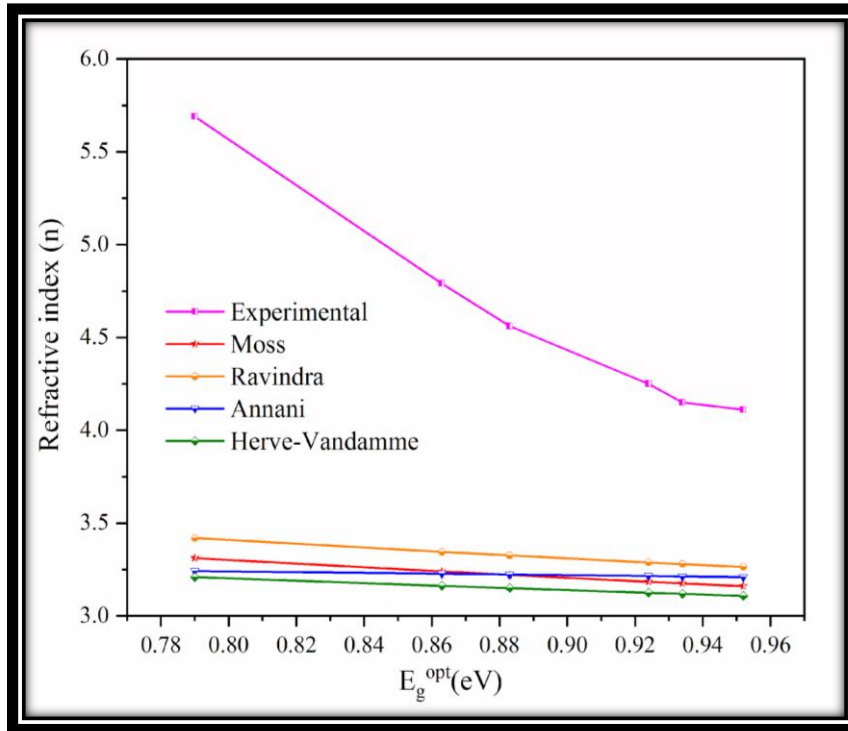
Figure 4.22: Plot of refractive index by various models with optical band gap

The deviation in the n values (calculated from different relation) from the experimentally observed values of the present system has been estimated and is depicted in figures 4.23 & 4.24.
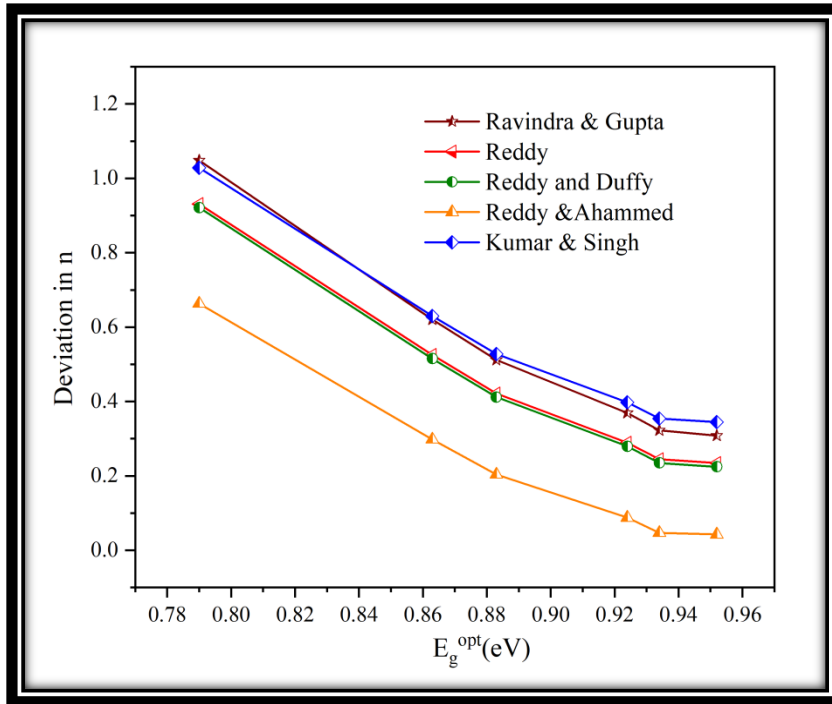
Figure 4.23: Plot of deviation in n with E_g^{opt}
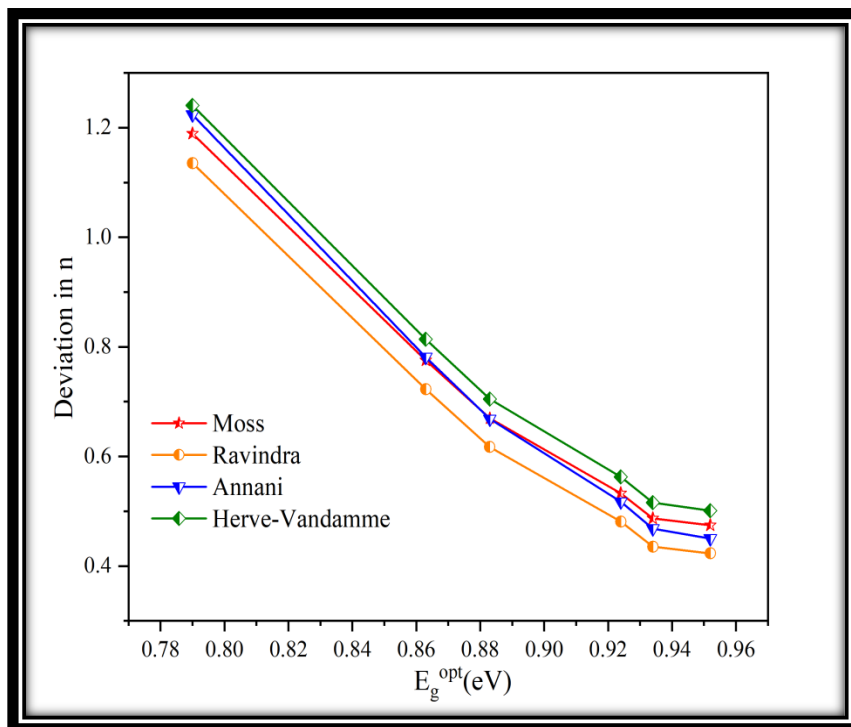
Figure 4.24: Plot of deviation in n with E_g^{opt} .

138

4.3 Conclusion

The transmission spectra for GeTeSeGa thin films have been discussed, which indicates that the absorption edge is shifting towards the higher wavelength. The optical parameters vary with the enhancement of Ga and decrement in Se concentration. With the enhancement of Ga amount in GeTeSeGa chalcogenide glassy thin films, the refractive indices rise and the optical band gap reduces. The single oscillator parameters such as E_o decreases from 2.26eV to 1.95 eV while E_d increases from 25.44 to 36.49, indicating that with the addition of Ga, the films become more stable and stiff. Drude theory has been applied for estimating electronic polarizability and other related parameters. The value of m<1 reveals the non-metallic nature of the material. Nonlinear parameters index of refraction (n_2) and non–linear susceptibility ($\chi^{(3)}$) rise with the incorporation of *Ga* in the GeTeSeGa material.

References

[1] R. Swanepoel., "Determination of the thickness and optical constants of amorphous silicon", J. Phys. E, vol. 16, pp. 1214, 1983.

[2] J. Tauc, R. Grigorovici, A. Vancu., "Optical properties and electronic structure of amorphous germanium", Phys. Stat. Sol, vol. 15, pp. 627–637, 1966.

[3] I. Sharma, & A.S. Hassanien., "Effect of Ge-addition on physical and optical properties of chalcogenide $Pb_{10}Se_{90-x}Ge_x$ bulk glasses and thin films", J. Non-Cryst. Solids, vol. 548, pp. 120326, 2020.

[4] M. M. Soraya., "Structural and optical properties of $Se_{85-x}Te_{15}In_x$ chalcogenide thin films for optoelectronics, Appl. Phys. A: Mater. Sci. Process, vol. 126, no. 8, pp. 1-9, 2020.

[5] S.S. Fouad, G.A.M. Amin, M.S. El-bana., "Physical and optical characterizations of $Ge_{10}Se_{90-x}Te_x$ thin films in view of their spectroscopic ellipsometry data", J. Non. Cryst. Solids, vol. 481, pp. 314–320, 2018.

[6] P. Sharma, S.C. Katyal., "Linear and nonlinear refractive index of As–Se–Ge and Bi doped As–Se–Ge thin films", J. Appl. Phys, vol. 107, pp. 1–6, 2010.

[7] E. Sharma, P. B. Barman & P. Sharma., "Evaluation of optical linear and non-linear parameters of thermally deposited GeTeSeGa thin films in NIR (1 µm -2.6 µm) wavelength range from their transmission spectra", Optik: Int. J. Light. Electron Optics, vol. 219, pp. 165181, 2020.

[8] A. Devi, A. Banotra, S. Kumar, A. K. Kapoor & N. Padha., "An effective alternative to SnSe nano-crystalline thin films for optoelectronic applications", Journal of Electronic Materials, vol. 48, no. 7, 4335-4341 (2019).

[9] T. A. Hegde, A. Dutta and G. Vinitha., "$\chi^{(3)}$ measurement and optical limiting behaviour of novel semi-organic cadmium mercury thiocyanate crystal by Z-scan technique", Applied Physics A, vol. 124, no.12, pp. 1-10, 2018.

[10]   J. N. Hodgson., "Optical Absorption and Dispersion in Solids", Chapman and Hall Ltd, 11 New Fetter Lane London EC4, 1970.

[11]   S. H. Wemple, M. DiDomenico., "Behavior of the electronic dielectric constant in covalent and ionic materials", Phys. Rev. B, vol. 3, pp. 1338–1351, 1971.

[12]   S. H. Wemple., "Refractive-index behavior of amorphous semiconductors and glasses", Phys. Rev. B, vol. 7, pp. 3767, 1973.

[13]   K. Tanaka., "Optical properties and photoinduced changes in amorphous As–S films", Thin Solids Film, vol. 66, pp. 271–279, 1980.

[14]   E. Sharma, H.H. Hegazy, V. Sharma, P. Sharma., "Topological behavior and glassy framework of GeTeSeGa chalcogenide glasses", Phys. B Phys. Condens. Matter, vol. 562, pp. 100–106, 2019.

[15]   A.I. Ali, J.Y. Son, A.H. Ammar, A.A. Moez, Y. Kim., "Optical and dielectric results of $Y_{0.225}Sr_{0.775}CoO_{3\pm\delta}$ thin films studied by spectroscopic ellipsometry technique", Results Phys, vol. 3, pp.167–172, 2013.

[16]   A. S. Hassanien, I. Sharma, "Band-gap engineering, conduction and valence band positions of thermally evaporated amorphous $Ge_{15-x}Sb_xSe_{50}Te_{35}$ thin films: Influences of Sb upon some optical characterizations and physical parameters", J. Alloys Compd, vol. 798, pp. 750–763, 2019.

[17]   A. S. Hassanien, A. A. Akl., "Influence of composition on optical and dispersion parameters of thermally evaporated non-crystalline $Cd_{50}S_{50-x}Se_x$ thin films", J. Alloys Compd, vol. 648, pp. 280–290, 2015.

[18]   F. Yakuphanoglu, M. Sekerci, O.F. Ozturk., "The determination of the optical constants of Cu (II) compound having 1-chloro-2, 3-o-cyclohexylidinepropane thin film", Optics Commun, vol. 239, pp. 275–280, 2004.

[19]   P. Kumar, M. C. Mathpal, G. K. Inwati, S. Ghosh, V. Kumar, W. D. Roos & H. C. Swart., "Optical and surface properties of Zn doped CdO nanorods and antimicrobial applications", Colloids and Surfaces A: Physicochemical and Engineering Aspects, vol. 605, pp. 125369, 2020.

[20]   D. R. Hang, Y.Q.Pan, K.H. Sharma, M.M.C.Chou, S. K. E. Islam, H. F. Wu and C. T. Liang., "2D CTAB-$MoSe_2$ nanosheets and 0D $MoSe_2$ quantum dots: Facile top-down preparations and their peroxidase-like catalytic activity for colorimetric detection of hydrogen peroxide. Nanomaterials", vol. 10, no.10, 2045, 2020.

[21]   M. Devi, A. Kumar and A. Kumar., "The synthesis, structural, optical and electrical characterizations of double perovskite oxide Y_2CuCoO_5," In AIP Conference Proceedings, vol. 2220, no. 1, pp. 020077, 2020.

[22]   M. Panday, G. K. Upadhyay, and L. P. Purohit., "Sb incorporated SnO_2 nanostructured thin films for CO_2 gas sensing and humidity sensing applications", J. Alloys Compd, vol. 904, pp. 164053, 2022.

[23]   K. R. Sharma and N. S. Negi., "Doping effect of cobalt on various properties of nickel oxide prepared by solution combustion method. Journal of Superconductivity and Novel Magnetism", vol. 34, no. 2, pp. 633-645, 2021.

[24]   N. F. Mott, E. A. Davis., "States in the gap and recombination in amorphous semiconductors", Philos. Mag, vol. 32, pp. 961–996, 1975.

[25]   A. Dahshan., "New amorphous As–Se–Sb–Cu thin films: theoretical characterization and evaluation of optical constants," Appl. Phys. A: Mater. Sci. Process, vol. 123, no. 3, pp. 210, 2017.

[26]   H. H. Hegazy, A. Dahshan & K. A. Aly., "Influence of Cu content on physical characterization and optical properties of new amorphous Ge–Se–Sb–Cu thin films", Mater. Res. Express, vol. 6, no. 2, pp. 025204, 2018.

[27]   H. E. Atyia, N. A. Hegab., "Optical spectroscopy and dispersion parameters of $Ge_{15}Se_{60}X_{25}$ (X =As or Sn) amorphous thin films", Eur. Phys. J. Appl. Phys, vol. 63, pp.10301, 2013.

[28]   N. Sharma, S. Kumar., "Effect of impurity (Te and Zn) incorporation in the density of defect states in thin films of $Se_{90}In_{10}$ and $Se_{75}In_{25}$ glassy alloys", J. Non-Cryst. Solids, vol. 357, no. 24, pp. 3940-3943, 2011.

[29]   E. Sharma, P. B. Barman, & P. Sharma., "Structural correlation of GeTeSeGa system by XRD and far-infrared spectroscopy", Appl. Phys. A: Mater. Sci. Process, vol. 127, pp. 345, 2021.

[30]   A. L. Pergament, E. L. Kazakova, and G. B. Stefanovich., "Optical and electrical properties of vanadium pentoxide xerogel films: modification in electric field and the role of ion transport", J. Phys. D, vol. 35, pp. 17 2187, 2002.

[31]   A. K. Walton, T. S. Moss., "Determination of Refractive Index and Correction to Effective Electron Mass in PbTe and PbSe", Proc. Phys. Soc, vol. 81, pp. 509, 1963.

142

[32]   M. A. Abdel-Rahim, M. M. Hafiz & A. Z Mahmoud., "Influence of thickness and annealing on optical constants of $Se_{82.5}Te_{15}Sb_{2.5}$ chalcogenide thin films," Solid State Sci, vol. 48, pp. 125-132, 2015.

[33]   E. G. El-Metwally, E. M. Assim, & S. S. Fouad., "Optical characteristics and dispersion parameters of thermally evaporated $Ge_{50}In_4Ga_{13}Se_{33}$ chalcogenide thin films", Opt. Laser Technol, vol. 131, pp. 106462, 2020.

[34]   A.A. Akl., "Thermal annealing effect on the crystallization and optical dispersion of sprayed V_2O_5 thin films", J. Phys. Chem. Solids, vol. 71, pp. 223–229, 2010.

[35]   A. Solieman, M.A. Aegerter., "Modeling of optical and electrical properties of In_2O_3: Sn coatings made by various techniques", Thin Solid Films, vol. 502, pp. 205–211, 2006.

[36]   A. S. Hassanien, K. A Aly, & A. A. Akl., "Study of optical properties of thermally evaporated ZnSe thin films annealed at different pulsed laser powers", J. Alloys Compd, vol. 685, pp. 733-742, 2016.

[37]   P. Nagels, L. Tichy, E. Sleeckx, R. Callaerts., "Photodarkening induced at low temperatures in amorphous Ge_xSe_{100-x} films", J. Non-Cryst. Solids, vol. 227, pp. 705–709, 1998.

[38]   S. Fouad, A. Bekheet, A. Farid., "Derivation of a relation between the conduction   mechanism and chemical bonding of amorphous $Ge_{15}Se_{85-x}Ag_x$ alloys", Phys. B Condens. Matter, vol. 322, pp. 163–172, 2002.

[39]   J. A. Duffy., "Trends in energy gaps of binary compounds: an approach based upon electron transfer parameters from optical spectroscopy", J. Phys. C. Solid State Phys, vol. 13, no. 16, pp. 2979, 1980.

[40]   R. R. Reddy, K.R. Gopal, K. Narasimhulu, L.S.S. Reddy, K.R. Kumar, C. K. Reddy, & S .N. Ahmed., "Correlation between optical electronegativity and refractive index of ternary chalcopyrites, semiconductors, insulators, oxides and alkali halides", Opt. Mater, vol. 31, no. 2, pp. 209-212, 2008.

[41]   D.C. Sati, S.C. Katyal, P. Sharma., "Role of composition and substrate temperature on nonlinear optical properties of GeSeTe thin 0.4–2.4-µm wavelength range", IEEE Trans. Electron Devices, vol. 63, pp. 698–703, 2016.

[42]   R. W. Boyd., "Nonlinear Optics", 2nd ed. Amsterdam, The Netherlands: Academic, 2003.

[43]   G. Lenz, J. Zimmermann, T. Katsufuji, M. E. Lines, H. Y. Hwang, S. Spalter, R. E. Slusher, S-W. Cheong, J. S. Sanghera, and I. D. Aggarwal., "Large Kerr effect in bulk Se-based chalcogenide glasses", Opt. Lett, vol. 25, no. 4, pp. 254-256, 2000.

[44]   J. M. Harbold, F. O. Ilday, F. W. Wise, J. S. Sanghera, V. Q. Nguyen, L. B. Shaw, and I. D. Aggarwal., "Highly nonlinear As–S–Se glasses for all-optical switching", Opt. Lett, vol. 27, no. 2, pp. 119-121, 2002.

[45]   Wang, Yingying, and S. Dai, "Mid-infrared supercontinuum generation in chalcogenide glass fibers: a brief review," *Photoni X* 2, pp. 11-23, 2021.

[46]   H. Ticha, L. Tichy., "Semiempirical relation between non-linear susceptibility (refractive index), linear refractive index and optical gap and its application to amorphous chalcogenides", J. Optoelectron. Adv. Mater, vol. 4, pp. 381–386 , 2002.

[47]   C.C. Wang., "Empirical relation between the linear and the third-order nonlinear optical susceptibilities", Phys. Rev. B, vol. 2, pp. 2045, 1970.

[48]   J. J. Wynne., "Optical third-order mixing in GaAs, Ge, Si, and InAs", Phys. Rev, vol. 178, pp. 1295, 1968.

[49]   J. Fournier, E. Snitzer., "The nonlinear refractive index of glass", IEEE J. Quantum Electron, vol. 10, pp. 473–475, 1974.

[50]   L. Petit, N. Carlie, H. Chen, S. Gaylord, J. Massera, G. Boudebs, J. Hu, A. Agarwal, L. Kimerling, K. Richardson., "Compositional dependence of the nonlinear refractive index of new germanium-based chalcogenide glasses", J. Solid State Chem, vol. 182, pp. 2756–2761, 2009.

[51]   T. S. Moss., "Relations between the refractive index and energy gap of semiconductors", Phys. Status Solidi, vol. 131, pp. 415–427, 1985.

[52]   N. M. Ravindra, V. K. Srivastava., "Variation of refractive index with energy gap in semi conductors", Infrared Phys, vol. 19, pp. 603–604, 1979.

[53]   V. P. Gupta, N. M. Ravindra., "Comments on the moss formula Phys. Status Solidi B, vol. 100, pp. 715–719, 1980.

[54]   R. R. Reddy, S. Anjaneyulu., "Analysis of the Moss and Ravindra relations", Phys. Status Solidi B, vol. 174, pp. K91–K93, 1992.

[55]   P. Herve, L.K.J. Vandamme., "General relation between refractive index and energy gap in semiconductors", Infrared Phys. Technol, vol. 35, pp. 609–615, 1994.

[56]   V. Kumar, J. K. Singh., Int. J. Pure. Appl. Phys, vol. 48, pp. 571–574, 2010.

[57]   M. Anani, C. Mathieu, S. Lebid, Y. Amar, Z. Chama, H. Abid., "Model for calculating the refractive index of a III–V semiconductor", Comput. Mater, vol. 41, pp. 570–575, 2008.

[58]   R. R. Reddy, Y.N. Ahammed, K. R. Gopal, D. V. Raghuram., "Optical electronegativity and refractive index of materials", Opt. Mater, vol. 10, pp. 95–100, 1998.

[59]   R. R. Reddy, Y. N. Ahammed., "A study on the Moss relation", Infrared Phys. Technol, vol. 36, pp. 825–830, 1995.

Thermal Properties of GeTeSeGa system

5. Thermal properties

Thermal transitions are transitions that occur as a result of a change in temperature. DSC can provide valuable information about thermal transitions in a sample. When an amorphous material is heated, the following basic phase changes occur:

> **"Glass transition":** It is a reversible phase change in which the structure of an amorphous material changes from a relatively hard state to a rubbery state. The temperature at which glass transition occurs (known as "glass transition temperature") is extremely important because it indicates the stability of the glassy or amorphous state.

> **Crystallization**: It is an irreversible phase change that involves the sequencing of the random orientation via nucleation and growth processes, resulting in the formation of crystalline structure.

> **Melting:** It is a phase transformation in which the crystalline lattice becomes disordered (solid to liquid transition "fusion"). In contrast to crystallization, which is a two-step exothermic process, it is a single - step endothermic process.

The aforementioned issue with tellurium-based glasses having high tendency to crystallize can be resolved by stabilizing the complete telluride matrix with a few additional elements. Nowadays, the main advancement is based on the $GeTe_4$ matrix, which can be further doped with stabilizing elements such as Se, Ga *etc*. By performing these activities, the glassy material's properties are improved for subsequent processing, such as fiber-drawing or moulding. Various thermal investigations of Ge-Te material doped with different forms of Se were carried out by "DSC" [1-4]. The common feature of these studies was an effort to identify the glass composition with the best stability and thermal charateristics. Maurugeon *et al.* [3] reported stability parameter (ΔT) value for pure $Ge_{20}Te_{80}$ glass is 79 °C where $\Delta T = T_o - T_g$ (T_o and T_g refer to onset of crystallization and glass transition temperature). According to the other studies [3, 5], the compositions of the Ge-Se-Te systems used were similar with the variation of Ge concentration where the amount of selenium used was kept below 5 at. % in order to maintain the best thermal stability.

5.1 "Experimental details"

The bulk samples of $Ge_{10}Te_{80}Se_{10-z}Ga_z$ ($z = 0$ to 10) chalcogenide glasses has been prepared by conventional "melt quenching technique". The details of the synthesis have already been discussed in chapter 2.

5.2 Results and discussions

The DSC thermograms of $Ge_{10}Te_{80}Se_{10-z}Ga_z$ ($z = 0$ to 10) powdered samples at single scan $10^{o}C$ have been shown in figure 5.1. The figure depicts normalized heat flow curves obtained by subtracting the baseline. The thermograms show well-defined endo and exothermic peaks in the temperature range room temperature ($28^{o}C$) to $450^{o}C$ which corresponds to the characteristic temperatures of the examined bulk samples. While the temperatures associated with endothermic peaks are the glass transition temperature (T_g) and melting temperature (T_m), temperature corresponds to the exothermic peaks are recognized as onset of crystallization (T_o) and peak crystallization temperature (T_c). Glass compositions with a higher T_c have better control over the nucleation and growth of crystals [6].

Most samples have broad crystallization peaks, indicating that at temperatures above 500 K, more than one compound crystallize. According to several authors, the crystallization temperature of about 500 K in binary glasses reveals the crystallization of the metastable $GeTe_2$ phase. The melting of this phase is evident by the presence of the melting peak's shoulder (T_m). The broadening of the crystallization peak in ternary glasses indicates the co-crystallization of several phases. The melting points are almost similar for all the compositions which can be attributed to the same phase. The values of T_g, T_o and T_c shifts towards the higher temperature with the Ga addition whereas the small variations in T_m values agrees with the literature data [7].
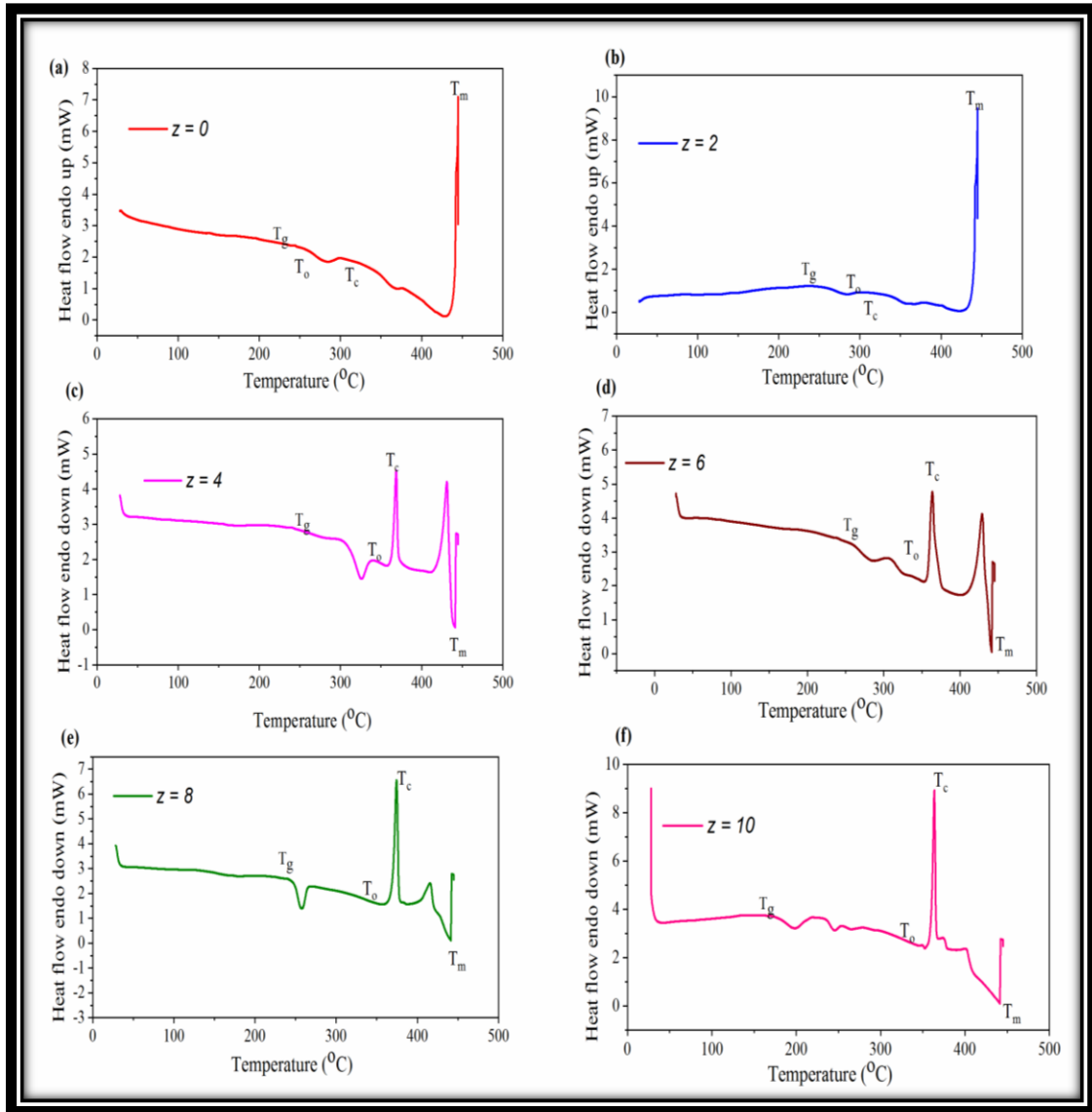
Figure 5.1: DSC thermograms of $Ge_{10}Te_{80}Se_{10-z}Ga_z$ *(z = 0 to 10)* chalcogenide glasses

5.2.1 Thermal Stability Parameters

T_g is a measure of chalcogenide glass structure rigidity or strength. As a result, T_g also provides relevant insight on the glassy state's thermal stability. However, it does not provide any information on the glass-forming tendency (GFT) by itself. The difference between T_o and T_g has been found to be a strong indicator for both thermal stability and GFT.

It is observed from the figure 5.1 that by adding Ga amoun, T_g increases. It is already discussed in chapter 3 that with the addition of Ga, the theoretical calculated parameter T_g

151

increases for all compositions. The glass forming ability increases with the increases of Ga for the present system.

Deiztal's criterion [7, 8] is the most commonly used criterion for determining glass thermal stability against crystallization, which is expressed by the relation:

$$\Delta T = T_o - T_g \tag{72}$$

The glass becomes more stable as ΔT rises. The obtained values of ΔT are tabulated in table 5.1. It is noted from the table 5.1 that by adding Ga concentration in the GeTeSeGa system the value of ΔT increases. The increases in thermal stability parameters may be due to the generation of Te-Ga covalent bonds. Also, with the generation of Te-Ga bonds the possibility of homopolar Te-Te bond is reduced (discussed in chapter 3).

Table 5.1: Values of stability parameter (ΔT), thermal stability criterion (H'), Hruby criterion (H_r, K_H), reduced glass transition temperature (T_{rg}) for $Ge_{10}Te_{80}Se_{10-z}Ga_z(z=0$ to 10) chalcogenide glasses.

z	ΔT	H'	H_r	K_H	T_{rg}
0	54.07	0.12	0.27	0.33	0.64
2	59.858	0.13	0.33	0.37	0.66
4	95.28	0.18	0.90	1.24	0.71
6	98.43	0.19	0.97	1.26	0.72
8	108.73	0.21	1.27	1.70	0.73
10	129.79	0.26	1.58	1.80	0.74

Saad and Poulain [9] discoveredthe additional criteria that provide information on thermal stability. The weighted thermal stability criterion (H') is represented by:

$$H^{'} = \frac{\Delta T}{T_g} \qquad (73)$$

By adding of Ga concentarion H' values increase. It is clear from equation 73 that H' value is directly proportional to ΔT. Hence increase in ΔT values leads to increase in H' values.

5.2.2 "Hruby Criterion and the Glass ‑ Formation Factor"

Hruby's criterion (H_r) is used to determine the thermal stability of glass using characteristic temperatures based on the following relationship [10].

$$H_r = \frac{\Delta T}{T_m - T_c} = \frac{T_o - T_g}{T_m - T_c} \qquad (74)$$

Further, the ability parameter or glass-formation factor (k_H) for the GeTeSeGa system is expressed by the relation:

$$k_H = \frac{\Delta T}{T_m - T_c} \qquad (75)$$

The k_H parameter used to quantify the glass-forming tendencies; higher values of criteria parameters suggest an improvement in the thermal stability of the glasses. The calculated values of both parameters (H_r & k_H) are depicted in table 5.1. It is observed from the table that by rising Ga in GeTeSeGa system, both the parameters increase. It is clear from equations 74 & 75 that Hr and k_H are directly proportional to ΔT. Hence an increase in ΔT values (table 5.1) The inclusion of Ga leads to increment in both the parameters.

The observed behaviour in thermal parameters (Hr, ΔT, H'& k_H) of present system can be explained using well-known principles of crystallization of glasses in the Ge – Ga – Te system. It is a double -stage procedure. First is mainly surface crystallization of tellurium followed by crystallization of GaTe and Ga_2Te_5 in a bulk autocatalytic manner [11]. The crystallization stability of Ge–Ga-Te glassy system is determined by formation of the tellurium phase. The presence of Te-Te bonds and chains of $-(Te-Te)_n-$ of varying lengths in the glass structure is one of the factors contributing to tellurium crystallization [12,13]. This describes the stabilization of Ge-Te system by the inclusion of Ga due to the

generation of structural tetrahedrons [GaTe$_{4/2}$], which further decrease the concentration of tellurium chains [12].

The ease of glass formation is obtained by estimating the reduced glass transition temperature (T$_{rg}$). The values so estimated follow the 'two-third rule' and is given by [14-16]

$$T_{rg} = \frac{T_g}{T_m} = \frac{2}{3} \qquad (76)$$

The obtained values of T$_{rg}$ for GeTeSeGa system are depicted in table 5.1 which strictly follows the 'two-third rule'. It is possible to generalize from the results (table 5.1) that the addition of gallium to the chalcogenide matrix (Ge-Te-Se) improves the thermal stability.

Also it may be ascribed that the Ga atom forms covalent bond with Te (Te-Ga) by trapping the metallic electrons and also reducing the probability of formation of tellurium microcrystal (discussed in chapter 3). Hence the connectivity of glassy network is enhanced and GFT increased consequently. Stronger glass forming ability and thermal stability indicates better anti-crystallization.

5.3 Conclusion

The DSC thermograms of $Ge_{10}Te_{80}Se_{10-z}Ga_z$ ($z = 0$ to 10) powdered samples at single scan 10°C has been analyzed. The value of T$_g$ increases from 417.413K to 517.562 K and the value of ΔT varies from 54.07 to 129.79 with the Ga addition. It is observed that with the addition of Ga the thermal parameters improve and also the glass forming ability increases.

References

[1] C. Conseil, V. S. Shiryaev, S. Cui, C. B. Pledel, J. Troles, A. P. Velmuzhov, A. M. Potapov, A. I. Suchkov, M. F. Churbanov and B. Bureau., "Preparation of High Purity Te-Rich Ge-Te-Se Fibers for 5–15 µm Infrared Range", J. Light. Technol. 31, 1703-1707, 2013.

[2] S. Maurugeon, B. Bureau, C. B. Pledel, A. J. Faber, X. H. Zhang, W. Geliesen and J. Lucas., "Te-rich Ge–Te–Se glass for the CO_2 infrared detection at 15 µm", J. Non-Cryst. Solids, vol. 355, pp. 2074–2078, 2009.

[3] S. Maurugeon, B. Bureau, C. B. Pledel, A. J. Faber, P. Lucas, X. H. Zhang and J. Lucas., "Selenium modified $GeTe_4$ based glasses optical fibers for far-infrared sensing", Opt Mater, vol. 33, pp. 660-663, 2011.

[4] S. Cui, C. B. Pledel, J. Troles and B. Bureau., "Telluride glass single mode fiber for mid and far infrared filtering", Opt. Mater. Express, vol. 6, pp. 971-978, 2016.

[5] S. Maurugeon, C. B. Pledel, J. Troles, A. J. Faber, P. Lucas, X. H. Zhang, J. Lucas and B. Bureau., "Telluride glass step index fiber for the far infrared", J. Light. Technol, vol. 28, pp. 3358-3363, 2010.

[6] P. Petkov, V.Ilcheva, T. Petkova, P. Ilchev., "Thermal Studies of Ge-Te-Ga Glasses", AIP Conf. Proc, vol. 203, no. 1, pp. 932-937, 2010.

[7] X. Huijuan, X. Wang, Q. Nie, Y. He, P. Zhang., "Glass formation and properties of $Ge-Ga-Te-ZnI_2$ far infrared chalcohalide glasses", J. Non-Cryst. Solids, vol. 383, pp. 212-215, 2014.

[8] S. Mahadevan, A. Giridhar & A. K. Singh., "Calorimetric measurements on As-Sb-Se glasses", J. Non-Cryst. Solids, vol. 88, no. 1, pp. 11-34, 1986.

[9] M. Saad & M. Poulain., "Glass forming ability criterion", Materials Science Forum, vol. 19, pp. 11-18, 1987.

[10] Hruby., "Evaluation of glass-forming tendency by means of DTA", J. Phys. B, vol. 22, no. 11, pp. 1187-1193, 1972.

[11]   R. Svoboda, D. Stritesky, Z. Zmrhalová, D. Brandova, & J. Malek., "Correlation of structural, thermo-kinetic and thermo-mechanical properties of the $Ge_{11}Ga_{11}Te_{78}$ glass", J. Non-Cryst. Solids, vol. 445, pp. 7-14, 2016.

[12]   Z. Chaker, G. Ori, M. Boero, C. Massobrio, E. Furet & A. Bouzid., " First-principles study of the atomic structure of glassy $Ga_{10}Ge_{15}Te_{75}$", J. Non-Cryst. Solids, vol. 498, pp. 338-344, 2018.

[13]   A. P Velmuzhov, M. V.Sukhanov, A.D. Plekhovich, N. S. Zernova & M. F. Churbanov., "Preparation and investigation of the properties of $Ge_{25-x}Ga_xTe_{75-y}I_y$ Glass System (x= 5, 10, 15, y= 0–6)", J. Non-Cryst. Solids, vol. 503, pp. 297-301, 2019.

[14]   W. Kauzmann., "The nature of the glassy state and the behavior of liquids at low temperatures", Chem. Rev. vol. 43, no. 2, pp. 219-256, 1948.

[15]   G. Kaur, T. Komatsu & R. Thangaraj Crystallization kinetics of bulk amorphous Se-Te-Sn system. J. Mater. Sci. 35(4), 903-906(2000).

[16]   B. S. Patial, S. Bhardwaj, A. M. Awasthi and N. Thakur., "On the crystallization kinetics of multicomponent nano-chalcogenide $Se_{79-x}Te_{15}In_6Pb_x$ (x= 0, 1, 2, 4, 6, 8 and 10) alloys", Nano Express, vol. 1 no. (3), pp.030021, 2020.

Summary & Future scope
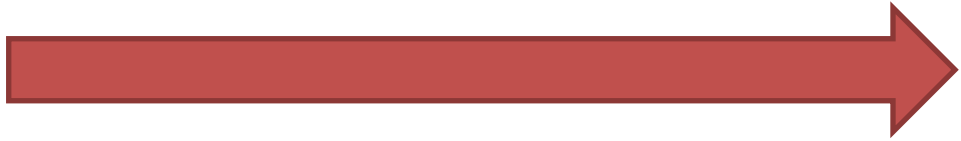
6. Summary and Future scope

6.1 Summary

Chalcogenide glasses are potential materials for IR applications. The studies have been performed on ternary and quaternary $Ge_{10}Te_{80}Se_{10-z}Ga_z$ (z = 0 to 10) chalcogenide glassy alloys. Due to their good "optical and thermal" properties, these glasses are becoming an attractive candidate for several applications. The GeTeSeGa glasses have been studied for their physical, structural, optical and thermal properties. The theoretical or physical studies report that the "average coordination number and number of constraints" increases with the Ga enhancement. The value "$<r> > 2.4$ and $N_c > N_d$", which reveals that the studied compositions possess over coordination and rigidity. The density of the studied system shows an increment in their values, which supports the decrease in free volume space. In the studied system, lone pair electrons decline with Ga addition but $L > 2$ for whole system. Thus, all the compositions of GeTeSeGa may be approved as good glass former. According to R parameter, the values of "transition temperature and mean bond energy" have been investigated. The "theoretical bandgap and mean bond strength" decreases with the Ga addition.

The bulk samples of $Ge_{10}Te_{80}Se_{10-z}Ga_z$ (z = 0 to 10) glassy system are prepared by traditional "melt quenching" method. The thin films of the bulk glasses have been deposited on glass substrates by the "thermal evaporation technique" in the vacuum coating unit.

The XRD technique has been adopted to confirm the "amorphous nature" of the samples. The HRSEM images also indicate the amorphous nature and presence of irregular shapes in all the compositions.

The qualitative and quantitative descriptions of absorption bonds have been realized by estimating theoretical calculations. The far-IR study reveals that the presence of Te-Ga and $GeTe_4$ and $GaTe_4$ with the rise of Ga concentration. The lesser bond energy leads to decline in the values of the mean bond strength of the material. Consequently, the calculated energy gap and optical bandgap of the material reduces. The bond $145cm^{-1}$-$151cm^{-1}$ corresponds to the homopolar Te-Te bond. The far –IR study supports the decrease in band gap of $Ge_{10}Te_{80}Se_{10-z}Ga_z$ (z = 0 to10 at. %).

The optical properties have been realized by "UV-Vis-NIR spectroscopy in the NIR range". The optical study reveals that by Ga addition, the absorption edge has moved towards a longer wavelength region. The index of refraction increases (n) with the enhancement of Ga concentration. The decrease in n values with the increase of wavelength indicates the normal dispersion behaviour of the system. The higher "refractive index" values of the samples make them appropriate for IR mirrors and filters. The values of "extinction coefficient and absorption coefficient" increase with the raising of Ga in the material. The refractive index, polarization, density and dielectric constant shows a similar trend with the Ga content. WDD parameters *viz.* E_o decreases from 2.26 eV to 1.95 eV. However, E_d increases from 25.44 eV to 36.49 eV. This indicates that with the enhancement of Ga, the thin films become more stable and stiff. The optical bandgap of the thin films has been estimated by the Tauc approach and the values decrease with the increase of Ga content. The optical band gap exhibits the similar pattern as the mean bond strength and theoretical bandgap with the Ga addition. The value of metallization character (M) < 1, which affirms the non-metallic nature of the material. The non-linear parameters have also been calculated. "Non–linear refractive index and non–linear susceptibility" increase by the inclusion of Ga concentration in the GeTeSeGa material.

The DSC thermograms of $Ge_{10}Te_{80}Se_{10-z}Ga_z$ (z = 0 to 10) powdered samples at single scan 10^oC has been analyzed. The value of ΔT varies from 54.07 to 129.79 with the Ga addition. It is observed that with the addition of Ga the thermal parameters improve and also the glass forming ability increases. By increasing Ga in the GeTeSeGa, the value of ΔT enhances. The increases in thermal stability parameters may be due to the generation of Te-Ga covalent bonds. Also, by the creation of Te-Ga bonds the possibility of homopolar Te-Te bond is reduced.

6.2 Future Scope

The future work of the present work is described in following points

> ➢ To study dark conductivity and photoconducting of prepared thin films.

> ➢ Study of thermal stability at different heating rates.

> ➢ In future, Machine learning techniques may be supplement with proper domain expertise to determine the optimal composition for achieving desired properties.